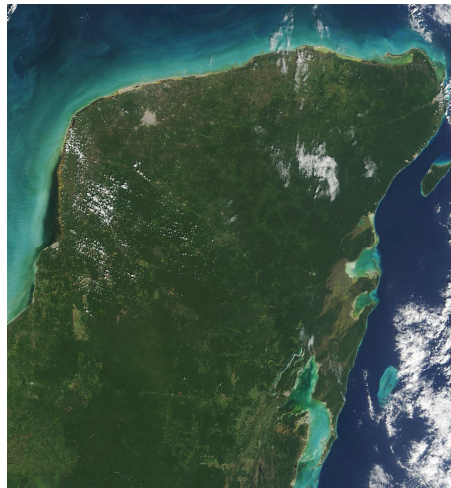


Estimation of actual evapotranspiration using remote sensing data for the Yucatan Peninsula, Mexico



MSc Thesis by Sara Lerer
July 2008

Supervised by Associate Professor Peter Bauer Gottwein

Abstract

Evapotranspiration (ET) is an important component of the hydrological cycle, and thus a key input to groundwater models. Remote sensing offers great opportunities for acquiring data on environmental variables for large and remote areas, and different methods have been developed for using this data to estimate ET. In this project, the so-called triangle method with Priestly-Taylor approach was applied to the Yucatan Peninsula in Mexico. Input data was MODIS images of NDVI (normalized difference vegetation index) and of day and night LST (land surface temperatures) for 491 days between January 1, 2007 and May 5, 2008. Output was 52 images of evaporative fraction (EF). The scatter plots of ΔLST vs. NDVI did not fully resemble the triangle/trapezoid shape expected due to the low representation of pixels with bare soil and low density vegetation, but for these 52 days the scatters were good enough to allow for an extrapolation into the model triangle.

Radiation data from ECMWF (European Centre for Medium Range Weather Forecast) combined with the NDVI images were used to derive images of available energy. Images of available energy and evaporative fraction were combined to produce images of spatially distributed actual evapotranspiration (aET). aET rates for the 29 images in 2007 varied between 0 and 6.95 mm day⁻¹ with a spatial and temporal mean of 2.99 mm day⁻¹. The variation in aET across the peninsula had a general decreasing trend from southeast toward northwest, with a stronger differentiation in the dry season, as expected. No correlation was found between EF and elevation, as opposed to the expectation that greater distance to the groundwater table would result in lower aET/PET ratio (imitated by the EF).

Sap flow was measured at eight sites on the peninsula, and results were used to estimate stand transpiration (sT). At two sites situated in high NDVI pixels the mean sT was 3.6 and 4.8 mm day⁻¹, and at a site in a low NDVI pixel the mean sT was 0.7 mm day⁻¹. The difference in mean sT between low and high NDVI sites is statistically significant despite the large variability in the daily results (related to daily variations in driving forces of ET and to measurement and scaling uncertainties). Similarly, the difference between the mean aET in the encompassing pixels of these sites during an overlapping period is statistically significant. This indicates an agreement between the results from the triangle method and from the sap flow measurements on the relative magnitudes of aET. Yet this is not sufficient for validating the results of either method.

Data for the Yucatan Peninsula violates some of the assumptions made in the triangle method, and it is therefore recommended to find means of validating the results before applying them in an operational model. There are possibly many improvements to the application of the method as done in this project, which should be tested once a means of evaluating the results is found.

Preface

This report presents a summary of the work done in my MSc thesis project from January 7th to July 11th, 2008, accredited with 30 ECTS points. The thesis is the last part required for graduating the MSc program in Environmental Engineering at the Technical University of Denmark. The work included a field trip to Yucatan, Mexico, from February 3rd to March 9th. Main supervisor was Associate Professor Peter Bauer-Gottwein from DTU Environment, and co-supervisors were Teis Mikkelsen, Senior Researcher at Risø DTU and Simon Stisen, Researcher at GEUS.

Lyngby, 11th of July 2008

Sara Lerer, s022863

Acknowledgements

This project was part of the larger research work being done in order to map and model the groundwater resources of the Sian Ka'an Biosphere Reserve, a work initiated and led by Associate Professor Peter Bauer-Gottwein and PhD Student Bibi Ruth Neuman Gondwe from DTU Environment. I am very grateful to the two of you for inviting me to be part of this work, and for all the inspiration and support you have given me.

The field work could not have been carried out without the invaluable financial and practical help from several institutions and people in Mexico. First and foremost Amigos de Sian Ka'an, who provided shelter, means of transport, expertise and practical help in the field. Especially thanks to Waldemar Santamaria Rivero and Alejandra Fregoso for their efforts to maintain my last experiment. Second, Prof. Luis Marin from the UNAM, who sent students to help in the field, and here I would especially like to thank Alexander for following me "through water and fire" across the peninsula for many tiring days. Last but not least, all the commissioners of common lands and other connoisseurs of the forest who shared their knowledge with us and dedicated time to help us with characterization of the vegetation at the different sites.

Planning of the field work could not have been done without the guidance of Senior Researcher Teis Mikkelsen from Risø DTU. Also thank you for fruitful discussions on interpretation of the results and dedicating time to do some testing at your field site at Sorø (results unfortunately not included in the report). Dr. Jose Luis Andrade, Dr. Cassandra Reyes-Garcia and Ing. Roberth from the Centro de Investigación Científica de Yucatán also generously shared with me their knowledge and practical experience with sap flow measurements.

I am thankful to Researcher Simon Stisen from GEUS for his intensive help to get me started with data processing in IDL+ENVI, and the many fruitful discussions we had about the triangle method. Research Assistant at DTU Environment Silvio Pereira Cardenal was very helpful with the ordering and handling of ECMWF data.

Finally, to friends and family, especially Maria, Alvaro and Faren, for love and moral support and help with all the small things that get me by.

List of Contents

1	Introduction	1
1.1	Motivation.....	1
1.2	Problem definition	1
1.3	The Yucatan Peninsula	2
1.3.1	Delineation	2
1.3.2	Topography	3
1.3.3	Climate	4
1.3.4	Vegetation	6
2	Theory	7
2.1	Physics of evaporation	7
2.2	Physics of radiant energy	8
2.3	The Surface Energy Balance.....	10
2.3.1	Net radiation	11
2.3.2	Surface Temperature	12
2.3.3	Soil heat flux	12
2.4	Transpiration.....	12
2.4.1	Stomata and cohesion-tension	13
2.4.2	Xylem and sapwood	14
2.4.3	Roots.....	15
2.5	Tropical forests	15
2.5.1	Water resources	16
2.6	Remote Sensing	17
2.6.1	Satellites	17
2.6.2	Sensors.....	17
2.6.3	Image restoration	17
2.6.4	Vegetation indices	18
2.6.5	Surface temperatures	18
3	Methods.....	21
3.1	The concept of evaporative fraction	21
3.2	The triangle method	21
3.2.1	Review.....	22
3.2.2	The Priestley-Taylor approach	23
3.2.3	NDVI.....	26

3.2.4	Δ LST	27
3.2.5	Evaporative fraction algorithm.....	27
3.3	Available energy	30
3.3.1	Net radiation	31
3.3.2	Soil heat flux	31
3.4	Sap Flow measurements	32
3.4.1	The heat dissipation method.....	32
3.4.2	Scaling from tree to stand.....	36
3.4.3	Site choice	38
4	Results.....	39
4.1	NDVI	39
4.1.1	Temporal variation	39
4.1.2	Spatial variation.....	40
4.2	Δ LST.....	42
4.3	Evaporative fraction.....	45
4.3.1	Scatter plots and triangles.....	45
4.3.2	Temporal and spatial variation	47
4.3.3	Analysis using regions of interest tool	49
4.3.4	Correlation with elevation	51
4.4	Available energy	52
4.5	Actual evapotranspiration	53
4.6	Sap flow	55
4.6.1	Test sites	56
4.6.2	Site 4.....	58
4.6.3	Site 5.....	61
4.6.4	Site 6.....	64
4.6.5	Site 7.....	67
4.6.6	Site 8.....	68
4.6.7	Summary	69
4.7	Comparison of actual evapotranspiration estimates from the triangle method and stand transpiration estimates from sap flow measurements	71
5	Discussion	73
6	Conclusion.....	77
	References.....	79
	List of abbreviations.....	85

Appendix E.....	87
Appendix F.....	88
Appendix G.....	97

List of Appendices

Appendix A	IDL scripts (on CD/DVD)
Appendix B	Technical specifications for Dynamax TDP (on CD/DVD)
Appendix C	Pictures of experimental installations (on CD/DVD)
Appendix D	Technical specifications for Campbell Scientific CR10X datalogger (on CD/DVD)
Appendix E	Coefficients used to calculate temperature measured by thermocouple type T
Appendix F	Scatter plots and modeled triangles for all “successful” days in 2007 and first four months of 2008
Appendix G	Description of experimental sites
Appendix H	Raw and processed sap flow data (on CD/DVD)
Appendix I	Produced images of NDVI, Δ LST, EF, R_n , G and aET for the Yucatan Peninsula (on CD/DVD)

1 Introduction

1.1 Motivation

Sian Ka'an is a biosphere reserve in the state of Quintana Roo on the Yucatan Peninsula, Mexico. It was established on the 20th of January 1986 and is part of UNESCO's Man and the Biosphere Program and a declared UNESCO World Heritage Site (UNEP-WCMC, 1996). The reserve covers an area of approx. 5300 km² and spans 120 kilometers from north to south (comprising almost one third of the Mexican Caribbean coast). Many different vegetation types exist within the reserve: tropical forests, flood forest, palm savanna, freshwater and saltwater marshes, hammocks, mangroves, dunes and keys. The habitat diversity gives rise to a large fauna diversity: a total of 103 species of mammals has been recorded in the reserve (including five big cats), some 339 species of birds (including many marine and wading birds) and 42 species of amphibians and reptiles (including four sea turtles).

About a third of Sian Ka'an is wetland, which is entirely fed by groundwater (Neuman and Rahbek, 2006). Groundwater of the Yucatan Peninsula is a thin lens of freshwater floating on saline water in a karstic limestone medium. The soil cover on top of the limestone is limited and the aquifer is highly permeable. Much of the groundwater flow occurs in matrix fractures and caves. All this makes the groundwater aquifer, and thus water resources of the reserve, very vulnerable to pollution.

The rapid expansion of tourism in the state of Quintana Roo since the late 1970's, which has entailed an extensive development and urbanization, especially along the coast from Cancun to Tulum, is a major threat to the state of the aquifer. Increased groundwater abstraction rates, pumping of wastewater into the aquifer and infiltration from landfills are just some of the examples of present hazards. Protection of the aquifer is crucial since it is the only significant source of freshwater in the state.

A model of the upland of Sian Ka'an's groundwater resources has been developed, and is continuously sought to be improved, by PhD student Bibi Neuman at DTU Environment. The objective of the modeling effort is to contribute to the sustainable management of the groundwater resource by facilitating simulation of different management scenarios. Neuman's current estimate of the upland area is 35,000 km², covering much of the state of Quintana Roo and some of the state of Campeche. One of the challenges in improving the model is acquisition of reliable input data such as maps of groundwater caves, groundwater and wetland water levels and recharge rates.

Determining the recharge to an aquifer is necessary in order to achieve quantitative description of groundwater flows and estimating groundwater residence times within the aquifer. Recharge, R , can be estimated from a simple water balance: $R=P-ET$, where P is precipitation and ET is evapotranspiration. Precipitation is relatively easy to measure and data for the Yucatan peninsula is available in reasonable quality. Evapotranspiration, on the other hand, is very complex to measure, and known estimates for the peninsula are between 40 and 85% of annual precipitation (Neuman and Rahbek, 2006).

1.2 Problem definition

Many methods for estimating evapotranspiration exist, and most require extensive input data such as local meteorological parameters, surface properties and soil moisture availability. Such data from ground observations is often scarce, especially in remote areas such as the Yucatan

Peninsula. Remote Sensing (RS) offers a great opportunity for acquiring distributed data for large areas, and researchers have shown that combinations of common RS parameters can be used to derive maps of actual evapotranspiration (aET) with reasonable accuracy. One such notable novel approach is the triangle method as presented by Jiang and Islam (2001) and improved upon by Wang et al (2006) and Stisen et al (2008).

The triangle method is designed for large study areas which include a large range of land cover types. The Sian Ka'an Basin is mostly covered by rather dense tropical forests. Therefore, in this project, the study area was expanded to include also the north-west part of the Yucatan Peninsula, where a drier climate and lower vegetation cover is found. At initiation of this project it was unknown whether this study area would fulfill all the requirements necessary for applying the triangle method. Furthermore, it was not known of any ground observations of aET which could be used to validate the results. As a fast and cheap means of obtaining ground observations, the measurement of trees' sap flow for estimating stand transpiration was considered. Thus, the objective of the project was to answer the following two main questions:

Can the triangle method be applied to the Yucatan Peninsula to produce improved quantitative estimates of actual evapotranspiration and qualitative distribution of evapotranspiration rates?

Can sap flow measurements at strategic sites on the peninsula be used to provide estimates of stand transpiration for validating the results of the triangle method?

1.3 The Yucatan Peninsula

1.3.1 Delineation

The name Yucatan (in Spanish: Yucatán) refers to two different places: a state in the Mexican Federation and a peninsula in Central America separating the Gulf of Mexico from the Caribbean Sea. The exact definition of the limits of the peninsula are unclear, but it normally includes the three Mexican states Campeche, Yucatan and Quintana Roo, the northern part of Belize and a small part of Guatemala. A map showing state and country borders, main cities and roads can be seen in Figure 1-1.

The name Yucatan in this report is used to refer to the peninsula, unless otherwise mentioned. All images of the Yucatan Peninsula, unless otherwise stated, have the following properties: they include 450 samples (columns) and 440 lines (rows), which makes a total of 198,000 pixels, of which approx. 136,000 are land pixels and the rest are ocean. Each pixel is 1 by 1 km, so the entire image represents 450 by 440 km. The projection is UTM zone 16 with datum WGS86, and the image encompasses the area from 80000-530000E / 196000-240000N (which corresponds approximately to latitude 17° to 21°, longitude 86° to 91°). Other maps were presented in a similar way as far as possible (e.g. the map in Figure 1-1 covers a slightly larger area than the one defined above).



Figure 1-1: Map of the Yucatan Peninsula (illustration taken from Infoplease, 2008).

1.3.2 Topography

A digital elevation map (DEM) of Yucatan obtained from the SRTM is displayed in Figure 1-2. The original data has 3 arc seconds spatial resolution and ± 10 m in vertical resolution (EROS, 2007), but the displayed image was resampled to a spatial resolution of 1 km^2 (and reprojected into UTM). Elevation varies between 0 and 363 m.a.m.s.l.; most of the blue pixels are lower than 40 m.a.m.s.l. All in all the peninsula is considered very flat.

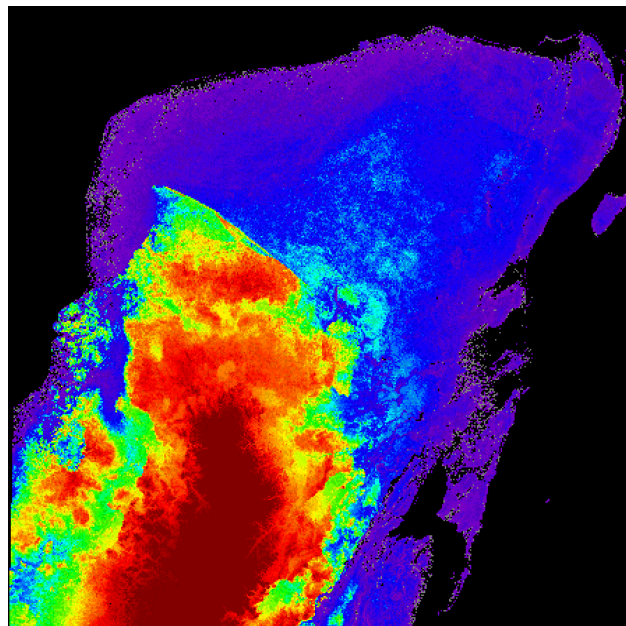


Figure 1-2: Digital elevation map of Yucatan, values range between 0 and 363 m.a.m.s.l. (from USGS SRTM).

1.3.3 Climate

Most of the peninsula – except the furthestmost northwestern part – belongs to the Aw group according to the Köppen classification (Wikipedia contributors, 2008a). Group A refers to tropical climates, characterized by constant high temperatures, while the subgroup Aw refers to tropical wet and dry or savanna climate, which have a pronounced dry season. In general there is a gradient of decreasing humidity on the peninsula from southeast toward northwest (Rzedowski, 1994).

Mean monthly temperatures, precipitation and evaporation rates from two opposite points on the peninsula, Merida in the northwest and Chetumal in the southeast, are presented in Figure 1-3 to Figure 1-6. Data represents the climatic normal for the years 1971-2000 according to the Mexican National Water Committee.

As expected from the climatic class, the temperatures at both sites are quite high and stable all year round. The annual mean for Merida is 26.5 °C (with a difference between the hottest and coldest month at 4.6 °C) and for Chetumal it's 26.9 °C (with a difference of 5.1 °C).

Annual precipitation, on the other hand, is significantly higher at Chetumal than at Merida (1327 mm compared to 1050 mm). The difference between the month of highest precipitation and the month of lowest precipitation is greater at Chetumal than at Merida (180 mm compared to 148.7 mm), but at Chetumal there are only two months with a precipitation lower than 50 mm (February-March), compared to five at Merida (December-April).

Pan evaporation rates reach a total of 1803 mm per year at Chetumal and 2023 mm per year at Merida. The seasonal pattern is very similar between the two sites, with a minimum in December-January and a maximum in May, and with the maximum almost two-fold the magnitude of the minimum.

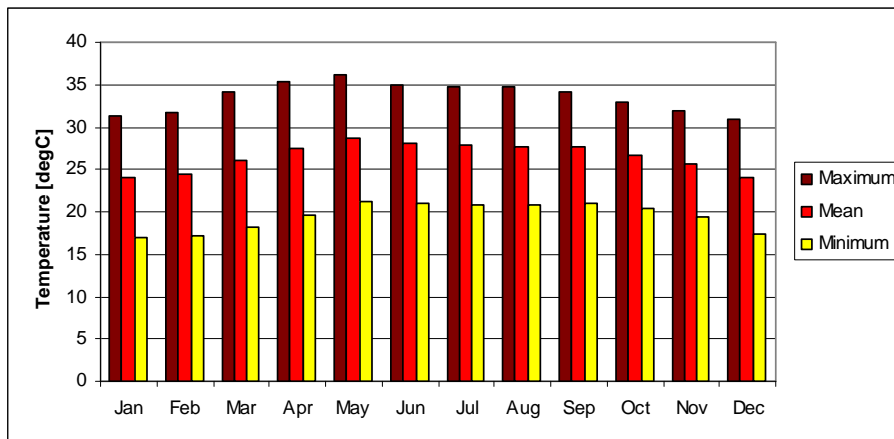


Figure 1-3: Mean, maximum and minimum monthly air temperatures in Merida, state of Yucatan, for 1971-2000 (CNA, 2008).

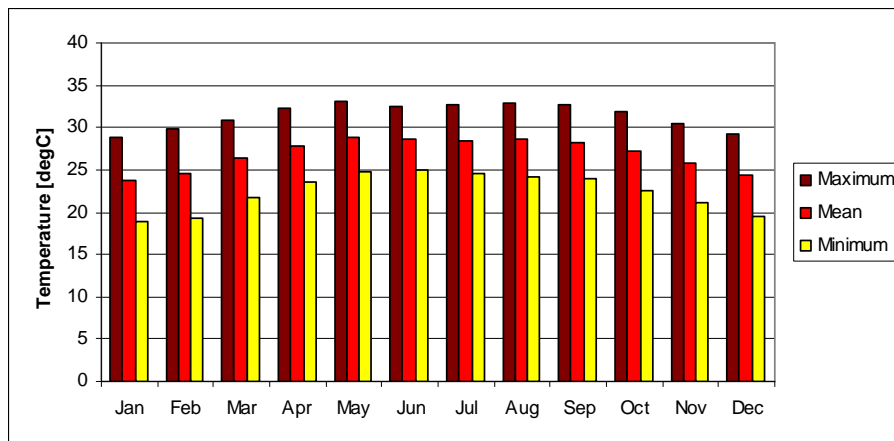


Figure 1-4: Mean, maximum and minimum monthly air temperatures in Chetumal, state of Quintana Roo, for 1971-2000 (CNA, 2008).

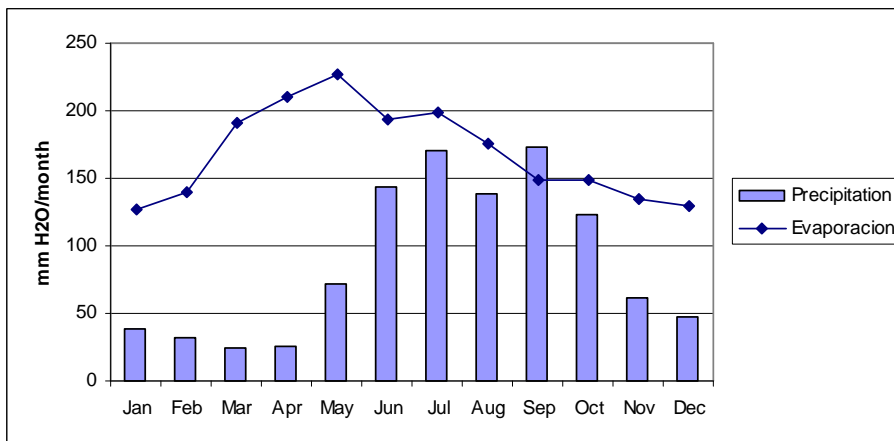


Figure 1-5: Mean monthly precipitation and pan evaporation in Merida, state of Yucatan, for 1971-2000 (CNA, 2008).

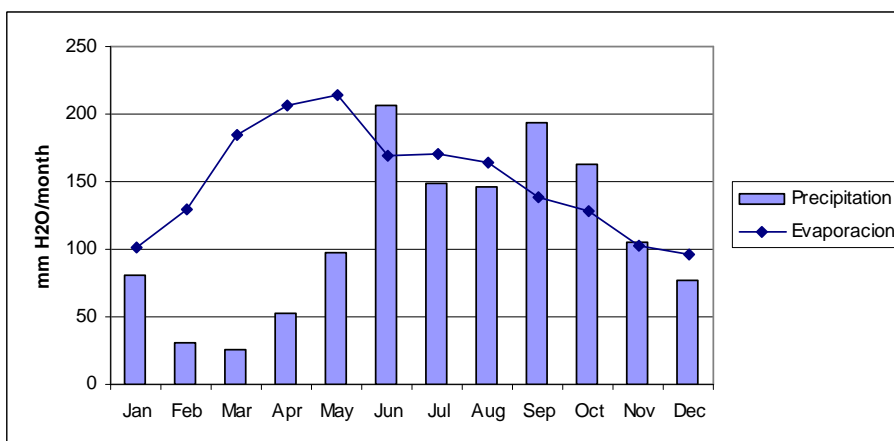


Figure 1-6: Mean monthly precipitation and pan evaporation in Chetumal, state of Quintana Roo, for 1971-2000 (CNA, 2008).

1.3.4 Vegetation

Most of the peninsula is covered by tropical forests (89% of the surface), divided into different sub-groups:

- high tropical forest (trees higher than 30 m)
 - o evergreen: 1%
 - o semi-evergreen (25-50% of the species lose their leaves in the dry season): 5%
- medium tropical forest (15-10 m high trees)
 - o semi-evergreen: 50%
 - o deciduous: 17%
- low tropical forest (trees lower than 15 m)
 - o semi-evergreen: 3%
 - o deciduous: 13%

The rest of the land surface is covered by hydrophilic vegetation or agricultural crops (or recovering from slash-and-burn agriculture), or supports human settlements (CNA, 2001). In general there is a gradient of decreasing vegetation density from southeast to northwest, linked to the gradient in humidity (Rzedowski, 1994). Practically all forests are affected to some extent by human activities (logging or slash-and-burn agriculture), thus they are considered “secondary” forests. Activities are usually regulated by local commissioners of communal lands. Forests are also affected by hurricanes and natural forest fires.

2 Theory

According to Dingman (2002), evapotranspiration (ET) can be defined as a collective term for all the processes by which water at or near the land surface becomes atmospheric water vapor. The word is composed of the term evaporation, referring to water vapor coming from liquid water such as rivers, lakes, bare soil and vegetation surfaces, and the term transpiration, referring to the water vapor originating from within the leaves of plants. Evaporation and transpiration are different processes governed by different rules, but since the earth's surface is often covered by a mixture of open water, soil and vegetation, it can be difficult to distinguish between the two fluxes, and for operational purposes they are often treated as one.

Direct measurement of ET is practically impossible, and therefore there exists a long list of methods to indirectly estimate ET. The theory reviewed in this chapter is the core of what is relevant for the two methods used in this project – the RS based triangle method and the ground based measurement of trees' sap flow. Section 2.1 introduces basic theory of evaporation, which is also relevant for understanding plant transpiration, further described in Section 2.4. Section 2.2 on basics of radiation is relevant for understanding the surface energy balance where ET is a key compound, as further described in Section 2.3, and also relevant for understanding how remote sensing works, as further described in Section 2.6. Section 2.5 gives a short introduction to some features of tropical forests, the dominating vegetation type on the Yucatan Peninsula, which are relevant for application of sap flow measurements and estimation of the degree at which the trees reach the groundwater.

2.1 Physics of evaporation

The rate of evaporation is the rate at which molecules of water move from the saturated surface layer just above a body of water into the air above; it is proportional to the difference between the vapor pressure of the surface layer and the vapor pressure of the overlaying air, Dalton's Law (Dingman, 2002):

Equation 2-1

$$E \propto e_s^* - e_a$$

Where E is the rate of evaporation, e_s^* is the saturation vapor pressure at the temperature of the surface and e_a is vapor pressure of the air measured at some representative height.

The difference can be positive (evaporation occurring), zero (nothing) or negative (condensation occurring). Evaporation will occur even if the relative humidity of the air equals 100%, as long as $e_s^* > e_a^*$ (under these conditions water will normally condense in the overlaying air to form fog or mist).

The latent heat of vaporization λ_v is the quantity of heat energy that must be absorbed to break the hydrogen bonds when evaporation takes place (the same quantity is released when condensation occurs). Thus evaporation is accompanied by a transfer of heat out of the water body (cooling of the body) and condensation on the surface by an addition of heat: latent heat transfer. The rate of latent heat transfer LE [$E T^{-1}$] and water transfer are directly proportional:

Equation 2-2

$$(a) LE = \lambda_v \cdot E$$

Where λ_v is the latent heat of vaporization [$E M^{-1}$] and E is the rate of evaporation or condensation in units of mass per time [$M T^{-1}$]; E is often expressed in units of length per time [$L T^{-1}$], in which case the equation becomes:

$$(b) LE = \rho_w \cdot \lambda_v \cdot E$$

Where ρ_w is the density of water [$M L^{-3}$].

The latent heat of vaporization decreases as the temperature of the evaporating surface increases, given approximately by:

Equation 2-3

$$\lambda_v = 2.495 - 2.36 \cdot 10^{-3} \cdot T$$

Where λ_v is in $MJ kg^{-1}$ and T in $^{\circ}C$. Since the variation of λ_v is relatively small over the range of normal earth surface temperatures, it is considered reasonable to use a single value of $2.45 MJ kg^{-1}$ corresponding to a surface temperature of $20^{\circ}C$ (Allen et al, 1998).

The vapor pressure gradient between the surface and the air is generated by the turbulence in the planetary boundary layer (PBL), which is the lowest layer of the atmosphere. The winds in the PBL are affected by the frictional resistance of the surface which produces turbulent eddies. These eddies have both horizontal and vertical components, thus spreading both sensible and latent heat in the atmosphere. The intensity of the turbulence can be characterized by the friction velocity, which is a component in the determination of the vertical distribution of wind velocity, which is used in one of the parameterizations of Dalton's Law:

Equation 2-4

$$LE = K_{LE} \cdot v_a \cdot (e_s - e_a)$$

Where K_{LE} is a bulk latent heat transfer coefficient and v_a is the time averaged velocity at a certain height above ground surface.

2.2 Physics of radiant energy

All matter at temperatures above absolute zero radiates energy in the form of electromagnetic waves that travel at the speed of light. The rate of emission is given by the Stefan-Boltzmann Law (Dingman, 2002), see also Figure 2-1(a):

Equation 2-5

$$R_L = \varepsilon \cdot \sigma \cdot T^4$$

Where R_L is the rate of energy emission per unit surface area per unit time [$E L^{-2} T^{-1}$], ϵ is the emissivity, T is the absolute temperature, and σ is the universal Stefan-Boltzmann constant [$E L^{-2} T^{-1} \Theta^{-4}$].

Values of emissivity range from 0 to 1, where most earth materials have emissivities between 0.95 - 0.99. An ideal surface with an emissivity of 1 is called a blackbody.

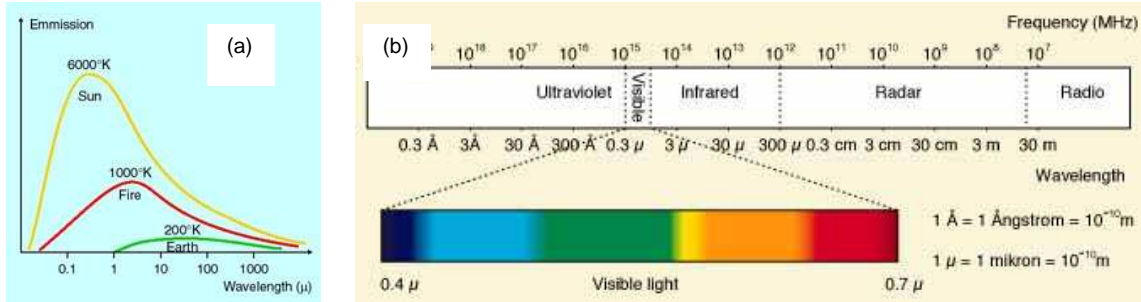


Figure 2-1: Illustration of the dependence between temperature and emissivity (a) and the electromagnetic spectrum (b) (taken from GO, 2008).

Electromagnetic radiation is described with wave length λ [L] and wave frequency f [T^{-1}], which are inversely related according to:

Equation 2-6

$$\lambda \cdot f = c$$

Where c is the speed of light ($2.998E8 \text{ m s}^{-1}$).

The wavelength from a surface decreases as its temperature increases according to Planck's Law. The wavelength at which maximum radiation λ_{\max} occurs is related to the absolute temperature via Wien's Displacement Law:

Equation 2-7

$$\lambda_{\max} \cdot T = 2897$$

Where λ_{\max} is in μm and T in degrees K.

Only radiation in the near-ultraviolet (0.2 - 0.4 μm), the visible (0.4 – 0.7 μm) and infrared (0.7 – 80 μm) ranges play a role in the earth's energy balance and climate, see Figure 2-1(b).

Electromagnetic energy is transmitted through a vacuum undiminished, but when it strikes matter it is partitioned: some of it will be absorbed (and cause an increase in the matter's temperature), some of it will be reflected (and continue to travel undiminished in a new direction) and some will be transmitted through the matter (and continue to travel undiminished in the same direction). The relative size of these fates depends on the type of matter and on the wavelength of the energy.

The reflectance of an object integrated over the visible wavelength is called the albedo; the albedo of an ideal white body is 1 and of an ideal blackbody 0. The albedo of the earth can

range from about 0.05 for dark and wet soil to 0.95 for fresh snow, the average of the earth being around 0.3; deciduous forests normally range between 0.15 and 0.2 (Dagmar, 2008).

2.3 The Surface Energy Balance

The energy balance for an ideal surface can be expressed as (Pal Arya, 2001):

Equation 2-8

$$R_n = H + LE + G$$

Where R_n is the net radiation (considered positive when directed towards the surface), and H , LE and G are sensible, latent and ground heat fluxes (considered positive when directed away from the surface) – all in units of energy per time per area [$E T^{-1} L^{-2}$].

During daytime the surface receives more radiative energy than it emits, and this surplus is converted into sensible heat conducted to the atmosphere (H) and to the ground (G) and into latent heat (LE). The partitioning between the three compounds depends on many factors such as the surface characteristics, the geographic location, the time and the weather.

During night time the surface emits more radiative energy than it receives, and this loss of energy is compensated by sensible heat conducted from the air and the ground towards the surface, and possibly also latent heat from condensation (dew formation). The absolute value of G during nighttime is roughly equal to its daytime value, thus G over 24 hours can be assumed to equal zero. The other compounds usually have greater magnitude during day than night.

The earth's surface is not an ideal surface as it includes horizontal inhomogeneities (such as vegetation, buildings and hills). It is therefore often more practical to regard it as a finite layer with its own mass and heat capacity so that energy can be stored in the layer. When considering vegetated surfaces it is most appropriate to include the whole canopy layer in the energy balance:

Equation 2-9

$$R_n = H + LE + G + \Delta H_s$$

Where ΔH_s is the change in energy storage per unit time per unit area over the depth of the layer, and H and LE are measured above the canopy.

The rate of energy storage in a vegetative canopy consists of two parts (physical and biochemical) and is rather complicated to measure and estimate; it is often added to the ground heat flux to produce a combined storage compound. The latent heat exchange is also complicated since besides evaporation from the surface it also includes transpiration from plant leaves. A typical diurnal variation of the energy balance compounds over a forest canopy can be seen in Figure 2-2.

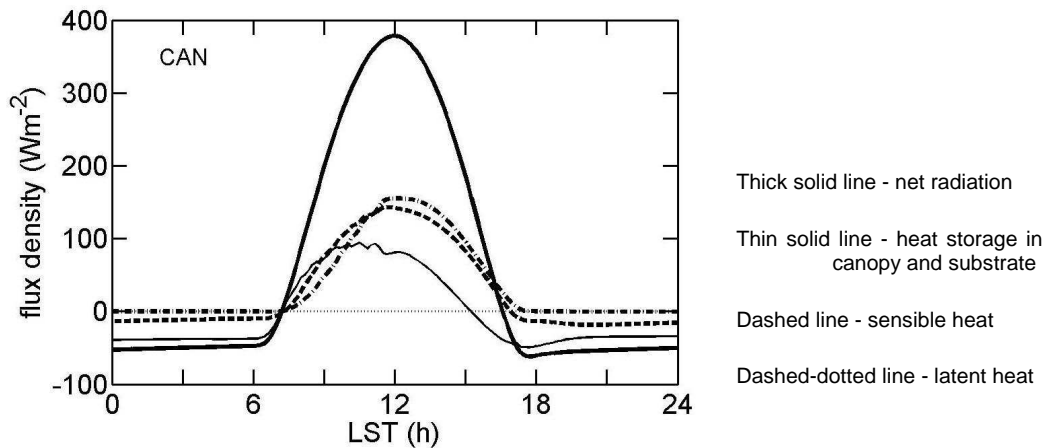


Figure 2-2: Model output results for the energy balance components of a forest canopy over the course of a day (illustration taken from Harman, 2007). LST here stands for Local Standard Time.

2.3.1 Net radiation

The net radiation R_n in Equation 2-9 is the result of radiation balance between shortwave and longwave radiation at or near the surface, which can be written as (Pal Arya, 2001):

Equation 2-10

$$R_n = R_{S\downarrow} + R_{S\uparrow} + R_{L\downarrow} + R_{L\uparrow}$$

Where $R_{S\downarrow}$ is the shortwave radiation downwards, $R_{S\uparrow}$ is the shortwave radiation upwards, $R_{L\downarrow}$ is the longwave radiation downwards and $R_{L\uparrow}$ is the longwave radiation upwards.

Shortwave radiation is also referred to as solar radiation since the ultimate source of all shortwave radiation received at or near the earth's surface is the sun. A large part of it comes directly from the sun and other parts come from radiation reflected and scattered from atmospheric compounds. The shortwave radiation at the top of the atmosphere can be determined with astronomical formulas from the day of year and latitude, but this amount is normally considerably reduced by passing through the atmosphere until it hits the earth's surface, thus making it dependent on weather variables. Also the amount of radiation coming in as reflected and scattered radiation from atmospheric compounds is, of course, dependent on weather variables. Some of the downwards radiation (also called incoming or incident radiation) is reflected by the surface, depending solely on the surface albedo.

The difference between the incoming and outgoing shortwave radiation is the net shortwave radiation, which on a diurnal scale is normally positive. A schematic overview of the global relative sizes of the shortwave radiation balance compounds can be seen in Figure 2-3(a).

Longwave radiation is also referred to as thermal radiation and it depends on the emitting body's temperature (see Stefan-Boltzmann Law Equation 2-5); outgoing longwave radiation from the earth thus depends on its surface temperature. Incoming longwave radiation comes primarily from clouds, but all gasses and aerosols in the atmosphere absorb and radiate energy each at its distinctive wavelength and thus the downwards longwave radiation is rather complicated to compute even given reliable measurements of atmospheric variables, and it is preferred to measure $R_{L\downarrow}$ directly.

The difference between the incoming and outgoing longwave radiation is the net longwave radiation, which on a diurnal scale it is normally negative. A schematic overview of the global relative sizes of the longwave radiation balance compounds can be seen in Figure 2-3(b).

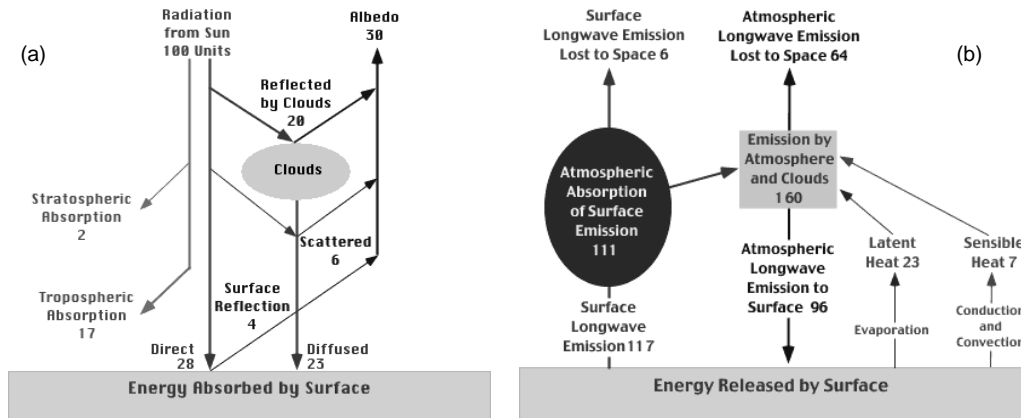


Figure 2-3: (a) shortwave radiation balance (b) longwave radiation balance (illustration taken from Pidwirny, 2006).

2.3.2 Surface Temperature

The temperature of the surface is given by the surface energy balance, thus depending on the radiation balance, atmospheric exchange processes, plant cover and thermal properties of the subsurface (normally soil) (Pal Arya, 2001). Surface temperature is quite difficult to measure directly and therefore often rather determined by extrapolation of measured temperatures in the above near-surface air and underlying soil. Another very common method is through remote sensors, see details in Section 2.6.5; in remote sensing it is common to distinguish between surface temperatures of land and sea, therefore surface temperature will in the following be referred to as LST – Land Surface Temperature.

On clear days the highest LST is typically reached an hour or two after midday, while the lowest LST is reached in the early morning hours. The maximum diurnal range is found at a relatively dry and bare surface, which in summer under clear skies and calm winds can reach 30-50 °C. The presence of moisture and vegetation greatly moderates the diurnal ranges of LST, due to increased G and ET.

2.3.3 Soil heat flux

Soil temperatures are affected by the same factors as the LST (Pal Arya, 2001), and may increase, decrease or vary nonmonotonically with depth, depending on the time of year and time of day. Diurnal variations in temperature normally do not penetrate deeper than about one meter, while annual variations penetrate to around 10 meters depth. The soil temperature and heat transfer through the soil depend on the soil's thermal properties, which include mass density, specific heat, heat capacity, thermal conductivity and thermal diffusivity.

2.4 Transpiration

Transpiration is the evaporation of water from the vascular systems of plants into the atmosphere, involving (Dingman, 2002):

1. absorption of soil water by plant roots,

2. translocation in liquid form through the vascular system of the roots, stem and branches to the leaves,
3. translocation through the vascular system of the leaf to the walls of the stomatal cavities where evaporation takes place,
4. movement of water vapor from these cavities through the openings in leaf surface called stomata to the ambient air.

These processes are reviewed in more detail in the following, though not strictly in the same order and categorization as above.

2.4.1 Stomata and cohesion-tension

Stomata are very small pores in the epidermal tissue of plant leaves, which permit gas exchange between the outside environment and the leaf's interior (Graham et al, 2006). Plants need CO_2 for photosynthesis, and CO_2 can enter the plant only when dissolved in water. Therefore plants must maintain these moist cavities permitting them to take up CO_2 from the atmosphere at the price of losing water vapor to the atmosphere. Air in the stomatal cavities is saturated at the temperature of the leaf, and water vapor moves from the cavities to the air due to vapor pressure differences. An illustration of leaf stomata is found in Figure 2-4.

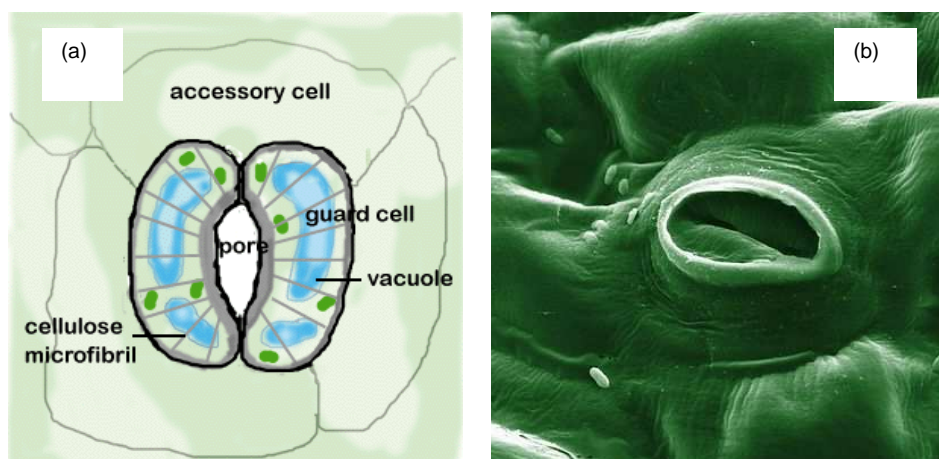


Figure 2-4: Two views of a plant stoma: (a) functional sketch (illustration taken from Cocks, 2008); (b) scanning electron microscope image of a tomato leaf (photograph taken from Howard, 2008).

Plants can control the rate of transpiration through the opening and closing of their stomata. Because CO_2 is needed when sunlight is available, most plants open their stomata during day and close them during night. Plants actively accumulate ions in the guard cells around the stomata under the influence of daylight, thus causing movement of water into the cells due to osmosis, which creates a turgor pressure that causes the cells to bend and create an opening into the stomatal cavity. At night, the reverse process closes the stomata.

Other factors can also influence trees' regulation of stomata. Water stress can entail the production of a plant hormone, which causes solutes to move out of the guard cells, thus causing loss of turgor pressure and closing of the stomata. In hot climates an increase in respiration rate around midday causes an increase in the concentration of CO_2 in the plant tissue, thus permitting plants to close their stomata and avoid water loss while maintaining photosynthesis using the excess CO_2 .

Water transport from the roots to the leaves is driven by potential energy gradients; evaporation from within the stomatal cavities causes a chain of tension (water deficit) through the different cell types where water is drawn by osmosis – the cohesion of water is so great that it can support this process even in tall trees. This is called the cohesion-tension theory and has been widely accepted until recently; a newer theory suggesting that living vascular tissue provides a tissue pressure in addition to the pulling force has challenged this and debate is ongoing.

2.4.2 Xylem and sapwood

The plant tissues that are responsible for most of the transport of fluids in plants are called xylem and phloem. Xylem conducts water and dissolved minerals, and is defined by the presence of lignin on walls of specialized water conducting cells called tracheids and vessel elements. Phloem conducts dissolved sugars and other photosynthates. Xylem and phloem are called vascular tissues and their presence is the condition for a plant to be considered a vascular plant (a group most land plants belong to). Vascular plants have stems, which enable them to increase their height, mass and surface; the vascular systems of plants also contribute to structural support.

Xylem and phloem are present in all tree organs- roots, stems and leaves. The fluid transported both in xylem and phloem is called sap. Stem xylem's main function is to transport water and minerals to other organs; in spring time it can also transport sugary solution converted from starch stored in the stem upward to supply the need of flower and leaf bud growth (maple syrup is produced from maple tree xylem sap).

Woody plants produce wood tissue by the action of vascular cambium, which is a localized region of cell division that increases plant girth. The girth increase of a tree trunk is known as secondary growth, while primary growth is a process that increases a plant's height or length. The mature vascular cambium is cylindrical, and produces secondary xylem to the inside, known as wood, and secondary phloem to the outside, which makes up the inner bark. Outer bark is produced by the cork cambium to protect the stem from pathogens and other damage.

During each growing season the vascular cambium produces new cylinders of secondary xylem adding to the stem's accumulation of wood and forming growth rings. Xylem produced in previous years may remain functional in water transport, but much of the older wood becomes nonfunctional due to clogging. The innermost and inactive wood is called heartwood while the outer and active xylem is called sapwood; heartwood is normally darker than sapwood and has a higher density. A typical cross section of a tree trunk can be seen in Figure 2-5.

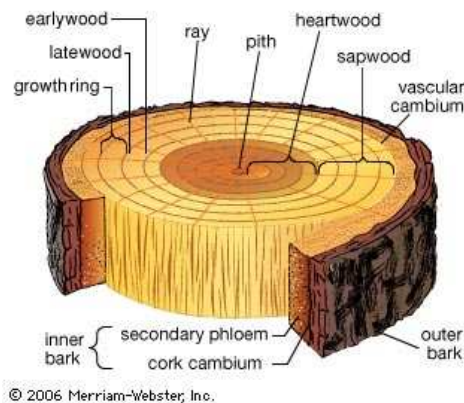


Figure 2-5: Cross section of a typical tree trunk (illustration taken from Britannica Online, 2008).

2.4.3 Roots

Roots of vascular plants normally lie below the surface of the soil and serve two main functions: absorbing water and inorganic nutrients and anchoring the plant body to the ground (Graham et al, 2006). There are many different types of roots and root systems, the two main ones being taproot system, where the primary root is dominant – pointing downwards and usually allowing for deeper roots reaching low groundwater tables; and diffuse root system where all roots are fibrous and branch in all directions.

In general, roots only grow where the physical and chemical environment is correct; they do not seek water, they grow where moisture is available (McDaniel, 1997). Nearly 99% of all tree's root mass is located in the upper ~1 m of the soil. Roots require sugar (which is transported to them through the phloem) and oxygen (which must be present in the soil) in order to perform active mineral uptake from the soil; the byproduct of this process is CO₂ which causes weathering of the subsurface soils and rocks (Graham et al, 2006).

2.5 Tropical forests

Moist deciduous and semi-evergreen seasonal forests are a type of tropical (moist) forests; they receive high overall rainfall with a warm summer wet season and a cooler winter dry season (Wikipedia contributors, 2008). They should not be confused with tropical rainforests which is another type of tropical forest differing by a higher annual rainfall, completely evergreen vegetation and (almost) no seasonality. Some trees in the semi-evergreen seasonal forest drop some or all of their leaves during the winter dry season. This is the predominant type of vegetation in the Yucatan Peninsula (see Section 1.3.4); the extent of tropical forests on earth is illustrated in Figure 2-6(a).

Tropical forests differ from temperate and boreal forests in several ways (Graham et al, 2006). They are layered, i.e. there are tall, medium and short trees where in temperate and boreal forests trees usually have about the same height (see schematic illustration in Figure 2-6(b)). Tropical forests are richer in tree species, and there is rarely one or few dominating species but rather up to 300 species per hectare (in comparison to at most 30 species per hectare in the richest temperate forest). In addition to trees tropical forests contain other species which are rarely found in temperate forests: giant herbs (such as ferns, palms and bamboos), epiphytes (plants that grow on surfaces of other plants such as orchids and bromeliads) and lianas (woody vines which grow on other tree trunks but root into the ground). Tropical forests have higher productivity than temperate forests.

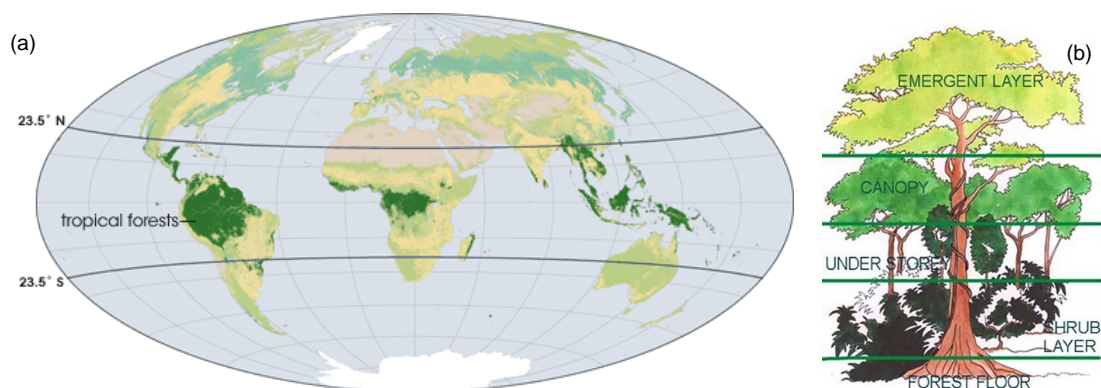


Figure 2-6: (a) map of the world marking with dark green the locations of tropical forests (illustration taken from Simon, 2007); (b) a schematic illustration of the layering in tropical forests (illustration taken from Rainforest Live, 2008).

Tropical forests often grow on relatively nutrient poor soils (Graham et al, 2006). Early farmers in the tropics learned to cope with this through the so-called slash-and-burn agriculture, where trees in a small forest area are cut down and burned, thus leaving the soil covered with nutrient rich ashes. These patches are then cultivated with multiple crops for 2-3 years until the nutrients are used up and the process is restarted at a new location.

Tropical trees typically have extensive systems of shallow feeder roots but no taproots, largely because tropical soils are thin and hard to penetrate (Graham et al, 2006). Tropical trees lacking tap roots often have buttress roots for structural support. It is, however, common that tropical storms topple tall trees, which creates small clearings in the tropical forests and is considered part of the natural regeneration pattern of the forest.

2.5.1 Water resources

In tropical forests that have a dry season it is interesting how the evergreen species get water – little is known about the different trees' water resources (Meinzer et al, 1999). Querejeta et al (2007) found that roots of trees in the seasonally dry tropical forest of Northern Yucatan were largely restricted to the upper 2 m of the soil/bedrock where the permanent water table was at a depth of 9-20 m. Their oxygen isotope data indicate that the trees use little or no groundwater and depend mostly on water stored within the upper 2-3 m of the soil/bedrock.

Meinzer et al (1999) used similar techniques (measurements of stable hydrogen isotope in xylem and soil water, soil volumetric water content and sap flow) in a seasonally dry tropical forest in Panama and could conclude that water uptake of some species was restricted to the upper 20 cm of the soil where volumetric water content dropped below 20% during the dry season, while others had access to water at depths greater than 1 m where the volumetric water content remained above 45% throughout the dry season. They found that the ability to tap progressively deeper source of soil water was related to smaller seasonal variability in leaf fall. They did not mention at which depth the groundwater table was and did not conclude anything regarding direct access to groundwater.

O'Grady et al (2006) investigated water use of tropical vegetation communities in Northern Australia using a combination of sap flow, isotopic and water-potential measurements, and concluded that all communities within the study showed some degree of groundwater use; it was, however, mainly riparian communities that used groundwater whereas the open forest communities depended principally on soil water. Drake and Franks (2003) also studied the water use of riparian seasonally dry tropical trees (in Northeastern Australia) and found that in the wet season all species were using soil water, while in the dry season some species probably used stream water and others remained dependant on soil water – none tapped directly from the groundwater.

On the other hand, Jackson et al (1999) found that several trees growing on a karst aquifer in Texas (not a tropical biome) had roots reaching below 5 m, the deepest of them reaching as deep as ~25 m. Using oxygen isotope measurements they showed that the deepest rooted trees used water from an underground stream while the shallow rooted plants used soil water. In a continuation at the same research site McElrone et al (2004) showed that these deep roots differ in xylem structure and hydraulic conductivity from their shallow counterparts, suggesting that they are specially optimized for deep water uptake. In a recent abstract Pockman et al (2008), again at the same site, report that contribution of roots 7 m below surface fluctuated with volumetric water content in the surface soil; during prolonged drought water transport in deep roots accounted for more than 60% of total daily transpiration, and occurred also during night when no transpiration was taking place – a process termed hydraulic redistribution.

2.6 Remote Sensing

Remote sensing may be defined as the science of “obtaining information about an object, area of phenomenon through the analysis of data acquired by a sensor that is not in direct contact with the target of investigation” (Ritchie and Rango, 1996 in Schultz and Engman, 2000). Remote sensors relevant to hydrology measure the electromagnetic spectrum to infer properties of landscapes or state of hydrological variables (Schultz and Engman, 2000). In the following remote sensing (RS) will refer to data acquired on board satellites (often also called earth observation, EO).

2.6.1 Satellites

Satellites used as platforms for remote sensing sensors can be polar orbiting or geostationary (with few exceptions falling between the two categories) (Schultz and Engman, 2000). Polar-orbiting satellites normally fly in a low earth orbit of some hundreds of kilometers, providing relatively high resolution measurements with repeating times of several or tens of days. Geostationary satellites orbit the earth with the earth’s rotation so that they observe the same point on earth continuously, but from a much higher altitude around 36,000 km. They provide data that is continuous in time but with a coarser spatial resolution. RS spacecrafts can also be categorized according to their main application being either earth observation, meteorological observation or oceanographic (Short, 2008).

2.6.2 Sensors

Common satellite sensors can be divided into visible and near infrared sensors, thermal infrared sensors, passive microwave sensors and active microwave sensors – also called space borne radars (Schultz and Engman, 2000). Data is acquired in “spectral bands” –finite ranges of the electromagnetic spectrum which are specific to each sensor design; narrower ranges are described as finer spectral resolution. The sensors measure radiance, which is the flux of radiant energy per unit time across an area into a cone defined by the unit solid angle.

The area the sensor covers at a single pass is called its swath, and it can vary between tens to hundreds of kilometers in width; in general, the greater the swath the lower the spatial resolution (CCRS, 2008). The radiometric resolution of a sensor refers to its sensitivity to the magnitude of received signal and is normally reflected in the number of bits used to store each pixel value. The spectral, spatial and radiometric resolutions of a sensor are conflicting by nature and sensor design implies a tradeoff between them.

Multispectral scanners (MSS) are sensors using a scanning system for acquiring data over a variety of wavelength ranges, and many of them include both thermal infrared and visible and near infrared spectra.

2.6.3 Image restoration

Image restoration (also called preprocessing) is the first step in the processing of raw RS data, and includes different systematic operations designed to compensate for data errors, noise, atmospheric scattering and geometric distortions (Sabins, 1987). The objective is to make the image resemble the original scene and is a prerequisite for using the data. The next steps in RS image processing are optional and more versatile: image enhancement (which alters the visual impact) and information extraction (such as recognition and classification).

2.6.4 Vegetation indices

A vegetation index is a numerical value, used to predict or assess vegetative characteristics such as plant leaf area, total biomass and general health of surface vegetation, derived from RS data using two or more bands within the visible and near infrared spectrum (AMS, 2008).

In general, visible and near infrared (NIR) bands are used to amplify or separate specific earth features such as vegetation or water due to their distinctive reflectance in different wavelengths (so-called spectral signature), as illustrated in Figure 2-7(a) (Williams, 2008). A way to increase the separability of different observed materials is multispectral analysis, which is based on plotting observed reflectance in different bands, as illustrated with two bands in Figure 2-7(b).

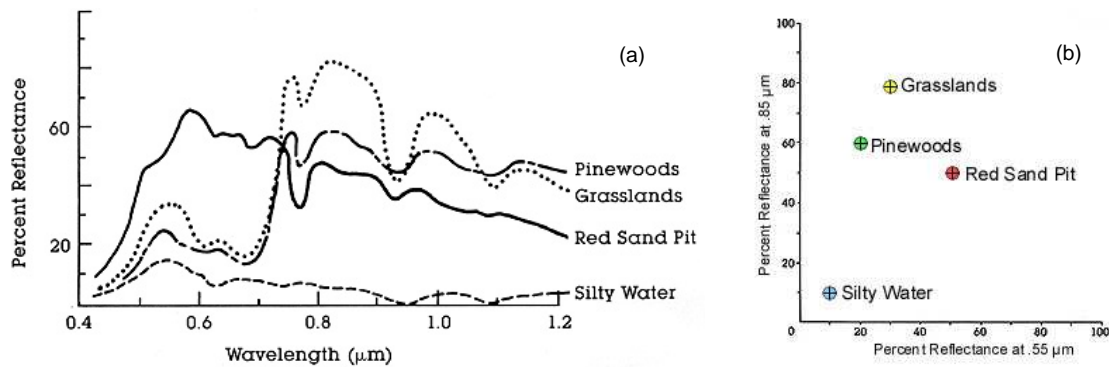


Figure 2-7: Reflectance of some common earth materials, (a) over a continuous scale of wavelengths (b) as a dual-band plot (illustration taken from Williams, 2008).

The normalized difference vegetation index NDVI, first presented by Tucker (1979), is the most commonly used vegetation index (Stisen et al, 2008), defined as:

Equation 2-11

$$NDVI = \frac{NIR - RED}{NIR + RED}$$

Where NIR stands for the measured radiance in a band in the near infrared spectrum (0.74 – 1.20 μm) and RED stands for the measured radiance in the visible red spectrum (0.63 – 0.69 μm).

RED shows a non-linear inverse relationship with green biomass as a result of strong spectral absorption of incident radiation by chlorophylls, and is thus sensitive to the presence of green or photosynthetically active vegetation (Tucker, 1979). NIR shows a non-linear direct relationship with green biomass as a result of the lack of appreciable absorption in the spectrum and a high degree of intra- and interleaf scattering in the plant canopy, and is thus enhanced over the level of radiance from the background material. The normal range of NDVI for green vegetation is 0.2 – 0.8 (ENVI User's Guide, 2007).

2.6.5 Surface temperatures

Estimates of the earth's surface temperature are derived from radiance in the thermal infrared spectrum (3-25 μm). Measured radiance at the RS sensor comes partly from radiation emitted by the earth itself and partly from the atmosphere (and some of the radiation emitted by the earth is absorbed by the atmosphere). The correlation between the earth's surface temperature and the energy it emits depends on its emissivity (see Section 2.2). Thus reliable estimates of the

surface temperature from measured radiance depend strongly on the efficiency of the atmospheric corrections applied and the accuracy of emissivity measurements (Norman et al, 1995).

Methods for atmospheric corrections of surface radiance can be categorized into two groups: direct methods (using atmospheric soundings of temperature and moisture with atmospheric radiative transfer models) and indirect methods (using only satellite data). A common indirect method is the so-called split-window algorithm, which is based on the fact that “the atmospheric attenuation suffered by the radiation emitted by the surface is proportional to the difference between the at-sensor radiances measured simultaneously in two different thermal channels” (McMillin, 1975 in Sobrino and Romaguera, 2004).

3 Methods

Actual evapotranspiration is estimated using the concept of evaporative fraction of available energy at the surface, which is explained in Section 3.1. The evaporative fraction is estimated from RS data using the triangle method, which requires NDVI and LST as input. The method and data sources used are described in Section 3.2. Estimation of the available energy at the surface is described in Section 3.3. sap flow measurements are described in Section 3.4.

3.1 The concept of evaporative fraction

The evaporative fraction EF is the ratio of latent heat exchange rate to total turbulent heat exchange at the earth's surface:

Equation 3-1

$$EF = \frac{LE}{LE + H}$$

The available energy AE is defined as the energy available for turbulent heat exchanges:

Equation 3-2

$$AE = R_n - G = LE + H$$

Combining Equation 2-2 and the two equations above, T can be calculated as:

Equation 3-3

$$ET = \frac{LE}{\rho_w \cdot \lambda_v} = \frac{EF \cdot AE}{\rho_w \cdot \lambda_v}$$

This is one of the methods used to estimate ET based on the surface energy balance with RS data; the most common one is the residual method (Jiang and Islam, 2001). All these methods require estimates of net radiation and soil heat flux, which can be achieved relatively easily and accurately. A drawback of the residual method is that the estimation of sensible heat flux includes large uncertainties when using RS data. The evaporative fraction, on the other hand, can be estimated reliably based on RS data only.

3.2 The triangle method

The so-called triangle method appears in different variations in the literature, where the common core element is that RS derived images of a vegetation index are plotted against images of a parameter related to temperature. Under the right conditions, this yields a scatter plot which resembles a triangle or a trapezoid. Based on a pixel's relative position in this scatter, a value related to water availability, such as soil moisture, is assigned to the pixel.

The first section below is a short review of the broader uses of this triangular space, and the second section focuses on use of the triangle method to estimate EF through the Priestley-Taylor parameter ϕ . The last three sections describe the data processing procedures applied to NDVI and LST data and finally the EF algorithm.

3.2.1 Review

According to Carlson (2007), the triangle concept was introduced for the first time by Price (1990). Price used AVHRR images over an area in western Nebraska, plotting NDVI against apparent surface temperature, where he discovered a triangular form, see Figure 3-1(a). He related the scatter to varying mixtures of vegetation, dry soil and wet soil in each pixel, and derived an index system where a pixel's ET was estimated as a weighted average of the expected ET from each of the three surface cover types. Thus the triangle was used as a means of scaling ET values, requiring an auxiliary model relating ET derived from classic meteorological data to remotely observed temperature data.

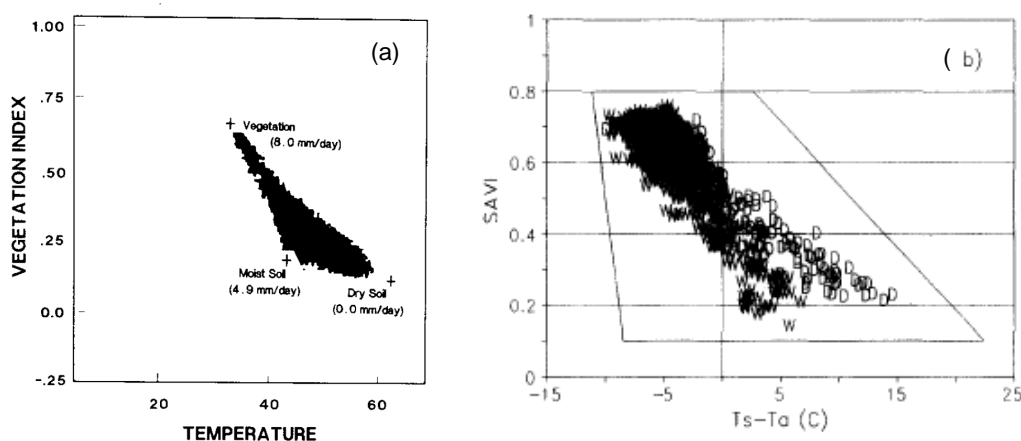


Figure 3-1: (a) Scatter plot of NDVI against LST of an area in western Nebraska on July 20, 1981 (illustration taken from Price, 1990); (b) Scatter plot of SAVI (soil-adjusted vegetation index) against the surface and air temperature difference of experimental alfalfa treatment plots over a 10 day period in summer 1985 (illustration taken from Moran et al, 1994).

In 1994, Moran et al presented the concept of a vegetation index/temperature trapezoid, which they used to derive a water deficit index (WDI), related to the ratio of actual and potential evapotranspiration. They evaluated the concept with a model and with data from an experimental field in Arizona, acquired with an aircraft carried sensor simulating Landsat TM. They plotted images of a vegetation index (SAVI, soil-adjusted vegetation index) against images of the difference between surface and air temperature and discovered a trapezoidal form, see Figure 3-1(b). The pixels are plotted with a W if they were in a well-irrigated field and with a D if they were in a dry field. The scatter thus includes pixels with a range of growing stages of alfalfa (range of vegetation cover) and a range of soil moisture (controlled by the two irrigation schemes). It is easy to note that one trapezoid edge is made up exclusively by “dry” pixels while the other is dominated by “wet” pixels. It is also obvious that the variation in temperature difference is bigger when the vegetation cover is low and smaller when the vegetation cover is high, although the dry and wet edges do not meet in a tip like they do in Figure 3-1(a). This variation at “the missing tip” demonstrates the possibility of variation in water availability and transpiration rate also within dense vegetation.

Gillies et al (1997) use the triangle concept to estimate soil water content, which, in combination with a SVAT (soil vegetation atmosphere transfer) model, can be used to compute sensible and latent heat fluxes at the surface. They emphasize that by definition, if the observations include a complete spectrum of vegetation amount and soil water content, the scatter plot will be bounded by limits of these variables: wet (cold) and dry (warm) edges and bare soil and full vegetation cover edges. Their scatters of NDVI against LST yield in one case (in Kansas) a trapezoidal form similar to the one of Moran et al (1994) and in the other case (in

Arizona) a triangular form similar to the one of Price (1990), see Figure 3-2. Both sites were dominated by low vegetation cover such as tallgrass prairie and desert grasslands, with the Kansas site also including some tree stands (about 10% of the area). In both cases the edges are quite clear, with the main difference being a larger variation in surface temperature at high NDVI values in the Kansas case, which could be related to the presence of tree stands. Gillies et al (1997) found that errors, between model derived fluxes and field observations of fluxes, were about 10-30% of the magnitude of the fluxes.

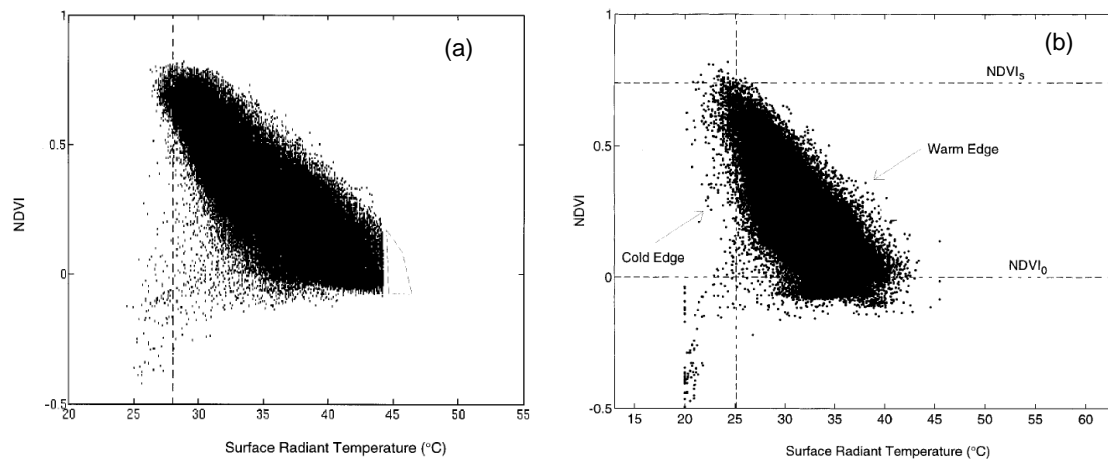


Figure 3-2: Scatter plots of NDVI against LST from two different experimental sites: (a) in Kansas, August 4, 1989, (b) in Arizona, August 9, 1990 (illustration taken from Gillies et al, 1997).

Sandholt et al (2002) develop a simplified version of the WDI by Moran et al (1994), and discuss the different possible interpretations of the so-called LST/NDVI “space”. They list five main mechanisms that determine the location of a pixel in this space:

1. Fractional vegetation cover is directly, though not necessarily linearly, related to the NDVI. It determines the integration over radiative temperature of bare soil surface fraction and of vegetation canopy fraction.
2. Evapotranspiration influences the LST through the energy balance of the surface – the less evapotranspiration, the more energy available to heating up the surface.
3. Thermal properties of the surface influence LST in the case of partly vegetated surfaces.
4. Net radiation directly affects LST, and affects plants’ transpiration rate thus indirectly affecting the partitioning of net radiation into sensible and latent heat fluxes.
5. Higher surface roughness entails more efficient mixing of the air and thus increased fluxes and lower LST. Higher NDVI normally implies higher roughness.

These factors and others are interacting and interlinked, and some may be more dominant than others depending on scale, suggesting that the different interpretations of the LST/NDVI space are not mutually exclusive (Sandholt et al, 2002).

3.2.2 The Priestley-Taylor approach

Jiang and Islam (2001) presented a method for estimating evapotranspiration using the LST/NDVI space and the Priestley-Taylor equation. The Priestley-Taylor equation can be written as:

Equation 3-4

$$LE = \phi \left[(R_n - G) \frac{\Delta}{\Delta + \gamma} \right]$$

Where ϕ is a parameter representing the effective surface resistance to evapotranspiration [-], Δ is the slope of the saturated vapor pressure curve [kPa K⁻¹] and γ is the psychrometric constant [kPa K⁻¹].

The Priestley-Taylor equation does not explicitly account for aerodynamic and physiological effects of the surface, but the advantage of using Equation 3-4 is that it is applicable to a large variety of surface conditions and pixel sizes, encompassing high heterogeneity.

Δ can be written as (Dingman, 2002):

Equation 3-5

$$\Delta \equiv \frac{de_a^*}{dT_a} = \frac{2508.3}{(T_a + 237.3)^2} \cdot \exp\left(\frac{17.3 \cdot T_a}{T_a + 237.3}\right)$$

Where T_a is the air temperature [°C].

The psychrometric constant γ is not strictly a constant but dependant on elevation; at low elevations a typical value of 0.066 kPa K⁻¹ can be used (Dingman, 2002).

$(\Delta+\gamma)/\Delta$ shows very small sensitivity to T_a (Jiang and Islam, 2001).

Combining Equation 3-4 with Equation 3-3 yields:

Equation 3-6

$$EF = \phi \left[\frac{\Delta}{\Delta + \gamma} \right]$$

Since EF can take values between zero and one, ϕ can take values between zero (corresponding to no evaporation, H=AE) and $(\Delta+\gamma)/\Delta$ (corresponding to full evaporation, LE=AE and H=0). Jiang and Islam (2001) assume that in RS images over very large areas, pixels with extreme EF (very high and very low evaporation) will be easily identified, and can be assigned limiting values of ϕ . Consequently, all other pixels need to be assigned intermediate values of ϕ according to their relative position in the LST/NDVI scatter plot. This procedure is explained in detail below.

Jiang and Islam (2001) assume that pixels with NDVI>0 can be divided into land surface types according to their NDVI value, ranging from bare soil to dense vegetation. Within each type of land surface the surface temperature ranges from a minimum (corresponding to a strong evaporative cooling) to a maximum (corresponding to a weak evaporative cooling). Thus the dry (warm) edge of the triangle is the lower bound of evaporation for different vegetation classes and the wet (cold) edge is the upper bound.

To determine the ϕ value of each pixel Jiang and Islam (2001) suggest a two-step linear interpolation scheme. The first step is to determine ϕ values at the edges: all pixels along the wet (cold) edge are assigned the ϕ_{\max} value (refer to the blue line in Figure 3-3), and pixels along the dry (warm) edge are assigned a value between ϕ_{\min} and ϕ_{\max} , linearly interpolated between the triangle corners (refer to the red line in Figure 3-3). In the second step, pixels within each NDVI class are assigned a value between the classes's maximum and minimum ϕ , which again is done as a linear interpolation (along the green line in Figure 3-3).

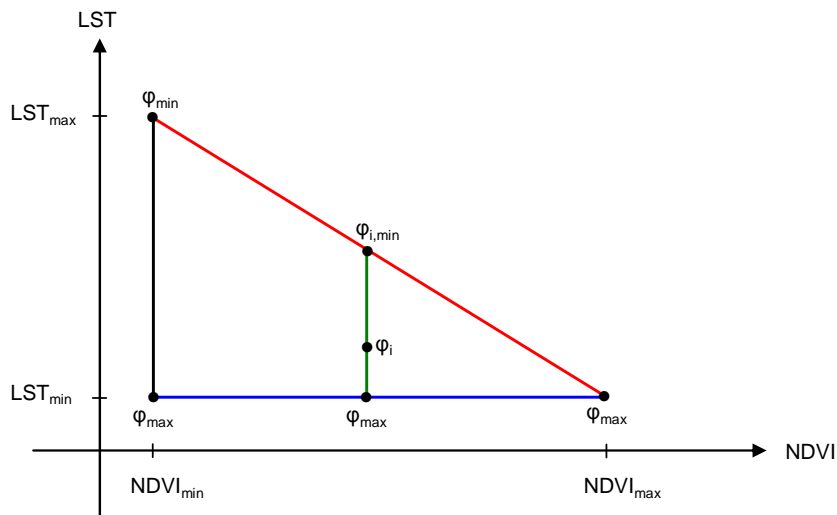


Figure 3-3: Illustration of the interpretation of ϕ values from the model triangle, adapted from Jiang and Islam (2001) and Stisen et al (2008). Note that the axes have been switched compared with previous figures.

Jiang and Islam (2001) applied this method to AVHRR images of the southern Great Plains (SGP) region in the US on six clear-sky days in the spring and summer of 1997. They compared their resulting estimates of LE with observations from several flux towers (both Bowen ratio and eddy correlation type) scattered in the region. They consider the bias (9.0 W m^{-2}) and correlation coefficient (0.80) to be acceptable and significantly better than those obtained with the original Priestley-Taylor approach (with a constant $\phi=1.26$). It should be kept in mind that the comparison between a derived pixel value and a flux tower observation is not straightforward since they represent different scales and there are also errors in the flux tower observations. Jiang and Islam (2001) also show that, when using their triangle method to estimate only EF and then combine it with ground observations of AE, the results' accuracy improves substantially.

Jiang and Islam (2001) note that their method produces instantaneous evaporation maps, but suggest that it can be extended to obtain daytime average evaporation. They cite Bastiaanssen et al (1999) for suggesting that EF is temporally constant and the difference between EF at satellite overpass time and EF derived from daily integrated energy balance is marginal and can be neglected on the regional scale. On the other hand, in case of topographic heterogeneity the method should be modified.

A major assumption necessary for the method is that variation in available energy is small, because the interpretation of the triangle assumes that the difference in surface temperature is primarily due to difference in evaporation rate for a given net radiation. Jiang and Islam (2001) suggest in case of heterogeneous R_n to normalize the surface temperature according to R_n .

Similarly, the effect of other atmospheric conditions could be minimized by using a normalized form of LST and NDVI, but the atmospheric forcings over the study area should be relatively uniform.

Wang et al (2006) proposed an improvement to the triangle method of Jiang and Islam (2001) by replacing the daytime LST with a difference between nighttime and daytime LST (Δ LST). They argue that the triangle method's principle lies in that the temperature change of a surface that evaporates is smaller than of a dry surface. Thus the use of a single temperature value relies on the implicit assumption that the surface temperature at night is uniform across the study region. They prove that this is not the case in nighttime LST MODIS images over the SGP, and that using Δ LST improves the accuracy of LE results over using only daytime LST (compared with ground observations).

Stisen et al (2008) proposed a further improvement to the temperature axis, replacing the day-night Δ LST with the gradient of morning rise in temperature (between 1.5 and 5.5 hours after sunrise). This is achieved using meteorological satellite data (MSG-SEVIRI) with a temporal resolution of 15 min. One of the advantages of this approach is that it decreases error and noise problems related to the LST values by fitting a gradient through up to 17 single values. This also means that fewer days are discarded due to cloud cover since a gradient can be fitted also when some of points in this time window are missing.

Stisen et al (2008) also suggest a slight modification to the interpolation scheme of Jiang and Islam (2001), where ϕ values along the dry (warm) edge are decomposed in a non-linear way:

Equation 3-7

$$\phi_{i,\min} = \phi_{\max} \left[\frac{NDVI_i - NDVI_{\min}}{NDVI_{\max} - NDVI_{\min}} \right]^2$$

Stisen et al argued that theoretically the relationship cannot be linear but admitted that the true relationship is unknown and the above equation is somewhat arbitrary. The interpolation for pixels between the dry (warm) and wet (cold) edges is still done linearly. They apply the method on 23 clear-sky days over the Senegal River Basin in 2005 and compare accuracy of LE results to LE results using the original Jiang and Islam (2001) method against field measurements from a single site using the flux profile method. Given that they only had one field site using a less accurate method and their pixel resolution is about 4 km², it was difficult to make any general conclusions, but the non-linear decomposition did result in EF estimates closer to the ground observations than the linear decomposition.

3.2.3 NDVI

NDVI images of the Yucatan Peninsula were obtained from MODIS for the period January 1, 2007 to April 22, 2008 through the EOS Data Gateway. MODIS is a RS sensor carried on board two satellites, Terra and Aqua, traveling on a sun-synchronous near-polar orbit (NASA, 2008). It has 36 spectral bands ranging in wavelength from 0.4 μ m to 14.4 μ m with a varying spatial resolution between 250 m and 1 km. Six different vegetation indices products are available, of which it was chosen to work with the 1 km resolution 16-days composite version 5, coded MOD13A2 (LPDAAC, 2008). NDVI is calculated from the red (centered at 645 nm) and near-infrared (centered at 858 nm) reflectance and has been atmospherically corrected and masked for water, clouds, heavy aerosols, and cloud shadows. Data is provided in tiles, each covering about 10 by 10 degrees lat/long in the Sinusoidal projection, in the HDF file format.

To cover the Yucatan Peninsula two tiles were necessary (h09v06 and h09v07). Using the MODIS Reprojecting Tool (MRT), the tiles were mosaiced, reprojected to UTM zone 16 datum WGS86, and a spatial subset defined by 80000-530000E / 196000-240000N was extracted and saved in the GeoTIFF file format. These files were read using ENVI+IDL, the scaling factor of 0.001 was applied, a value of -99 given to invalid pixels, and statistics for the year 2007 extracted. The IDL script can be seen in Appendix A (electronic).

3.2.4 Δ LST

Difference in day-night surface temperature was extracted from MODIS LST product with 1 km spatial resolution version 5, coded MOD11A1, also retrieved through the EOS Data Gateway. MODIS LST is produced with the generalized split-window LST algorithm using multi-band data including other MODIS data products (such as geolocation, cloudmasking, atmospheric temperature and land cover) and is view-angle dependent, yielding at optimal conditions an accuracy of 1 K (Wan, 2006). As with MODIS NDVI data, the two tiles necessary to cover the Yucatan Peninsula were mosaiced, reprojected and spatially subset using the MRT. Using ENVI+IDL, the scaling factor of 0.02 and the invalid code -99 were applied, and if the portion of valid pixels in both night and day image was higher than 10% an image of the temperature difference was saved with the percent of valid pixels in the file name. The IDL script can be seen in Appendix A (electronic).

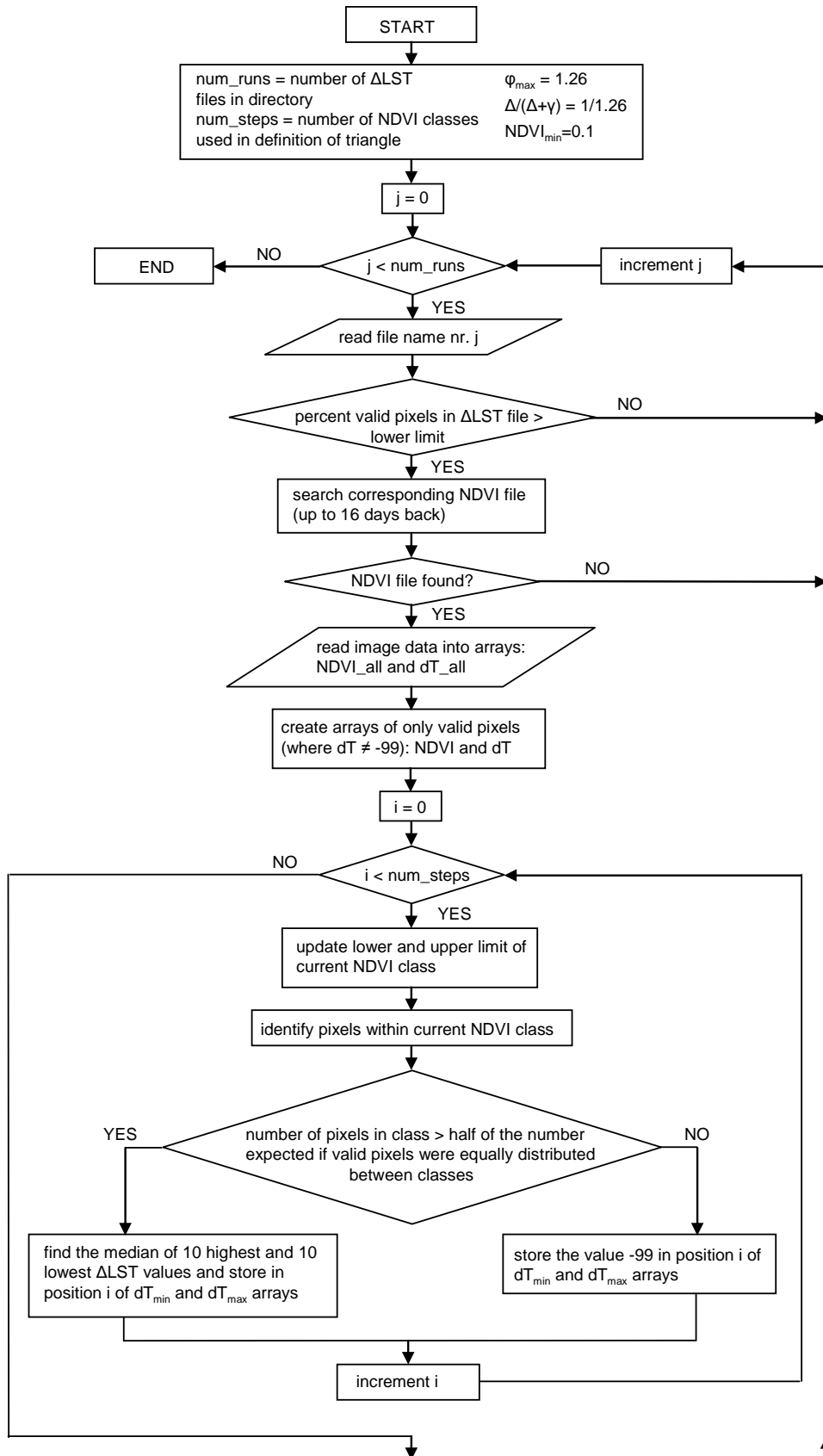
3.2.5 Evaporative fraction algorithm

The algorithm used to derive maps of EF from NDVI and Δ LST follows the triangle method with Priestley-Taylor approach as introduced by Jiang and Islam (2001), with the temperature axis replaced by the day-night temperature difference as introduced by Wang et al (2006) and the decomposition of values along the dry (warm) edge done non-linearly as suggested by Stisen et al (2008). The algorithm was written in IDL utilizing ENVI procedures and the script can be seen in Appendix A (electronic). Main steps in the algorithm are described schematically in the flowchart in Figure 3-4. The script processes a batch of Δ LST images by running a loop through all relevant file names found in a given directory. Five stages in the processing of each image can be defined:

1. Data reading: data from the current Δ LST image and the corresponding 16-day NDVI image are read into data arrays, and smaller data arrays containing only values for valid Δ LST pixels are created to ease the calculation load.
2. Triangle definition: minimum and maximum Δ LST values for each NDVI class are found as the median of the 10 lowest and 10 highest Δ LST values, and the dry (warm) edge line (DEL) and the wet (cold) edge line (WEL) are defined according to these values.
3. Quality check: three conditions must be fulfilled before EF values are calculated:
 - a. The number of NDVI classes used to define the DEL must higher than a given limit, which is arbitrarily set to 20 out of 40 possible (otherwise the triangle is defined based on too thin evidence and does not truly reflect the shape of the scatter).
 - b. The slope of the DEL must be negative (despite the above condition, some WELs have positive slopes, which is not acceptable).

- c. The WEL (the mean of the median of the lowest 10 Δ LST values for each NDVI class) must be positive (if it is negative it means there is a substantial amount of Δ LST values smaller than zero, which means there was a significant part of the pixels where night temperature was higher than day temperature – this implies that there must have been a swift change in weather conditions, which violates one of method’s assumptions - that changes in surface temperature are mainly due to partitioning of surface energy fluxes).
4. EF calculation: minimum ϕ values are assigned to each pixel according to its normalized NDVI value using a non-linear decomposition between overall minimum ϕ and overall maximum ϕ , ϕ values are assigned according to position in the triangle using linear interpolation between the pixel’s minimum ϕ and the overall maximum ϕ , and EF values are calculated by multiplying ϕ with $\Delta /(\Delta+\gamma)$.
5. Data writing: EF image file is created and statistic objects and files are updated.

Note that for simplicity, ϕ was set to have maximum and minimum of 1.26 and zero, respectively, and $\Delta /(\Delta+\gamma)$ was set to be equal (1/1.26). A more precise estimate of $\Delta /(\Delta+\gamma)$ would require data for air temperature; this could be derived from the surface temperature. EF values outside the range zero-to-one were considered invalid and changed to -99. This applies to few outliers.



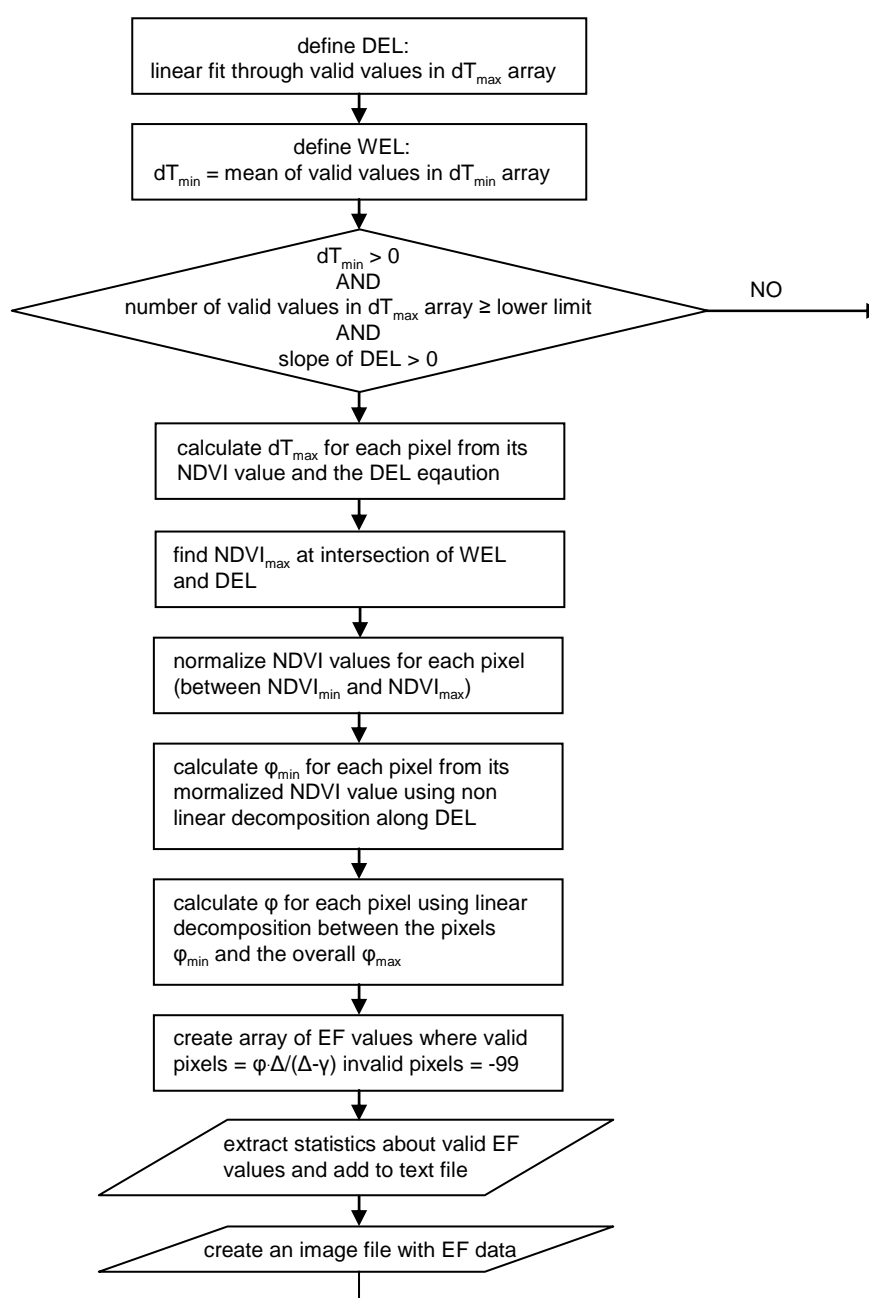


Figure 3-4: Flow chart describing main functions carried out in the EF algorithm. The complete script can be seen in Appendix A (electronic).

3.3 Available energy

Available energy for partitioning between sensible and latent heat fluxes was estimated as the difference between net radiation and soil heat flux on a 12-hour basis (from 06:00 to 18:00 local time, where it is assumed that EF is relatively constant). Net radiation was calculated from ECMWF data, as described below in Section 3.3.1. Soil heat flux was estimated as a fraction of net radiation dependant on NDVI, as described in Section 3.3.2.

3.3.1 Net radiation

The European Center for Medium-Range Weather Forecast (ECMWF) keeps a record of all operational datasets, including surface analysis (where ground observations are interpolated into grid data) and forecast (where state variables are calculated using the surface analysis data and a simulation model). Unfortunately, short and longwave incoming and outgoing radiation are not featured in the surface analysis records, but only in the forecast records. Due to time limitations and the uncertainty related to estimation of compounds of net radiation based on available parameters, it was considered reasonable to use this forecast dataset.

Net radiation was thus calculated as the sum of net shortwave radiation (Surface Solar Radiation, SSR, ECMWF parameter number 177) and net longwave radiation (Surface Thermal Radiation, STR, ECMWF parameter number 176), both parameters obtained from the ECMWF forecast archive through DMI (Danish Meteorological Institute). The data was delivered in the GRIB file format, which was decoded using a supplementary package of IDL programs available on ITT's infoNET. There were two files per day, each file containing data for 3, 6, 9, and 12 hours after forecast start (at midday and midnight) of accumulated short and longwave net radiation. Data had global coverage in lat/long equidistant cylindrical projection with grid size of 0.25 degrees. The 12 hours accumulated values were read into an IDL array, added, and divided with a time factor transforming them into equivalent average daily radiation. A spatial subset corresponding to an area somewhat larger than the Yucatan peninsula was extracted, and saved as an image file in the original projection. This image was then reprojected into UTM zone 16 WGS86, resampled to 1 km resolution, and a final spatial subset defined by 80000-530000E / 196000-240000N was extracted and saved as a new image file (corresponding to the same image size and location as NDVI and Δ LST files). The script can be seen in Appendix A (electronic).

3.3.2 Soil heat flux

Energy conduction to the soil can roughly be assumed to equal zero on a 24-hours basis (Kustas and Daughtry, 1990), but since it was decided to look at available energy for daytime hours 06:00-18:00), such an assumption would have caused overestimation of available energy at the surface. Instead, it is assumed that the ratio G/R_n is relatively constant over daytime hours, but dependant on the amount of vegetation cover on the soil. Kustas et al (1993) investigated the use of different vegetation indices for predicting midday G/R_n , and found that, although theoretically, a non-linear relationship between G/R_n and NDVI was expected, the best fit to data was obtained with the following equation:

Equation 3-8

$$\frac{G}{R_n} = 0.40 - 0.33 \cdot NDVI$$

Jacobsen and Hansen (1999) confirmed that a linear model was the best to fit their data from an arctic environment, though they found slightly different coefficients. Santanello and Friedl (2003) examined the G/R_n diurnal behavior, and claim that it can be highly variable, suggesting a method to predict it on hourly timescale. However, their model has high data requirements (input includes soil type and moisture), making it too complex for the task at hand. It seems that high values and large variations of G/R_n are expected at surfaces with sparse vegetation cover. Thus considering the dense vegetation on the Yucatan Peninsula the ratio and variations can be assumed to be less significant and the above equation a reasonable estimate. The script used can be seen in Appendix A (electronic).

3.4 Sap Flow measurements

Sap flow was measured using the heat dissipation method in order to estimate stand transpiration. In the following is a description of the heat dissipation method for measuring sap flux density, methods for measuring sapwood depth and estimating sapwood area and methods for scaling up from tree to stand transpiration. It is also mentioned which equipment was used and which sampling strategies were followed.

3.4.1 The heat dissipation method

The heat dissipation method was first presented by Granier in 1985 (Granier, 1987). The original apparatus consisted of two cylindrical probes of 2 mm diameter which were inserted 20 mm into the sapwood of the tree trunk, one above the other about 10 cm apart. The upper probe contained a heating element of constantan which was heated at a constant power. Each probe contained a copper-constantan (type T) thermocouple in the middle. The temperature difference between the two probes was influenced by the sap flux density in the vicinity of the heated probe (sap flux density is defined as the sap flow per unit area). The mean sap flux density along the probe u was found by calibration with different species to be:

Equation 3-9

$$u = 0.0119 \cdot K^{1.231}$$

Where u is in cm s^{-1} and K is a dimensionless value defined as:

Equation 3-10

$$K = \frac{\Delta T_M - \Delta T}{\Delta T}$$

Where ΔT_M is the temperature difference between the two probes for no flow and ΔT is the temperature difference for positive xylem flow ($u > 0$).

Total sap flow F is calculated as:

Equation 3-11

$$F = u \cdot A_{\text{SW}}$$

Where A_{SW} is the cross-sectional area of sapwood at the heating probe.

A schematic illustration of the probes setup in the heat dissipation method can be seen in Figure 3-5.

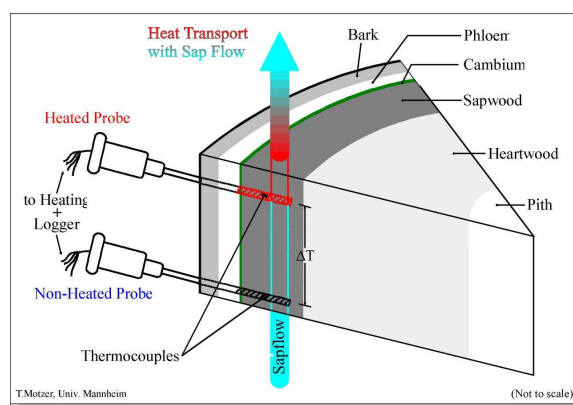


Figure 3-5: A schematic illustration of probe installation in the thermal dissipation method (illustration taken from Motzer, 2004).

Granier's heat dissipation method is one of several different methods of estimating sap flux density, which can be grouped according to two different thermal principles: the heat pulse velocity and the heat balance methods (Granier's method belonging to the second group) (Köstner et al, 1998). The main difference lies in that heat pulse velocity methods are based solely on heat transfer theory while heat balance methods require empirical calibrations. However, the Granier method requires less power, the equipment costs are lower and the installation easier (Smith and Allen, 1996).

Smith and Allen (1996) claim that Granier method should be calibrated for species on which it hasn't been previously validated. However, several studies have confirmed the comparability of Granier's method's results with other methods (e.g. Granier et al, 1996a, Köstner et al, 1998 and Gonzalez-Altozano et al, 2008).

Sap flux density

Sap flux density was measured in this project using thermal dissipation probes (TDPs) produced by Dynamax Inc, Huston USA based on the Granier design with Dynamax upgrades (Dynamax, 2008). There were 6 TDPs of type TDP50, which are 50 mm long with a diameter of 1.65 mm, containing one thermocouple type T in the middle of the probe. For more technical details as well as illustration of probe design see Appendix B (electronic). Installation and insulation of the probes was done following the Dynamax's user's guide. Selected pictures illustrating the setup can be seen in Appendix C (electronic).

Probes were connected to 6 differential channels in a datalogger type CR10X from Campbell Scientific Inc, Utah, US. In the range of voltage measured (± 2.5 mV) the nominal resolution is $0.33 \mu\text{V}$ and the accuracy $\pm 1.25 \mu\text{V}$. Further technical specifications can be seen in Appendix D (electronic). Data recording and transfer was controlled using the PC400 software from Campbell scientific, Inc. Recording intervals were changed between sites, varying from 1 minute samples to 5 minute averages. As a backup, a datalogger from the older 1200 series from Grant Instruments, Cambridgeshire, GB, was occasionally used.

Data was stored as the raw differential voltage measured and converted to temperature difference using the following polynomial approximation (NIST, 1995):

Equation 3-12

$$\Delta T = \sum_{n=0}^N a_n \cdot v^n$$

Where ΔT is the temperature difference in °C, N is the number of coefficients (in this case $N=6$), a_n is the coefficient and v is the measured differential voltage in mV. Coefficients were taken from NIST (1995) and can be seen in Appendix E.

The no flow reference temperature difference ΔT_M was estimated by subjective inspection of the nighttime ΔT values, often calculating an average of maximum values for two consecutive nights to be used for the daytime period in between (as recommended by Mikkelsen, pers.comm., 2008). The subjective element is introduced due to the high level of noise and high variability in the data collected, which made it complicated to develop a simple and robust algorithm for determination of ΔT_M (see results for each site in Section 4.6).

Granier's method assumes that the measured sap flux density is a representative mean of the sap flux density all along the sapwood depth at the heating probe. However, several studies have shown that the sap flux density varies radially, and that significant errors in estimates of sap flow can result from using the simple relation in Equation 3-11 (e.g. James et al, 2002 and Cohen et al, 2008). There seem to be two types of radial pattern: one where the highest u is near the cambium decreasing toward the heartwood and another where u is low near the cambium, increasing toward a certain depth and then decreasing toward the heartwood. Radial patterns certainly vary between species, but sometimes also between individuals of same species and over time, probably correlated with environmental conditions (e.g. water availability).

In order to fully capture the variability in u the recommendation is to use multiple probes of 10-20 mm length inserted at consecutive depths along the radius of the trunk. This was not possible with the available equipment in this project, and it is difficult to assess what degree of radial variability in sap flux density should be expected in the trees studied. Clearwater et al (1999) claim that the heat dissipation method systematically underestimated mean u when gradients in u exist, and give examples of errors in the order of magnitude 8-45%.

Another source of error arises when probes are inserted to a depth where they are partly in contact with inactive xylem in the heartwood or with bark (Clearwater et al 1999). Errors occur because the relationship between ΔT and u is not linear, and therefore mean ΔT along the probe is not a measure of mean u . If a portion of the probe is inserted into inactive xylem while the remainder of the probe is in sapwood with relatively uniform sap velocity, then it can be assumed that the measured ΔT is a weighted average of ΔT in the sapwood and ΔT in the inactive xylem (Clearwater et al 1999):

Equation 3-13

$$\Delta T = a\Delta T_{SW} + b\Delta T_M$$

Where ΔT_{SW} is the ΔT in the sapwood, ΔT_M is ΔT in the inactive xylem, and a and b are the proportions of probe in sapwood and inactive xylem, respectively ($a+b=1$).

This approach assumes that the thermal properties of the inactive xylem are the same as sapwood with no sap flow (ΔT_M value used in Equation 3-13 is the same as in Equation 3-10, i.e. the ΔT registered during nighttime). Rearranging Equation 3-13 yields the following

equation, which was used to correct sap density flux measurements in cases where the xylem was less deep than 50 mm:

Equation 3-14

$$\Delta T_{SW} = \frac{\Delta T - b\Delta T_M}{a}$$

In cases where sap wood depth was not measured, no correction to the measured temperature difference was made and the calculated sap flux density was multiplied with the length of the probe (as recommended by Granier, pers.comm., 2008).

Sap flux density also varies circumferentially around the tree trunk (e.g. James et al, 2002 and Cohen et al, 2008). James et al (2002) report that whole tree water use calculated from replicate series of probes at different positions around the trunk differed by as much as 100%, mostly due to variability of sap flux density in the outermost sapwood layers. Cohen et al (2008) found that the variability in radial distribution of sap flux density around the trunk of one tree had a coefficient of variation similar to that between trees of the same species (up to 28%). They also report that the amplitude of circumferential variation changed during the day (high in mornings and evenings and low at noon), and depended more on the structure of each individual trunk than on the position with respect to the sun.

Given the limited amount of probes available for this project it was decided to place only one probe per tree thus capturing more interspecies variation in the stand rather than finding more accurate values for each tree.

Sapwood cross-sectional area

Sapwood cross-sectional area A_{SW} is calculated from sapwood depth as follows:

Equation 3-15

$$A_{SW} = \pi \left((r_T - d_B)^2 - (r_T - d_B - d_{SW})^2 \right)$$

Where r_T is the radius of the tree trunk, d_B is the depth of the bark and d_{SW} is the depth of the sapwood (all measured at breast height).

Sapwood depth can be difficult to determine and variable over time, between species, between individuals and around the trunk circumference (Cermak and Nadezhdina, 1998). Basically, the transition from sapwood to inactive xylem is “fluid”, and the only accurate means of measuring sapwood depth is by measuring the radial variation of sap flux density as described in the previous section. This was not possible in this project.

Sapwood depth was estimated using an increment borer (also known as a Pressler drill) and natural food coloring, applying the method described by Meinzer et al (2001). A solution of food coloring in water was injected into a hole in the trunk, and 1-2 h later core sample was extracted about 1-2 cm above the injection point. Meinzer et al (2001) validated their results by measuring sap flux density at incremental depths (using specially constructed dissipation probes). This project’s results could not be validated and are estimated to be quite uncertain due to practical limitations in the field:

- The depth of coloring injection was limited by the length of the drill bits used (6-7 cm) thus limiting the depth at which coloring could be observed in the core samples.
- The hardness of the wood made it very difficult to use the increment borer, and core samples were often partly damaged in the process of extraction.
- The transport of the coloring was very uneven through the core samples and it was often difficult to judge where the coloring border was in effect.

3.4.2 Scaling from tree to stand

Using measurements of individual trees' transpiration to estimate stand transpiration (sT) requires adapting a strategy for scaling the results from water use per individual per unit time to water transpired per unit area per unit time. A main challenge is to determine which and how many trees should be sampled in order to account for the variation within the stand. Granier et al (1996a) compared results from several studies and found that coefficients of variation of among-tree variability in sap flux densities were 10-15% in temperate forests but 35-50% in tropical forests. They mention that the high variability in tropical forests is related to the high variability in species and sizes.

The best approach would be to sample all trees in a representative area as done by Köstner et al (1992), but this was not possible given the equipment limitations. An effective limit on the number of trees sampled was given by the number of available channels in the datalogger, which dictated the number of sap flow probes acquired. Thus the variability had to be captured as well as possible within this limitation, and the guidelines adapted were to look for the biggest (most dominant) trees in a limited area and choose a variety of species among those. The motivation for choosing the biggest trees comes from Köstner et al (1992), who report that 50% of sap flux density in the plot they monitored originated from 3 of 14 trees which emerged 2-5 m above the canopy. Granier et al (1996b) also found that sap flux density depended on crown status, i.e. for a given species codominant trees exhibited lower u than dominant trees. Cermak et al (2004) claim that in general, dominant trees stand for two-thirds of a stand's transpiration, medium trees for one-quarter and suppressed trees for 5-10%.

The plot (the area within which trees were sampled) was limited by the length of the cables connecting sensors to datalogger, by the accessibility through the dense vegetation and by a consideration of keeping the chosen trees within a reasonably sized plot (for the purpose of characterizing all trees within the plot). Since there were usually not many very big trees within a plot and since the dominant trees were often of the same species, a trade off between size and species was made at each site.

A popular scaling parameter when sampling dispersed trees within a plot is sapwood area, as described by Granier et al (1996b):

Equation 3-16

$$T = A_T \cdot \sum (F_i \cdot p_i)$$

Where A_T is the sapwood area per unit ground area, F_i is the mean sap flux density of trees in class i , A_i is the sapwood area of the trees in class i and $p_i = A_i/A_T$. Classes are usually defined according to diameter at breast height (DBH).

Obviously this method relies on accurate measurement of sapwood cross-sectional area in a representative sample of the plot trees, which was not possible in this project (see discussion in

previous section). Saugier et al (1997) also admit that their estimation of sT suffered from the spatial variability of sapwood cross-sectional area throughout the forest. They studied a boreal forest of a single species, thus the uncertainty is expected to be substantially higher in a species rich tropical forest. Other possible scaling parameters include stem diameter, stem basal area, and leaf area (Smith and Allen, 1996).

In their review of the sap flow method, Cermak et al (2004) also recommend dividing the stand into classes and suggest an elaborate statistical method for choosing sample trees to represent the different DBH classes. However, they also describe a much simpler scaling method based on a ratio of a readily measurable biometric parameter. They recommend its application in cases where only a small number of sample trees is available, which does not allow for calculation of a reliable regression for the DBH classes, or where the variation in sap flow between individual trees is large (due to e.g. stress). The simple ratio method was applied by e.g. Cermak et al (1995) in a sub-boreal forest in Sweden.

The simple ratio method is expected to overestimate the transpiration of trees in small DBH classes and underestimate transpiration of trees in large DBH classes. Nonetheless, given the small samples that were achievable in this project (and the lack of consistent regressions between DBH and sap flow as can be seen in Section 4.6), this method is considered a reasonable choice. The following equation is used:

Equation 3-17

$$T = \left(\frac{\sum_{i=1}^N B_i}{\sum_{i=1}^k B_i} \right) \cdot \sum_{i=1}^k F_i \cdot \frac{1}{A_{plot}}$$

Where T is transpiration rate [mm day⁻¹]; the term in parenthesis is the scaling factor, in the numerator is the sum of B_i, a biometric parameter of tree i, for N trees in the plot, and in the denominator is the sum of B_i for k trees in the sample; F_i is the daily transpiration [L day⁻¹] of sample tree i out of k sample trees; and A_{plot} is the plot area [m²]. Two different biometric parameters were used: DBH and basal area (A_B).

Plot areas used varied between sites from 100 to 800 m². Within each plot all trees with a trunk circumference at breast height above 10 cm were counted and their circumference and species noted. Species identification was done using the knowledge of local experts, usually the commissioner of communal lands from the nearest village or someone appointed by him. Species were identified by their local names (in Spanish or Maya) and wherever possible translated into Latin using a key developed by a forest engineer working for the local organization U'yo'olché (copyright by U'yo'olché A.C. 2007, permission to use granted by the director).

From stand transpiration to pixel evapotranspiration

Stand transpiration from a dense forest is expected to be the main, but not single, contributor to total evapotranspiration over the forest. Other compounds that must be accounted for are transpiration from undergrowth, evaporation from forest floor and evaporation from canopy interception. All these parameters could not be directly assessed or measured in this project. A very rough estimate of their contribution would be between 10 and 30%.

3.4.3 Site choice

Sites for sap flow measurements were chosen so that they reflect the expected extremes of pixel actual ET within the peninsula, considering only pixels covered with tropical forests. Since it was not possible to create maps of estimated actual ET before the field work, the identification of appropriate sites had to be done based on substitute indicators. The main parameters for site choice were:

- NDVI
 - It was aimed at having at least 1-2 sites of respectively relatively low and relatively high NDVI.
 - It was preferred to have a site in an area where pixels had relatively equal values of NDVI, assuming that this would increase the probability of homogeneous vegetation within the area and reduce the effects of uncertainty in georeferencing.
- Land cover type
 - It was aimed at finding sites within larger areas classified as tropical forest, assuming this would decrease the probability of some of the area within the pixel being milpa (transformed recently from forest to cultivation).
- Accessibility
 - Site had to be within short walk from a road manageable by private car, and within reach of a few hours drive from a base town.

At each site it was aimed at having at least 3-4 consecutive days of measurement in order to increase the chance of measuring on a clear-sky day and increase data reliability by showing reasonable day-night-day variations.

4 Results

This chapter starts with results obtained using RS methods (Sections 4.1-4.5), continues with results from sap flow measurements (Section 4.6) and ends with a comparison between the two (Section 4.7). RS results are presented in five steps: Sections 4.1 and 4.2 shortly analyze the NDVI and Δ LST images for 2007, Section 4.3 describes and analyses the results from using these images to calculate the evaporative fraction, Section 4.4 shortly describes the results from estimating available energy and Section 4.5 analyses the results from using the evaporative fraction results together with the available energy results to produce actual evapotranspiration. All images produced (of NDVI, Δ LST, EF, AE and aET) can be found in Appendix I (electronic) in the appropriate folders, together with Excel files where extracted statistics are treated.

4.1 NDVI

In the following is a short presentation of the temporal and spatial variation of NDVI values during 2007.

4.1.1 Temporal variation

The mean NDVI on the peninsula is quite stable and quite high all year round, as can be seen in Figure 4-1. The lowest value is 0.66, reached towards the end of April, and the highest value is 0.83, reached at the beginning of November. The slight decrease in the beginning of September which is coupled with an increase in standard deviation could be related to Hurricane Dean which hit the peninsula on August 21. The overall mean is 0.76, with a standard deviation of 0.15, corresponding to CV of 20%. These statistics include all land pixels, i.e. human settlements and inland water bodies have not been masked out.

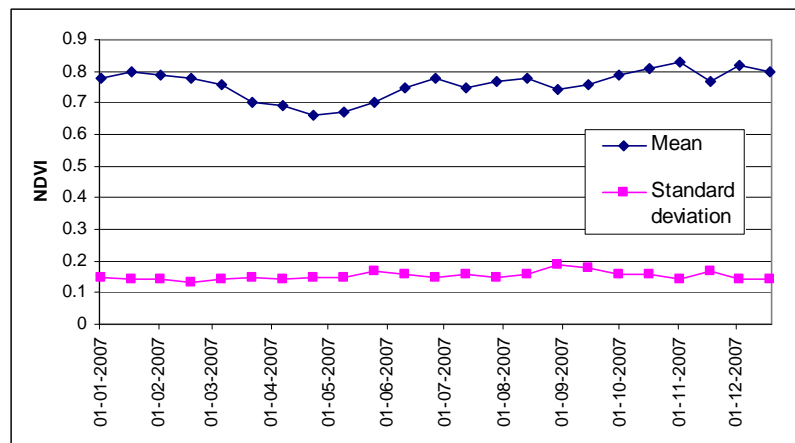


Figure 4-1: Spatial mean of 16-days NDVI values over the Yucatan Peninsula in 2007 together with standard deviation from the mean.

However, when looking specific pixels the variation over time is much larger, as expected. Figure 4-2 shows trajectories of NDVI for some selected pixels, whose approximate location is indicated in Figure 4-3. The pixel denoted with pink rectangles (X:85, Y:164) is located in the northern part of the western coast, an area that has a lower annual average NDVI than the average on the Peninsula, and the drop in NDVI in April corresponds well to the seasonal shedding of leaves in the dry season. The pixel denoted with blue diamonds (X:80, Y:161) is

from the same area and shows similar behavior but with a longer period of low NDVI, probably corresponding to a vegetation composition where more species shed their leaves in the dry season. The pixel denoted with purple crosses (X:335, Y:246) is in the wetlands of Sian Ka'an, displaying an overall significantly lower NDVI than the average on the peninsula; it is unknown what the drops in June and August are related to. The pixel denoted with orange triangles (X:238, Y:305) is in the southeastern part of the peninsula, an area that was severely affected by Hurricane Dean, which could explain the drastic drop in NDVI in September. The pixel denoted with green crosses (X:319, Y:239) is close to Felipe Carillo Puerto in a forest within the Sian Ka'an reserve, showing a high and relatively stable level of NDVI (no clear decrease in NDVI in the dry season).

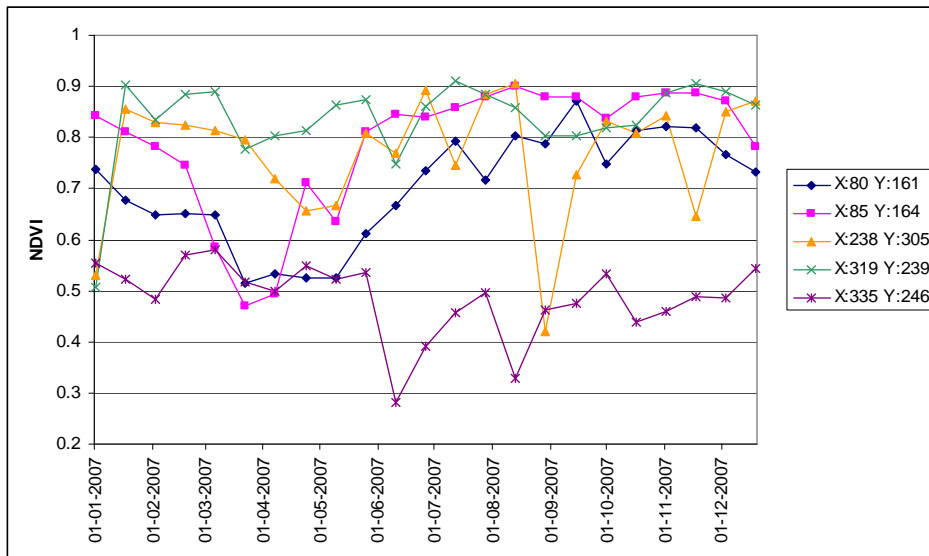


Figure 4-2: Trajectories of selected pixels' NDVI values in 2007. Pixel location is given by image sample number (X) and line number (Y), and the approximate location is indicated by white arrows in Figure 4-3.

4.1.2 Spatial variation

NDVI values in each pixel were averaged for 2007 in the image which can be seen in Figure 4-3. Four cross-sections of this image are presented in Figure 4-4: two horizontal (east-west) and two vertical (north-south), their approximate position indicated with black arrows in Figure 4-3. Both figures illustrate that NDVI values on the peninsula are generally quite high and quite constant in space. The few pixels with a yearly average below 0.6 seem to be along the coast, in wetlands and in urban areas.

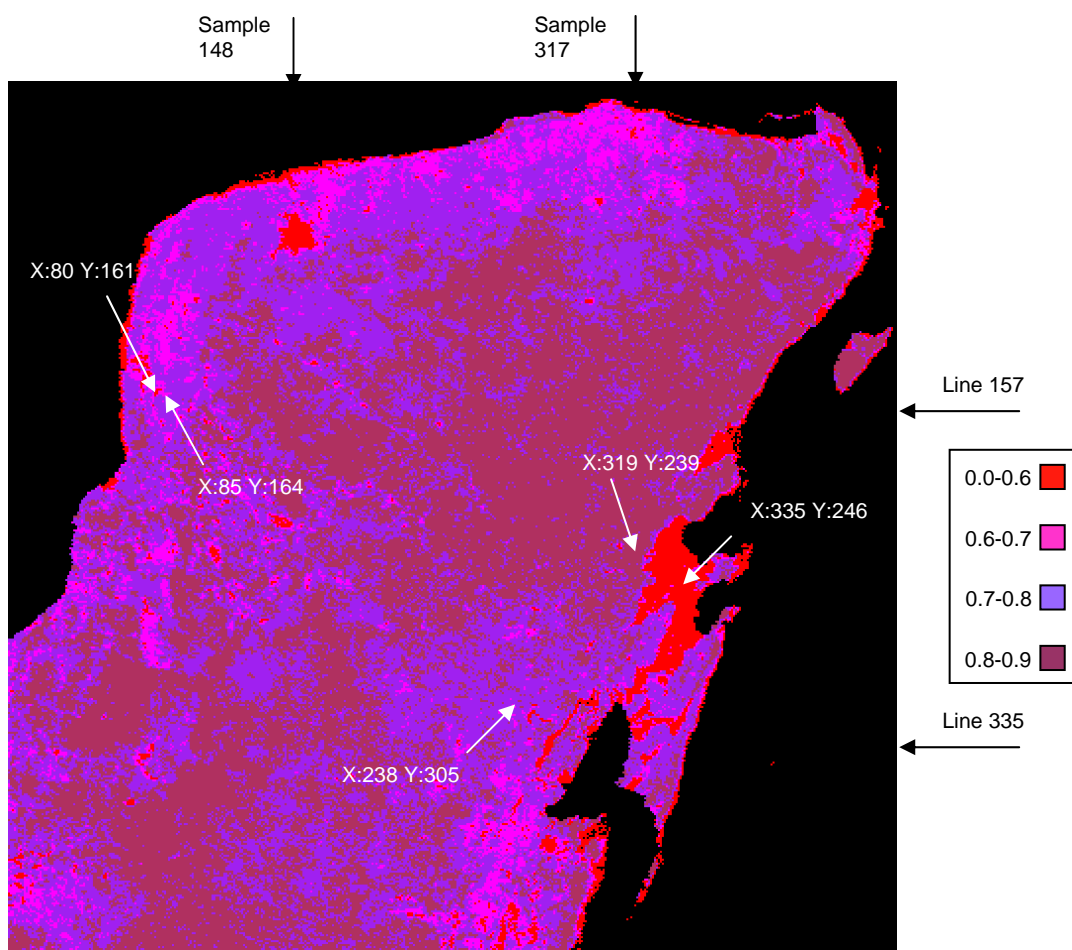
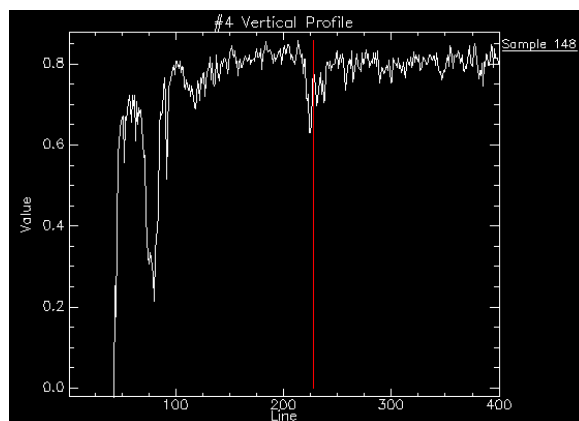
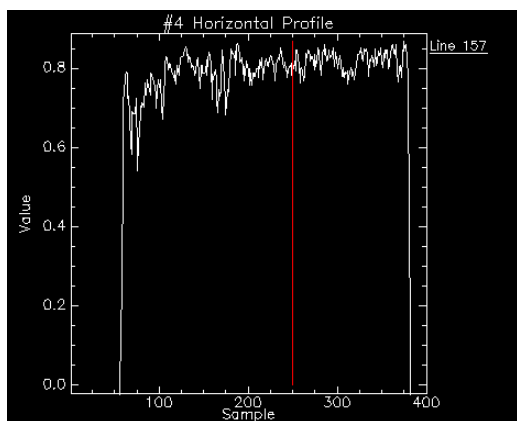


Figure 4-3: Grouped pixel average NDVI [-] values in 2007. White arrows denote the approximate location of pixels depicted in Figure 4-7 and Figure 4-11; black arrows depict the approximate location of the horizontal and vertical profiles in Figure 4-4.



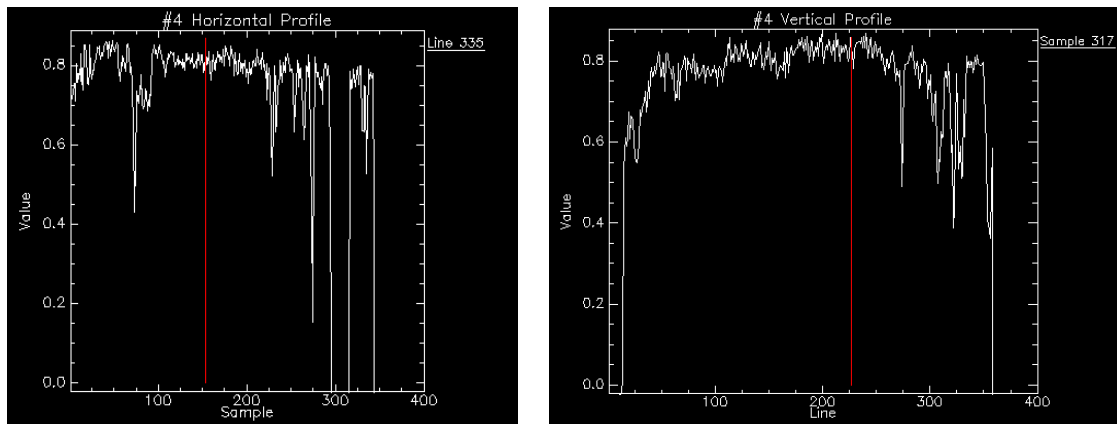


Figure 4-4: Horizontal and vertical profiles of pixel average NDVI values in 2007. Approximate locations of profiles are indicated in Figure 4-3.

4.2 LST

In 2007 there were 192 days (53% of the year) where more than 10% of the land pixels had both daytime and nighttime valid Δ LST value (invalid values occur when pixels have been masked out due to clouds or cloud shadows). Images with less than 10% valid Δ LST pixels were abandoned and are not included in the following analysis. The percent of pixels with valid day, night and both day and night values is displayed in Figure 4-5. There does not seem to be any seasonal pattern in either of the three parameters, suggesting that cloud cover is more or less equally probable at day as at night and in the rainy season as in the dry season.

The average fraction of valid Δ LST pixels per image in 2007 was 21% considering all 365 images; considering only the days which pass the 10% threshold, the average was 38%. The average of valid day pixels was 66% and the average of valid night pixels was 56% (obviously a significant part of the valid pixels are different between the corresponding day and night images). Only 54 images had more than 50% valid Δ LST pixels, and only 6 images had more than 80% valid Δ LST pixels (a single image passed the 90%).

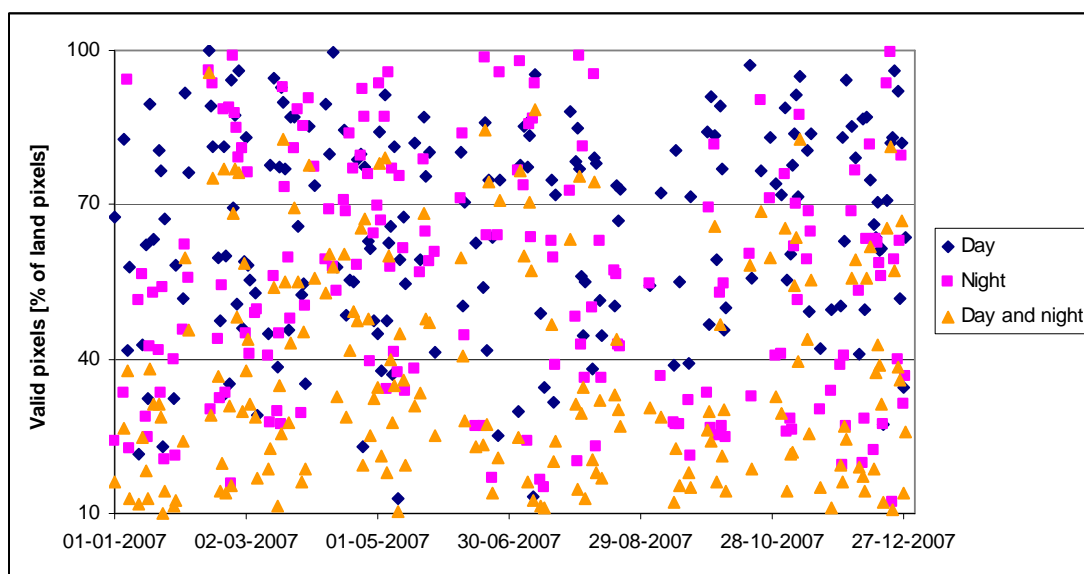


Figure 4-5: Daily percent of land pixels which had a valid day, night or day and night value in 2007 (includes only days with more than 10% pixels with valid day and night values).

The pixel Δ LST in 2007 varied from -9.8 to 36.3 °C, with a temporal and spatial mean of 7.2 °C. The temporal variation of the spatial mean can be seen in Figure 4-6, together with the standard deviation from the mean for each image (the figure includes only the images that pass the 10% threshold). Here there is a rather clear seasonal trend, with a maximum in April-May and a minimum in September-October.

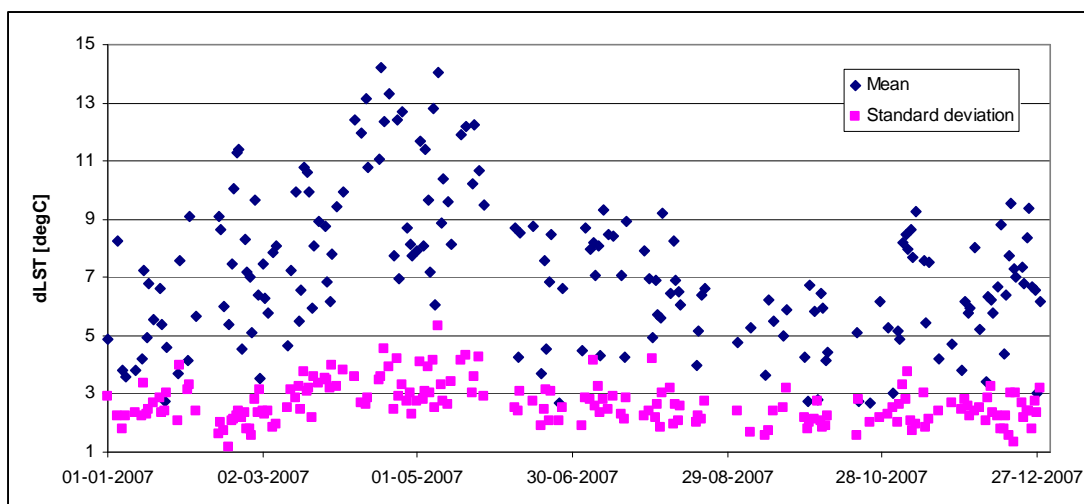


Figure 4-6: Spatial mean and standard deviation of Δ LST in 2007 (includes only days with more than 10% pixels with valid day and night values).

The seasonal pattern is not as clear when observing values for single pixels, as shown with five arbitrary pixels in Figure 4-7. The two pixels located in the northwestern part of the peninsula with the seasonally low NDVI (denoted with blue diamonds and pink rectangles) generally have the highest Δ LST values, both with a very high degree of scattering, possibly with a peak around April and lower and more stable levels in November-December. The two pixels in the southeastern part of the peninsula (denoted with orange triangles and green crosses), located in

4 Results

forests with relatively stable and high NDVI, generally have lower Δ LST values and lower degree of scattering than the former two, in general showing slightly higher values in the first half of the year than in the second half. Δ LST in the Sian Ka'an wetlands (pixel denoted with purple asterisk) is generally the lowest of these five pixels and has generally lower values in November-December than the rest of the year.

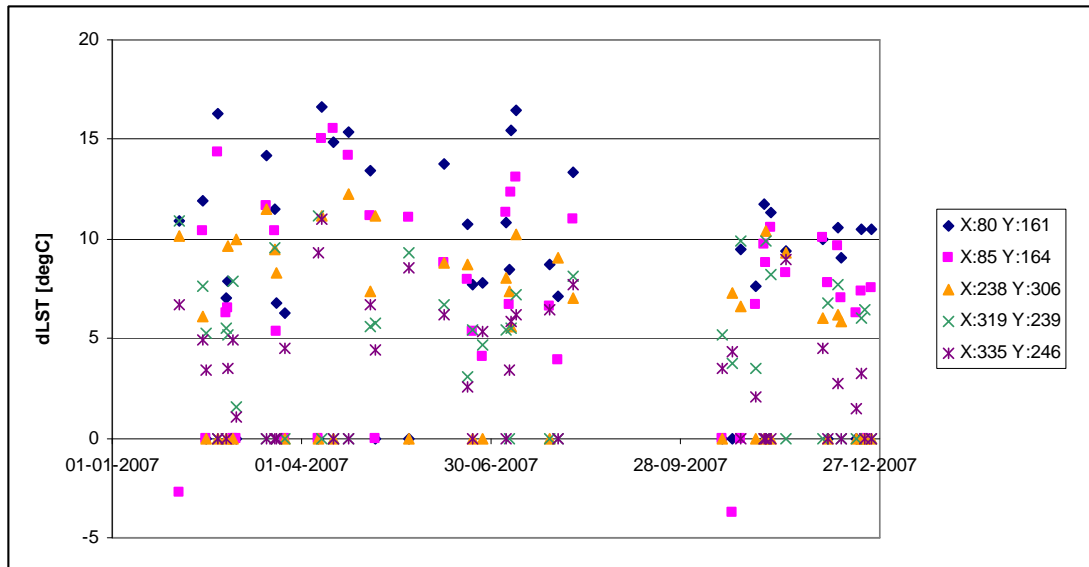


Figure 4-7: Temporal variation in Δ LST in 2007 for 5 arbitrary pixels. Pixel location is given by image sample number (X) and line number (Y), and the approximate location is indicated by white arrows in Figure 4-3. Note that values of exactly zero are actually invalid values and should be ignored.

The spatial variation on a particular day (February 13, 2007, the day with highest percentage of valid land pixel values) can be seen in Figure 4-8. Small differences between day and night surface temperatures are found along the coast, in wetlands and in an area in the middle of the peninsula. Large differences are found mostly in the western and southern parts of the peninsula.

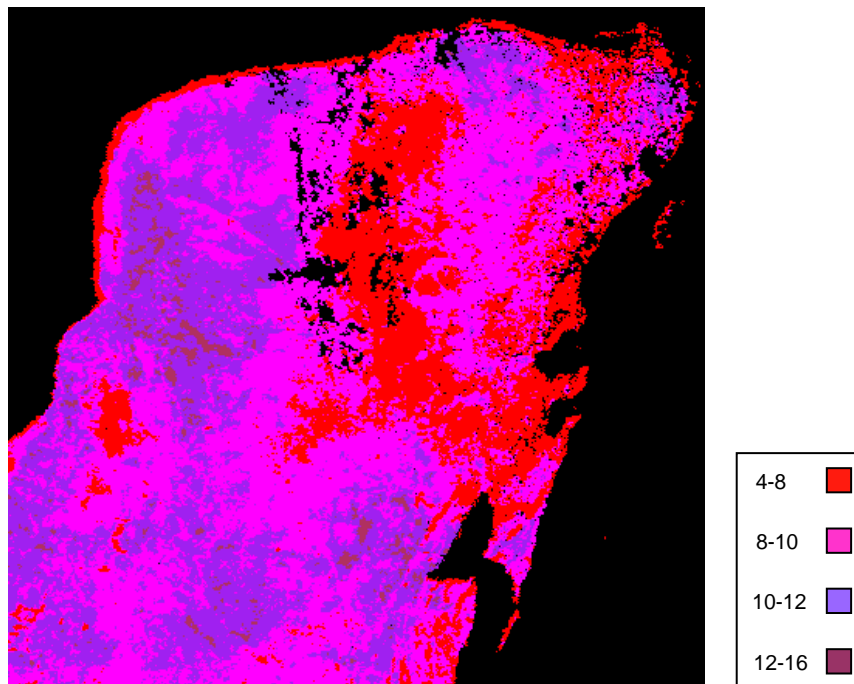


Figure 4-8: Grouped pixel Δ LST values [°C] for February 13, 2007 (valid values in 94% of land pixels).

4.3 Evaporative fraction

4.3.1 Scatter plots and triangles

After some trial-and-error it was decided, somewhat arbitrarily, to apply the triangle method only to images with a fraction of valid Δ LST land pixels above 50%. This threshold left 54 images for 2007, of these 29 passed the other three quality criteria, as explained in Section 3.2.5. Scatter plots of these images' Δ LST against NDVI, including the algorithm-defined DEL and WEL, can be seen in Appendix F, together with 23 scatter plots for the period January 1 to May 5, 2008. A few selected examples from 2007 are shown in Figure 4-9.

The first two examples of scatter plots in Figure 4-9 (a and b) resemble the expected triangle/trapezoid. They lack the “tip” of the triangle, i.e. the DEL and WEL meet outside the plot range, but they are not exactly trapezoids either in that the right-hand edge is not “flat”. In the low NDVI end they have very few pixels, all with low Δ LST, so the maximum Δ LST corner of the triangle is defined only by the slope of the DEL and the arbitrary definition of minimum NDVI (set at 0.1, line not displayed in the figures). The hypothetical maximum Δ LST resulting for these two days is about 30 °C, which seems reasonable. The DEL in both cases seems to describe the upper boundary of the triangle well. In a, the WEL also seems to follow the lower boundary well, but in b the real boundary seems to have a slight slope (while the WEL was arbitrarily set to be horizontal going through the mean minimum Δ LST).

4 Results

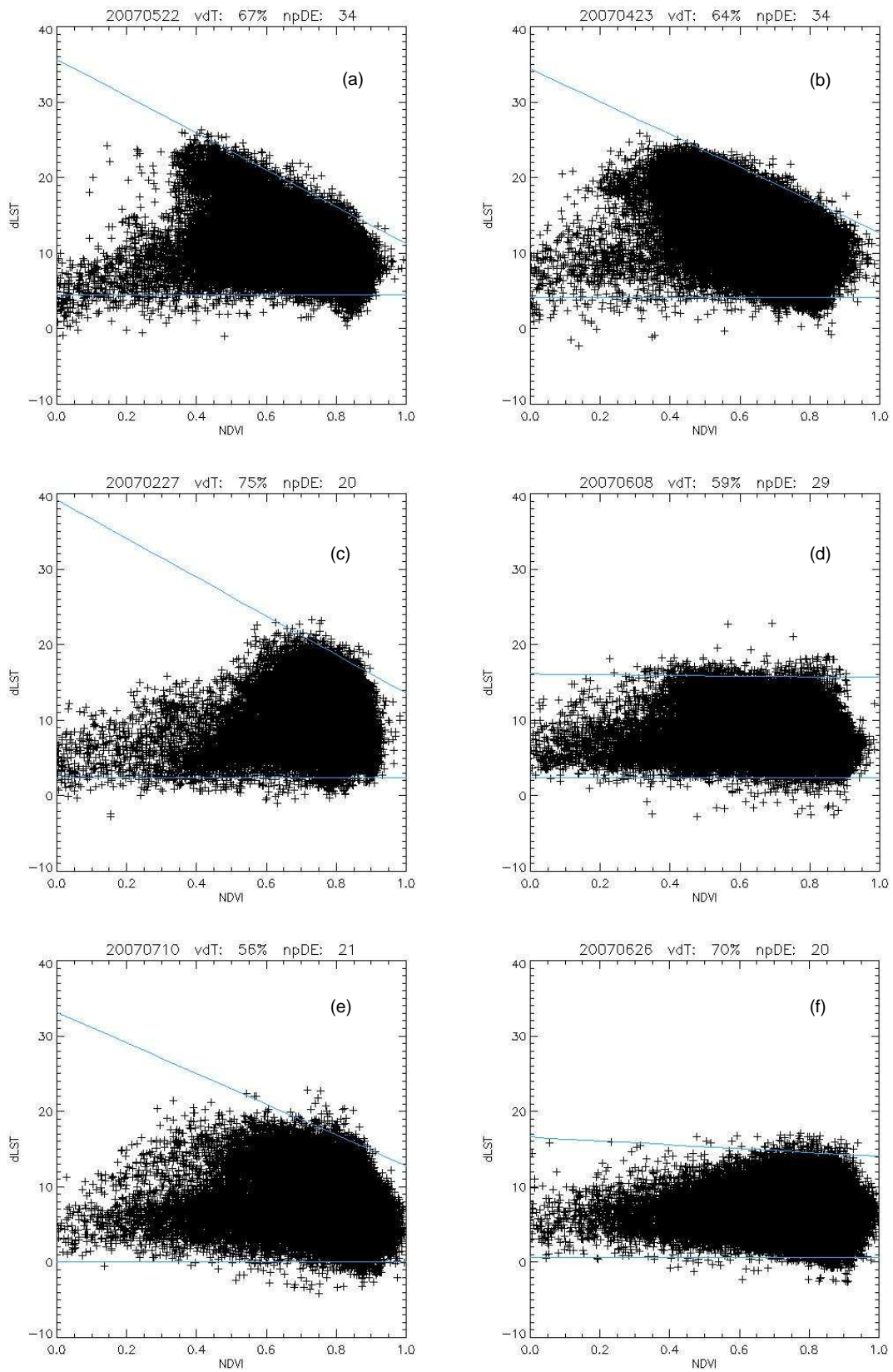


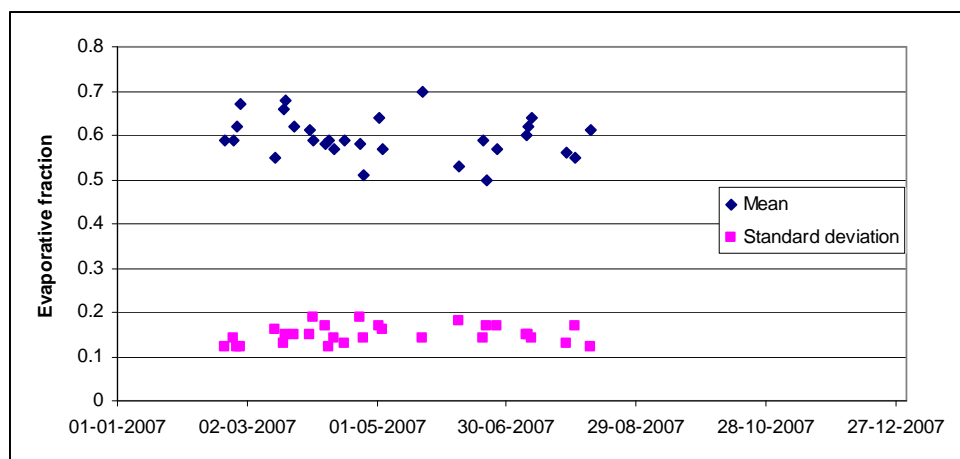
Figure 4-9: Selected scatter plots of ΔLST [°C] against NDVI [-] for six days in 2007; (a) May 22 (b) April 23 (c) February 27 (d) June 8 (e) July 10 (f) June 26. Blue lines denote DEL (sloping) and WEL (horizontal).

The last four examples of scatter plots in Figure 4-9 (c-f) do not resemble in their shape the triangle/trapezoid expected. In (c), the WEL is clearly defined but the DEL is only defined between NDVI 0.7 and 0.9, below 0.7 the slope changes and becomes unclear. In (d), the lower boundary has a little slope while the upper boundary and thus the DEL is almost horizontal. In (e), there seem to be two slopes within the upper boundary, and the DEL captures a mean of the two slopes. The horizontal WEL again does not represent well the slightly sloping lower front. In (f), there seems to be an “opposite” triangle, since the upper boundary has a very clear but positive slope. The calculated DEL results in a slightly negative slope, but similar plots resulted in negative DEL slopes and were thus disqualified from further analysis.

Note that the quality differences between these six example plots cannot be explained by the percentage of valid pixels in the corresponding Δ LST images (denoted vdT in the plot headings). A high number of points (30-40) included in the definition of the DEL (denoted npDE in the plot headings) seems to guarantee the expected triangular shape in the scatter, but there are also examples of reasonable triangular shapes with lower npDE (between 20 and 30). The number of plots where the DEL was defined based on more than 30 points in 2007 is 10, in 2008 (January-May) there are 7.

4.3.2 Temporal and spatial variation

The spatial mean of the resulting estimates of EF for the 29 “successful” days in 2007 are plotted in Figure 4-10, together with standard deviations. Unfortunately, these days are not evenly distributed around the year, the first day is February 20 and the last day is August 8. It is difficult to see any clear trend in the values, although one could spot a possible correlation between a decrease in the mean and an increase in the standard deviation, culminating in May-June. This could suggest an increased differentiation in EF around the peninsula at the end of the dry season, where some very dry areas “pull” the average down.



NDVI (denoted with orange triangles and green crosses), generally have higher EF values and lower degree of scattering than the former two. EF in the Sian Ka'an wetlands (pixel denoted with purple asterisk) generally has highest EF values among these five pixels. This ranking corresponds well to the expectations.

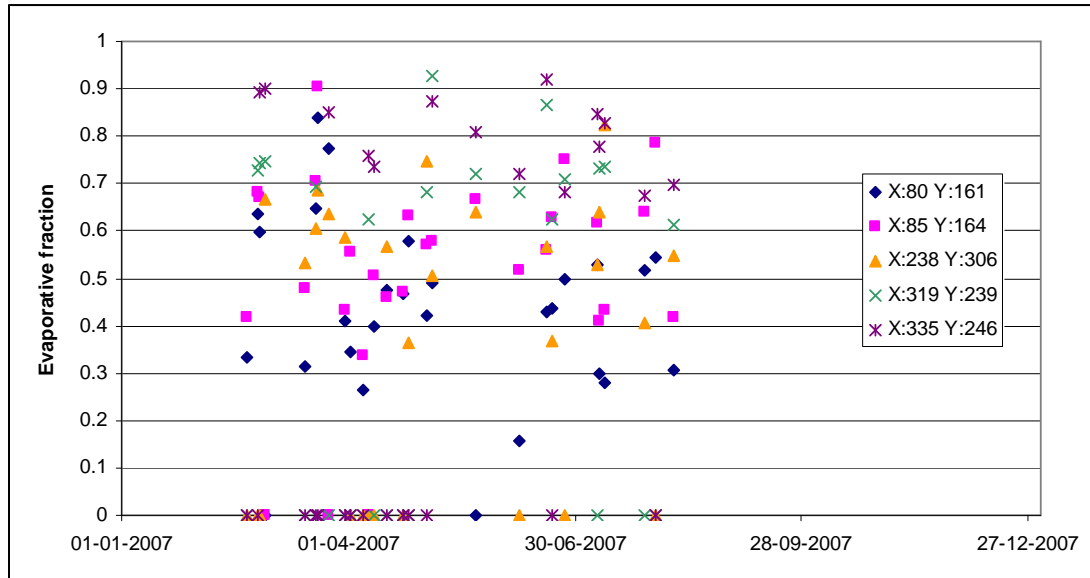


Figure 4-11: Evaporative fraction for five arbitrary pixels on 29 days in 2007. Pixel location is given by image sample number (X) and line number (Y), and the approximate location is indicated by white arrows in Figure 4-3.

The spatial distribution of pixels' average EF in 2007 can be seen in Figure 4-12. In general there is a decreasing trend from south-east to north-west, as expected from the similar trend in annual precipitation and pan evaporation data. Areas with lower EF are mostly close to the northern and western coasts, while areas with higher EF are on the eastern coast - especially in the Sian Ka'an wetlands and further south towards the border with Belize.

Distribution of EF values on two specific days in 2007 can be seen in Figure 4-13. On April 7 (a) the distribution is similar to the distribution of yearly averaged values in Figure 4-12, but more extreme. This is in the dry season, and some areas have EF values even lower than 0.3 or higher than 0.9 (thus not colored). On August 8 (b) (in the rainy season), the distribution seems more random and less pixels have values outside the range 0.3-0.9.

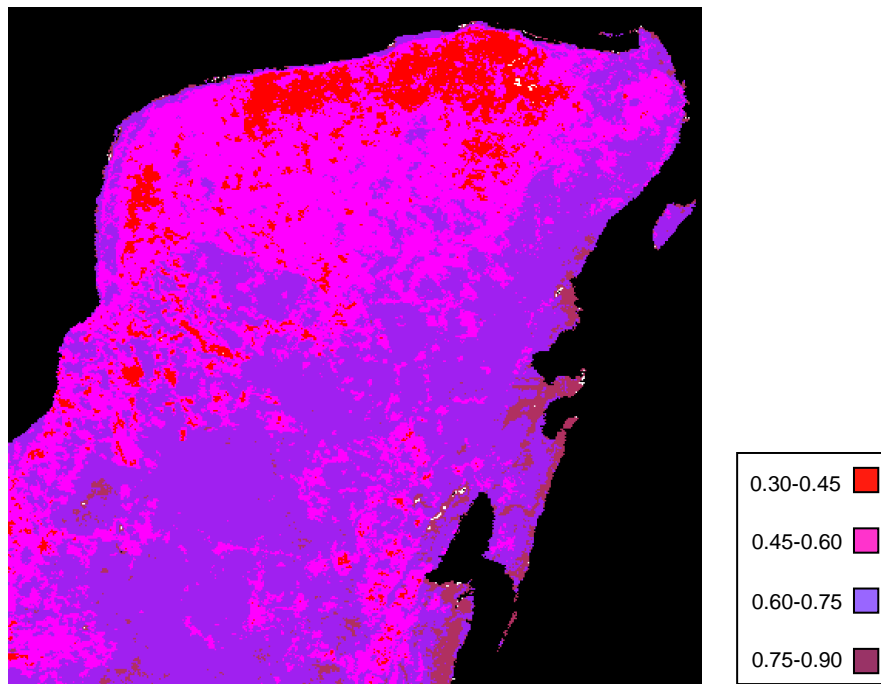


Figure 4-12: Grouped pixel average EF [-] values in 2007.

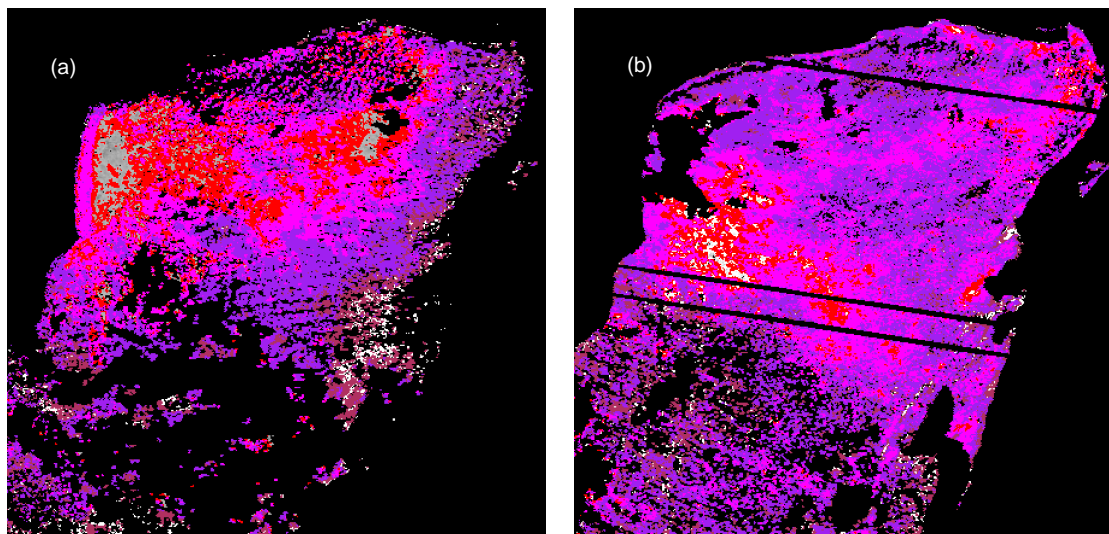


Figure 4-13: Grouped pixel EF [-] values on: (a) April 7, 2007 (b) August 8, 2007. Color scale is the same as for Figure 4-12.

4.3.3 Analysis using regions of interest tool

Scatter plots of ΔLST against NDVI for several days in 2007 were also created using ENVI, where regions of interest (ROIs) can be marked manually, and pixels in the ROI can be highlighted simultaneously in another image. This was used to explore which pixels make up the wet (cold) edge (WE) and the dry (warm) edge (DE). The scatter plots were also “density sliced”, revealing the density patterns of pixels within the triangle area.

Figure 4-14 displays two of these density-sliced scatter plots, highlighting the pixels that were classified as DE (with red) and WE (with blue). The first plot (a) is an example of a “good”

triangle, although it is obvious the “core” of the pixels does not resemble the triangle/trapezoid expected. The second plot (b) is an example of a day that “passed” the quality check in the EF algorithm although the triangular shape is only obvious when using imagination/interpolation to extend the DEL. Here the “core” of pixels resembles even less the triangle/trapezoid expected.

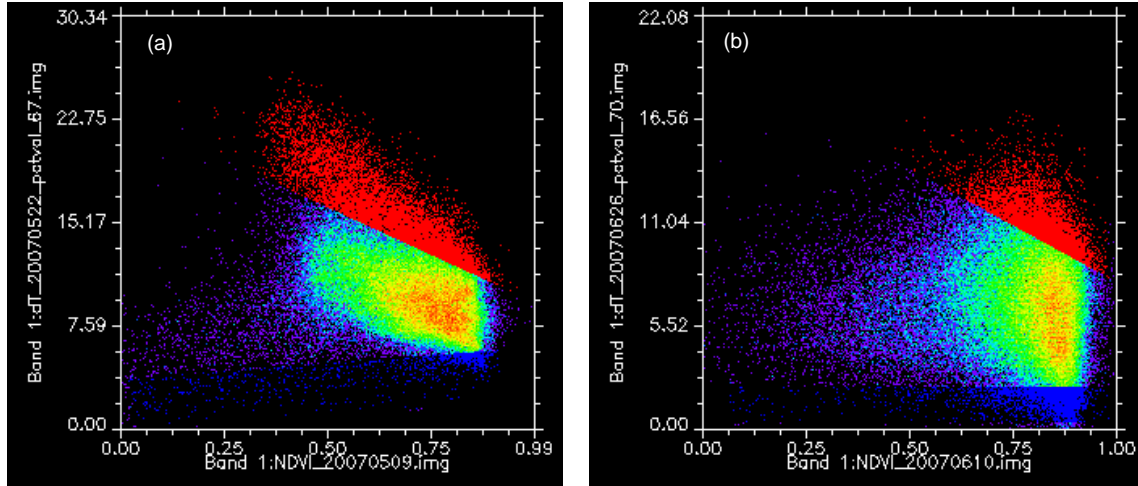


Figure 4-14: Scatter plots of Δ LST against NDVI, with color scale (blue to red) indicating relative density of pixels and DE and WE pixels highlighted with red and blue (respectively), for two different days: (a) May 9, 2007 (b) June 10, 2007.

Figure 4-15(a) displays the location of all pixels that were on any of the analyzed days classified as DE (red) or WE (blue). In all there were approx. 75,000 pixels classified as DE in this manner and 43,000 as WE; of these 18,000 pixels (marked with yellow) have been classified both as WE and as DE (on different days, obviously). Not a single pixel is included in the DE or WE of all days. When gathering the pixels that were part of the DE and WE in three groups and intersecting these groups a few pixels did repeat, displayed in Figure 4-15(b). The overall trend in both a and b resembles, as expected, the overall picture from the EF maps: the WE is defined by pixels in the southeastern wetlands and the DE by inland pixels in the low NDVI areas of the northwest.

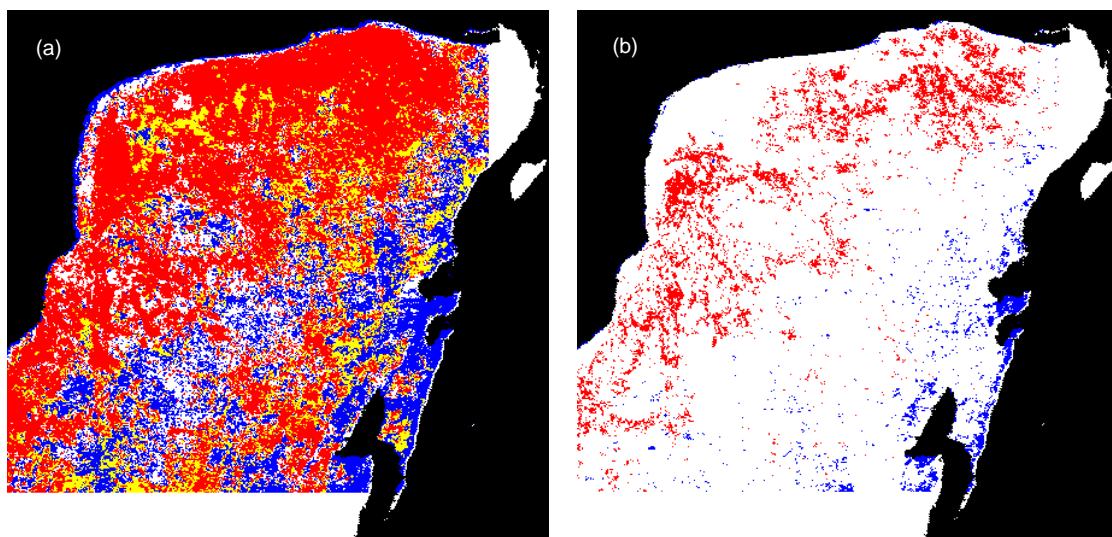


Figure 4-15: pixels defined as DE (red), WE (blue) and overlaps (yellow): (a) in any day analyzed in 2007, (b) those reoccurring in three seasonal groupings. Pixel analysis does not cover the entire image due to a technical error.

4.3.4 Correlation with elevation

Some EF maps were plotted against a DEM of Yucatan (from SRTM, resampled to 1 km² spatial resolution) to test the hypothesis of a correlation between depth to groundwater and relative rate of evapotranspiration. This assumes that the depth to the groundwater is correlated with the elevation, which is largely the case in Yucatan (Bauer-Gottwein, pers. comm., 2008). Four of these scatter plots are displayed in Figure 4-16.

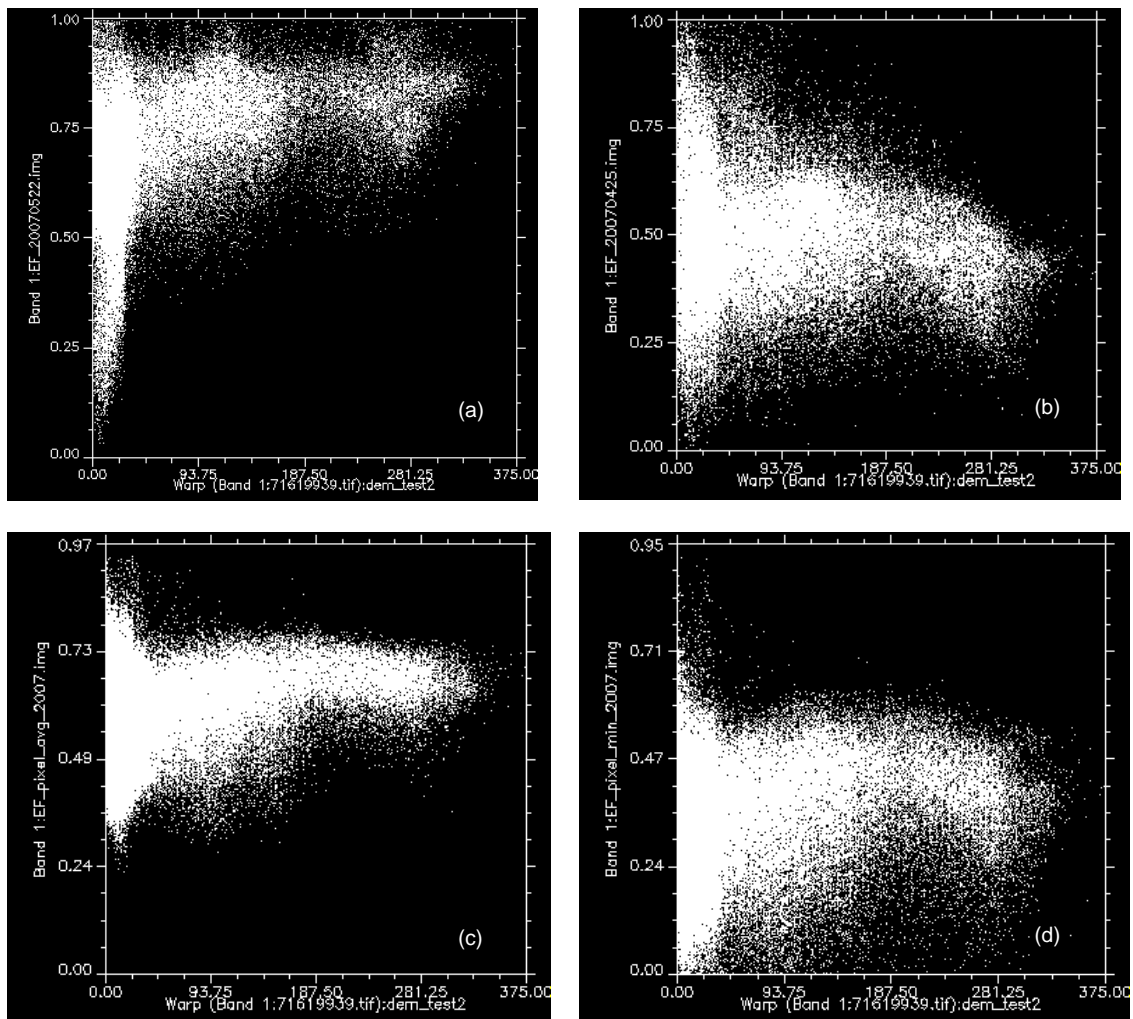


Figure 4-16: scatter plots of different EF maps in 2007 against DEM; (a) EF on May 22, (b) EF on April 25, (c) pixel average EF for 2007, (d) pixel minimum EF for 2007.

The expectation was that EF would decrease with increased depth to the groundwater in the dry season, reflecting a species adaptation to availability of water: in periods with low precipitation trees depend on soil moisture and groundwater for maintaining maximum transpiration rates. This would be expressed in the scatters as a negative slope: decreasing EF with increasing elevation. It is hard to say that any of the above four scatters fulfills this expectation. The two first plots (a and b) are both from the end of the dry season (May 22 and April 25, 2007), where pan evaporation is highest and average NDVI lowest. The upper edge of the pixel cloud in (b)

could seem to have a negative slope, but the lower edge has a positive slope. The upper edge in both (a), (c) and (d) is quite horizontal. If anything, these plots suggest that the EF increases with increased elevation.

4.4 Available energy

The spatial mean of net radiation for daytime hours given in W m^{-2} can be seen for 2007 in Figure 4-17, together with the standard deviation from and each day's minimum and maximum pixel values (note that the pixel size of the original ECMWF data is 0.25 degrees, thus the real variation in 1 km^2 pixels is expected to be higher). The mean varies between approx. 62 and 288 W m^{-2} with the expected seasonal pattern. The standard deviation varies between approx. 8 and 60 W m^{-2} with a mean of 22 W m^{-2} . This indicates a reasonably low spatial variation, which satisfies one of the assumptions necessary for using the triangle method. Of course, the large pixel size is partly the reason for this low variation.

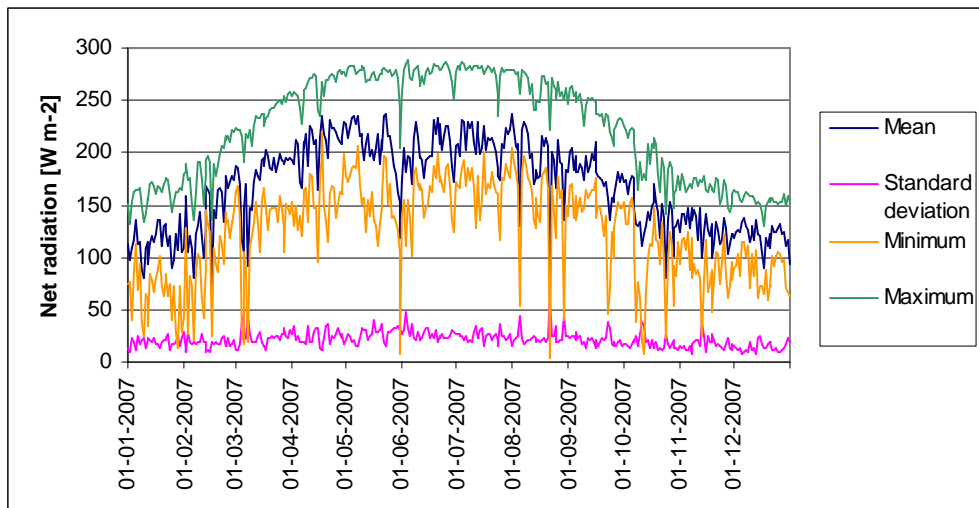


Figure 4-17: Spatial mean, standard deviation from mean and minimum and maximum net radiation on the Yucatan peninsula in 2007.

The spatial mean of soil heat flux for daytime hours given in W m^{-2} can be seen for 2007 in Figure 4-18, together with the standard deviation from the mean and each day's minimum and maximum pixel values (here the pixel variability is influenced both by pixel size of results the pixel size of NDVI data and the pixel size of R_n data). The mean varies between approx. 9 and 43 W m^{-2} with the expected seasonal pattern. The standard deviation varies between approx. 4 and 15 W m^{-2} with a mean of 9 W m^{-2} . This corresponds to a higher coefficient of variation for G than for R_n , which is expected from the influence of the spatial resolution of the NDVI factor. In average G corresponds to approx. 15% of R_n , which is in the order of magnitude expected.

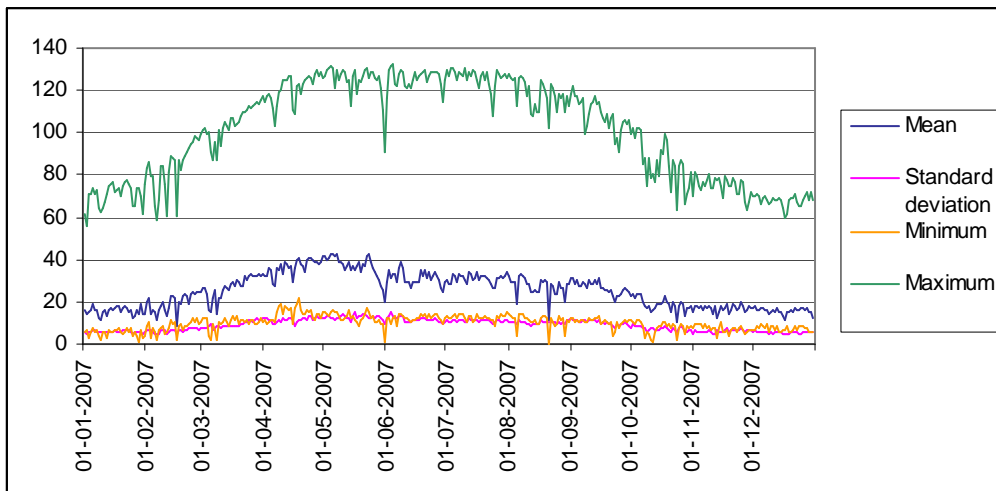


Figure 4-18: Spatial mean, standard deviation from mean and minimum and maximum soil heat flux on the Yucatan peninsula in 2007.

4.5 Actual evapotranspiration

Spatial mean rates of daily actual evapotranspiration for the 29 “successful” days in 2007 are plotted in Figure 4-19, together with standard deviation from the mean, minimum and maximum. As with the EF plots (Figure 4-10), it is hard to identify any trends, although the actual evapotranspiration seems somewhat higher in June-July than in March-April, which is to be expected from the higher AE. The minimum pixel evaporation is 0 mm day^{-1} and the maximum pixel evaporation is 6.95 mm day^{-1} . The spatial mean varies between 2.47 mm day^{-1} and 3.82 mm day^{-1} with an overall mean of 2.99 mm day^{-1} . If the overall mean was assumed to represent the annual mean, the annual aET would be at 1090 mm day^{-1} , which is clearly too high considering the annual precipitation rates. But this assumption is dubious, since the 29 days are not evenly distributed over the year. Furthermore it is likely that they represent days with less cloud cover than normal, which entails higher ET than normal.

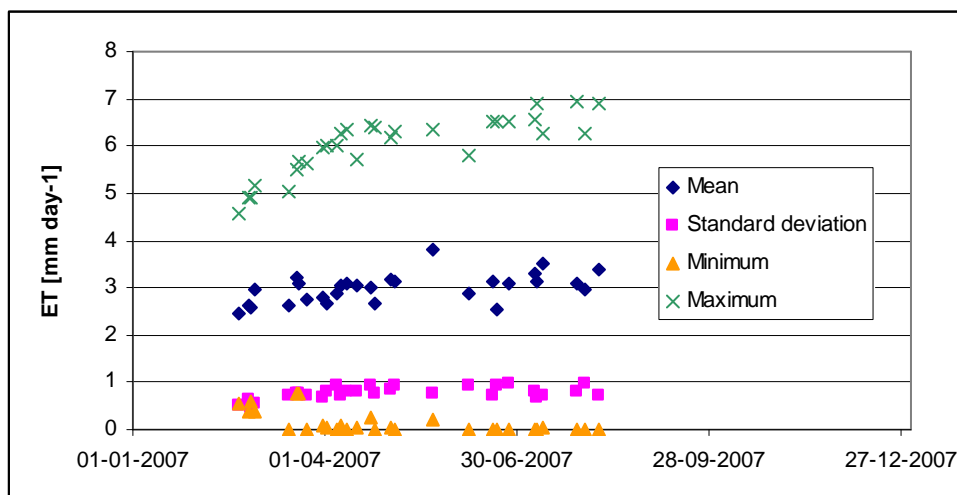


Figure 4-19: Spatial mean of ET [mm day^{-1}] on 29 days in 2007, together with standard deviation from the mean, minimum and maximum.

Figure 4-20 shows the spatial distribution of pixel averages of aET in the 29 days of 2007. The overall pattern is, as expected similar to the one in Figure 4-12 (spatial distribution of average EF). Figure 4-21 shows the spatial distribution of aET on two specific days in 2007. May 22 (a) is an example of a “good” day (compare to scatter plot in Figure 4-9(a)), the spatial variation is high and resembles the overall trends. February 27 is an example of a less “good” day (compare to scatter plot in Figure 4-9(c)), the spatial variation is lower and it seems that cloud cover has a significant effect on the distribution, which shouldn’t be the case since it is unlikely that the same clouds were covering the same areas all the time between the day and night images were taken.

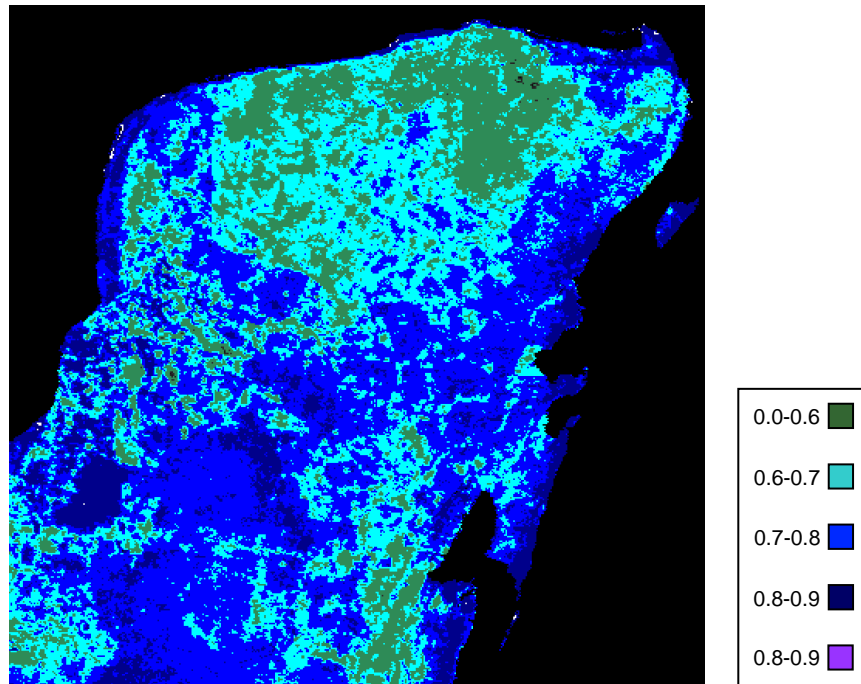


Figure 4-20: Grouped averages of ET [mm day^{-1}] for 29 days in 2007.

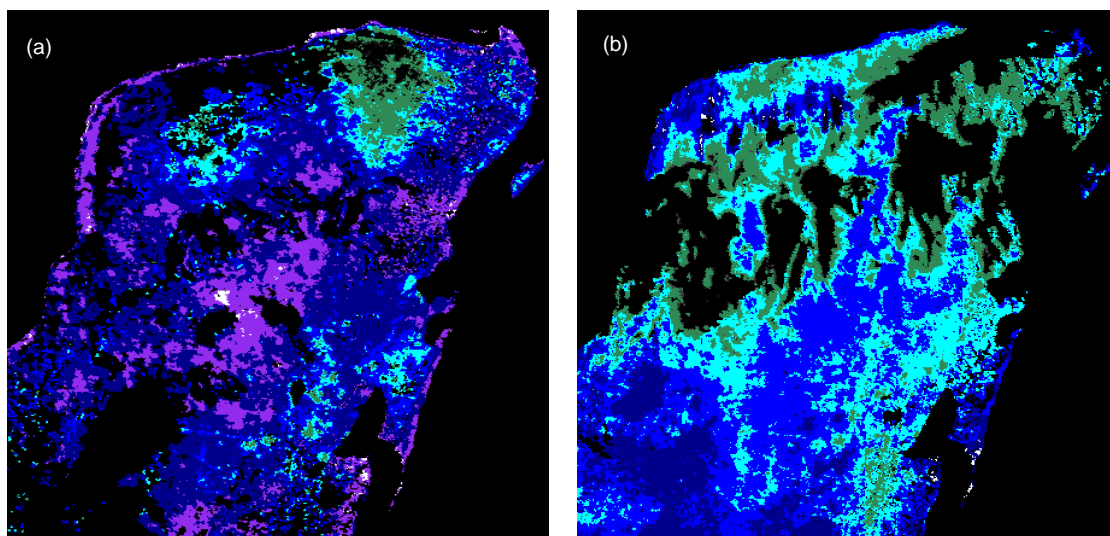


Figure 4-21: Grouped average of ET [mm day^{-1}] for two days: (a) May 22, 2007 (b) February 27, 2007. Color scale is the same as for Figure 4-20.

4.6 Sap flow

In all eight setups of sap flow measurements at different sites were made in the period from February 7 to March 9, 2008. Of these the first three are considered test setups, sites 4 and 5 are considered main attempts at measuring transpiration in an area with high NDVI, sites 6 and 7 as attempts at measuring in an area with low NDVI and site 8 as an attempt at getting a longer time series of data for monitoring seasonal changes in transpiration rate.

Location of the five full setup sites can be seen in Figure 4-22, and a description of all sites' location and setup can be seen in Appendix G. As can be seen, sites 4, 5 and 8 are located in areas of relatively high NDVI, although the NDVI at site 4 is rather inhomogeneous. This is because this location was chosen based on an older NDVI map than the one presented here. The land cover classification at these three sites is medium sub-deciduous tropical forest (according to land cover map from SEMARNAP, 2000). Sites 6 and 7 are located in areas classified as low deciduous and sub-deciduous tropical forest with secondary vegetation of shrubs and herbaceous plants (according to same map). Note that the area with very low NDVI (indicated with blue color) in the north-west corner corresponds to the city of Merida and the one on the north-east coast to the city of Cancun. It is assumed that most of the scattered pixels in the "blue" range correspond to human settlements, except for those within the Sian Ka'an wetlands (south-east of site 8).

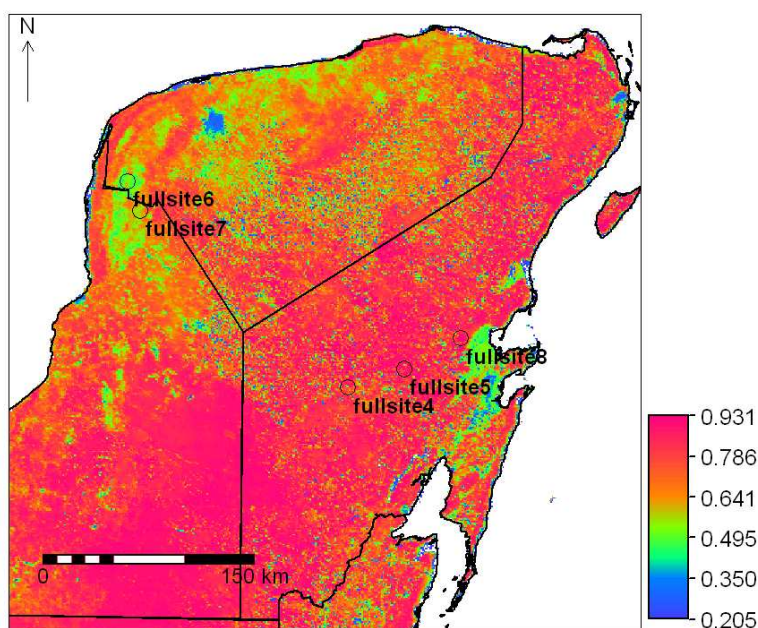


Figure 4-22: Map indicating location of sites of sap flow measurement (fullsite4 to fullsite8). Exact locations are given in Appendix G. Background raster is MODIS 16-days NDVI for February 2, 2008. Black lines indicate state and country borders.

This section includes a short description of the results obtained at the three test sites, followed by a more thorough description of the results at the main sites. The results at the successful main sites are presented in four steps: characterization of the trees at the site, presentation of the measured temperature differences, presentation of the calculated sap flux densities and finally the results for whole tree and stand daily transpiration rates. All raw data, calculations, tree characterizations and additional graphs can be found in Appendix H (electronic). Photographs are provided in Appendix C (also electronic).

4.6.1 Test sites

Sites 1-3 were made with the aim of learning to work with the equipment. Site 1 taught us that drilling in the local trees was very difficult, and that a method for measuring sapwood depth other than visual inspection was needed.

Site 2 showed that the spare datalogger (Grant) was useful although the resolution is quite coarse. The results have the expected night-day trend as can be seen in Figure 4-23. The three lines in the figure represent data from three probes installed at different circumferential positions in the trunk of the same tree, thus they also indicate a rather homogeneous sap velocity regime around the trunk in this specific tree. The estimates of whole tree transpiration for this *Melicocca bijugatus* on February 9 based on the three different sensors range between 96 and 195 L day⁻¹, corresponding to a CV (coefficient of variation) of 34%.

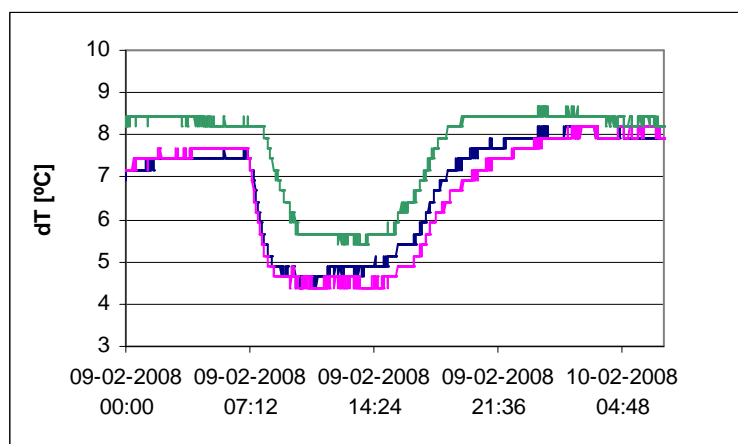


Figure 4-23: Measured temperature difference between probes at three points around a tree's circumference at site 2.

Setting up site 3 confirmed that the drilling was a critical issue. The Campbell datalogger CR10X proved to have a much higher sensitivity than the Grant, as expected. Despite its high sensitivity the noise on the data from this site was rather small. However, the night time values are not as stable as was expected, as can be seen in Figure 4-24: tree 1 has a pronounced drift downwards in the night values, both from night to night and during each night; tree 2 has a slight drift upwards during the first night followed by a slight drift downwards during the second and third night; tree 3 has a pronounced drift upwards during the first night, a stable level during the second night and an unstable level during the third night. There was found no explanation for this inconsistency in night levels. On the other hand, the daytime values seem to correlate nicely: morning onset of sap flow is detected approximately at the same time for all three trees (around 08:00), as is a drop in flow around 10:30 on the first day and around 14:30 on the second day.

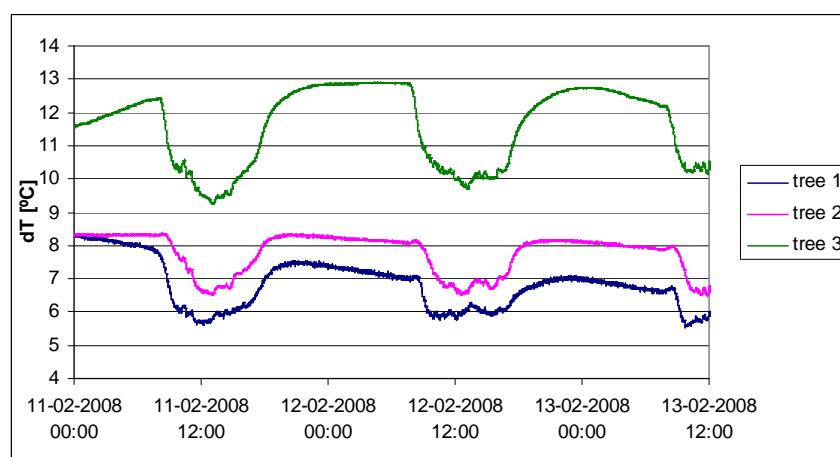


Figure 4-24: Measured temperature differences between probes in three different trees at site 3.

Estimates of whole tree transpiration are summarized in Table 4-1. There can be seen no clear correlation between tree size and daily transpiration rates. Trees 1 and 2 lost more water during the second day, but tree 3 lost less water on the second day compared to the first day.

Table 4-1: Calculated whole tree daily transpiration for three trees sampled at site 3.

		Tree 1	Tree 2	Tree 3
DBH [cm]		14.6	27.4	24.8
F [L day ⁻¹]	11-02-2008	19.0	15.1	14.7
	12-02-2008	22.7	18.9	11.8

The vegetation at site 3 illustrated the variability in the local forest. Within an area of 100 m² there were counted 20 individuals with a DBH larger than 3.2 cm (incl. the three trees sampled), corresponding to a density of 0.18 trees m⁻². Trees represented 14 different species and with DBH varying between 3.8 and 47.7 cm. The number of seedlings (very young trees of DBH smaller than 1.6 cm) was roughly estimated to be equal to the number of bigger trees, and there was also a big variety of other types of vegetation (Lianas, epiphytes, herbaceous plants etc.). Due to the density of the vegetation it was quite difficult to take pictures that show this clearly, but a photograph taken from a helicopter flying over a similar forest illustrates the variability in size and species visible in the canopy layer, Figure 4-25. According to the local forest experts, tree species seem to cluster in this area, thus an area of 100 m² and three sample trees cannot be considered representative of the stand. Nonetheless, an attempt to estimate sT was made, yielding 2.7 mm for February 11 and 2.9 mm for February 12.



Figure 4-25: Photograph of tropical forest near Tulum, Quintana Roo, taken from helicopter, February 2008.

4.6.2 Site 4

Trees

Within a plot size of approximately 400 m² there were counted in all 84 individual trees of a DBH larger than 3.2 cm, corresponding to a density of 0.21 trees m⁻². The biggest tree had a DBH of 44.6 cm and the mean DBH was 11.6 cm; size distribution is illustrated with the histogram in Figure 4-26(a). The trees belonged to 15 different species, of which two were very dominant: *Pouteria unilocularis* (34) and *Pouteria izabalensis* (17). Measured depth of sapwood as a function of DBH is illustrated in Figure 4-26(b). A photograph of the vegetation containing some of the equipment can be seen in

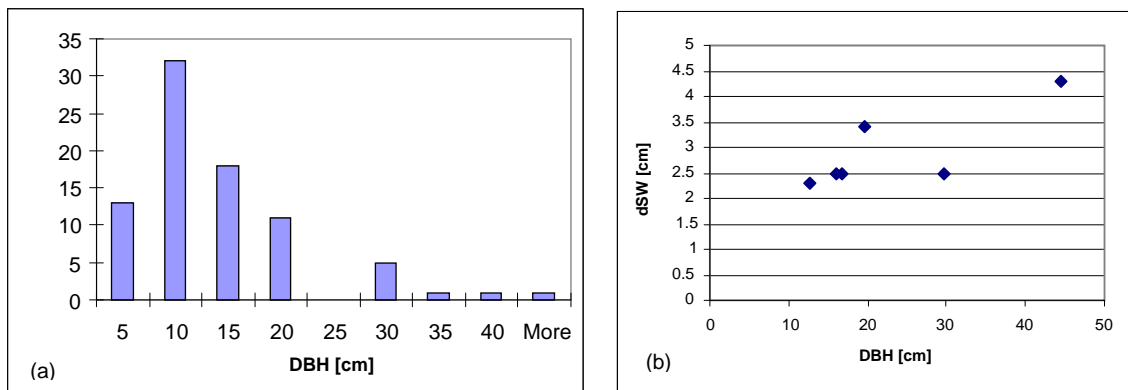


Figure 4-26: Characterization of trees at site 4: (a) Histogram of trees sizes within plot; (b) Measured depth of sapwood in sample trees.



Figure 4-27: A photograph from site 4 showing some of the sample trees (covered with insulation and aluminum foil) and the datalogger (in the white box).

Temperature data

Temperature differences between probes in the six sample trees averaged every 10 minutes can be seen in Figure 4-28. The 10 minute averaging removes much of the noise recorded by the 1-minute samples, except for at tree 1 where there is clearly something wrong with the data. The reason for this is unknown and tree 1 has been omitted from the further analysis. Tree 3 also exhibits a trend different from the remaining trees, which is attributed to the fact that it seemed to be hollow in the center of the trunk. It is estimated that a little part of the probe may have been in contact with the air in this hole, but the data was further processed as usual (I found no way to account for the disturbance). Data for trees 2, 4, 5, and 6 seems reasonably reliable with rather stable nighttime values.

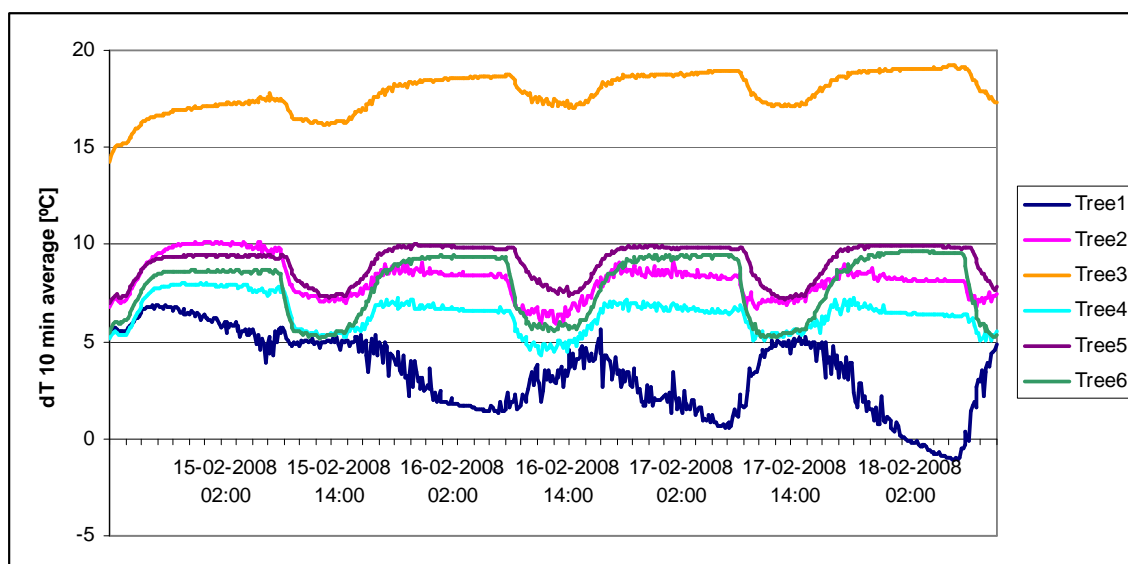


Figure 4-28: 10 minute averages of temperature differences between probes installed in six sample trees at site 4.

Sap flux density

Sap flow in the five trees starts at around 08:00 and stops around 20:00, as can be seen in Figure 4-29. Variation in sap flux densities between the trees is rather big, as is also illustrated in Figure 4-30. There seems to be no consistent clear correlation between DBH and calculated sap flux density; the correlation pattern with basal area is very similar (not shown).

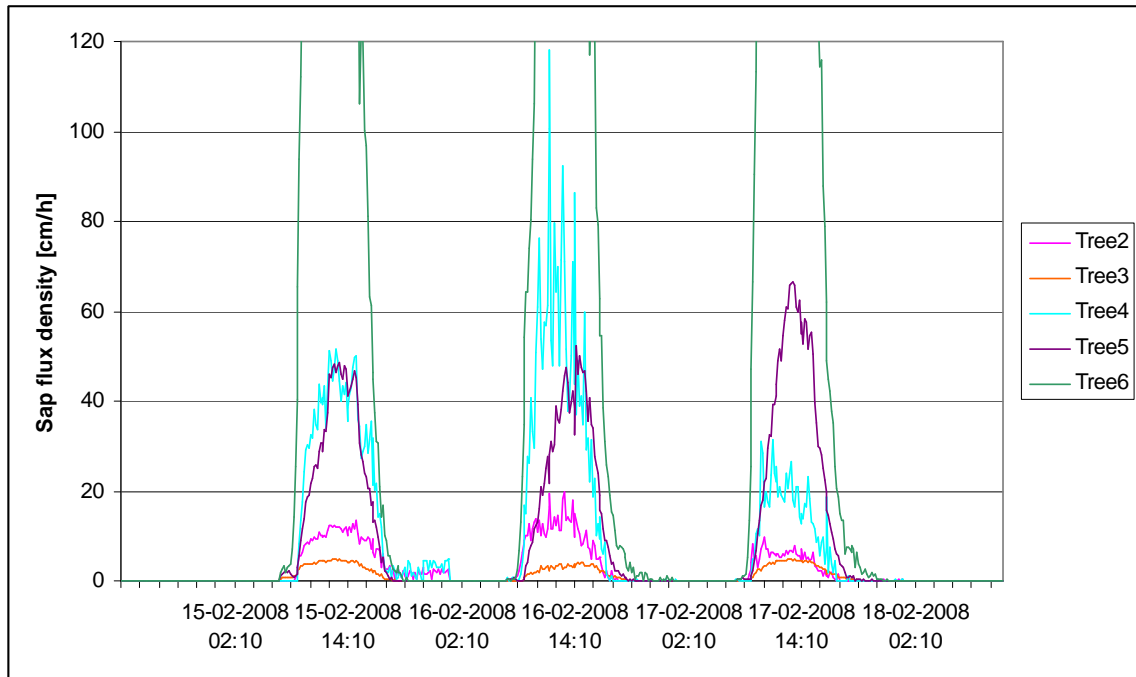


Figure 4-29: Calculated sap flux densities for five sample trees at site 4. Tree 6 reaches a maximum of 66.2 cm h⁻¹ with a daytime average of 21.9 cm h⁻¹.

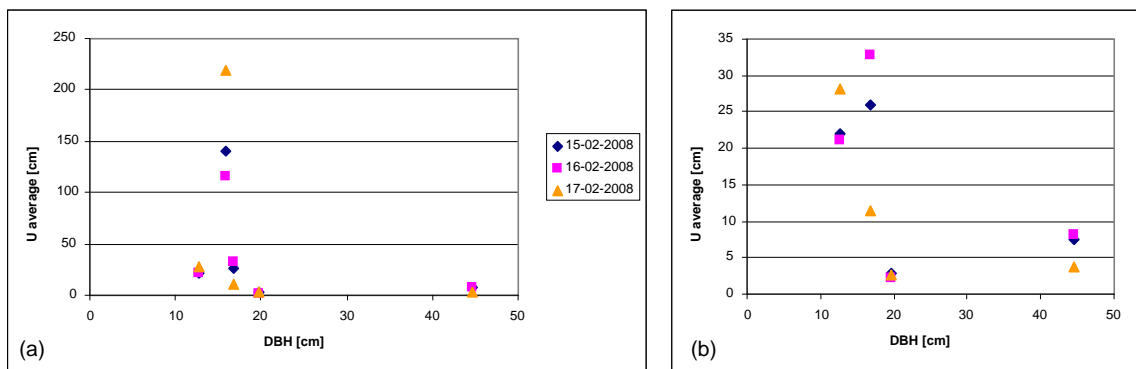


Figure 4-30: Calculated daytime average sap flux density plotted against DBH for (a) trees 2-6 and (b) trees 2-5 at site 4.

Tree and stand transpiration

Daily transpiration rates for trees 2-6 can be seen in Table 4-2. As for the sap flux velocity there seems to be no clear correlation between daily transpiration and DBH or basal area. Despite some inconsistencies it can be noted that most trees transpired most on February 17th and least on February 16th.

Table 4-2: Calculated whole tree daily transpiration for five trees at site 4.

		Tree 2	Tree 3	Tree 4	Tree 5	Tree 6
DBH [cm]		53.4	5.8	34.9	18.9	170.7
F [L day ⁻¹]	15-02-2008	52.8	4.4	42.0	18.1	140.1
	16-02-2008	24.4	5.5	14.7	24.1	265.4
	17-02-2008	53.4	5.8	34.9	18.9	170.7

The sT calculated using two different biometric parameters is presented in Table 4-3. The scaling parameter resulting from DBH (7.36) was substantially higher than when using A_B (4.94).

Table 4-3: Estimated daily transpiration rates from stand at site 4 using two biometric parameters: DBH and A_B .

Date	T [mm day ⁻¹]	
	B=DBH	B= A_B
15-02-2008	5.2	3.5
16-02-2008	4.7	3.2
17-02-2008	6.2	4.1

4.6.3 Site 5

Trees

Within a plot size of approximately 375 m² there were counted in all 65 individual trees of a DBH larger than 3.2 cm, corresponding to a density of 0.18 trees m⁻², very similar to that at sites 3 and 4; also the general impression of the vegetation at this site resembles the previous. The biggest tree had a DBH of 55.7 cm and the mean DBH was 13.3 cm; size distribution is illustrated with the histogram in Figure 4-31(a). The trees belonged to 16 different species, of which three were very dominant: *Pouteria unilocularis* (24), *Gymnanthes lucida* (12) and *Pouteria izabalensis* (7). Measured depth of sapwood as a function of DBH is illustrated in Figure 4-31(b).

4 Results

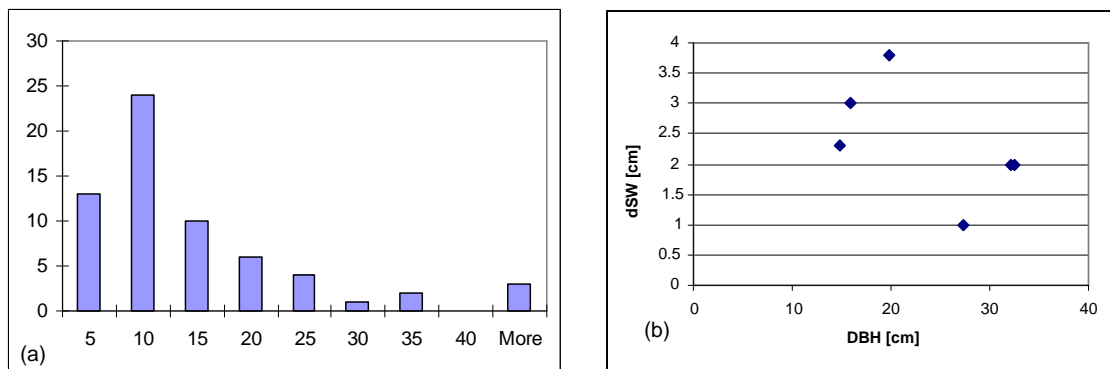


Figure 4-31: Characterization of trees at site 5: (a) Histogram of trees sizes within plot; (b) Measured depth of sapwood in sample trees.

Temperature data

Temperature differences between probes in the six sample trees averaged every 10 minutes can be seen in Figure 4-32. Again data for tree 1 exhibits some strange pattern for which there could be found no explanation (it is unknown whether the probe used for tree 1 at this site is the same as for tree 1 at site 4; probes and cables were numbered when taking down the setup at this site in order to clear this question at the next site, where it turned out there was no specific problem with the equipment connected to datalogger channel 1). Tree 1 has been omitted from the further analysis. Trees 2-6 seem to converged towards stable nighttime values, but are then interrupted by some very notable noise which starts at the same time for all trees, a time that becomes earlier for each night (ca. 04:00 on the first night and ca. 20:00 on the fourth night). It was suggested that the cause of the noise could be either electromagnetic signal interference or condensation in the datalogger, and attempts at solving the problem at the next site indicate that it was probably condensation in the datalogger. It is unknown why there is more noise around midday on the data from trees 2 and 6 than trees 3, 4 and 5.

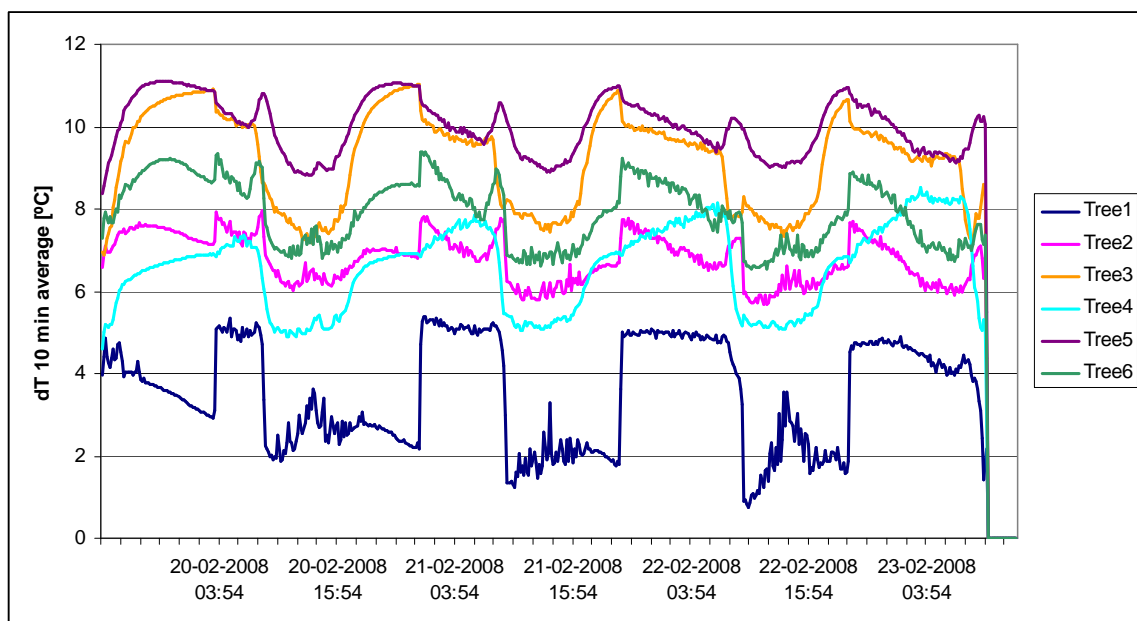


Figure 4-32: 10 minute averages of temperature differences between probes installed in six sample trees at site 5.

Sap flux density

Sap flow in the five trees starts at around 08:00 and starts decreasing sharply around 17:00, though completely stable night values are not reached before around 22:00 (see Figure 4-33). Variation in sap flux densities between the trees is much smaller than at site 4, with daytime averages ranging between 2.2 and 29.0 cm h^{-1} . Again there seems to be no consistent clear correlation between DBH or basal area and calculated sap flux density.

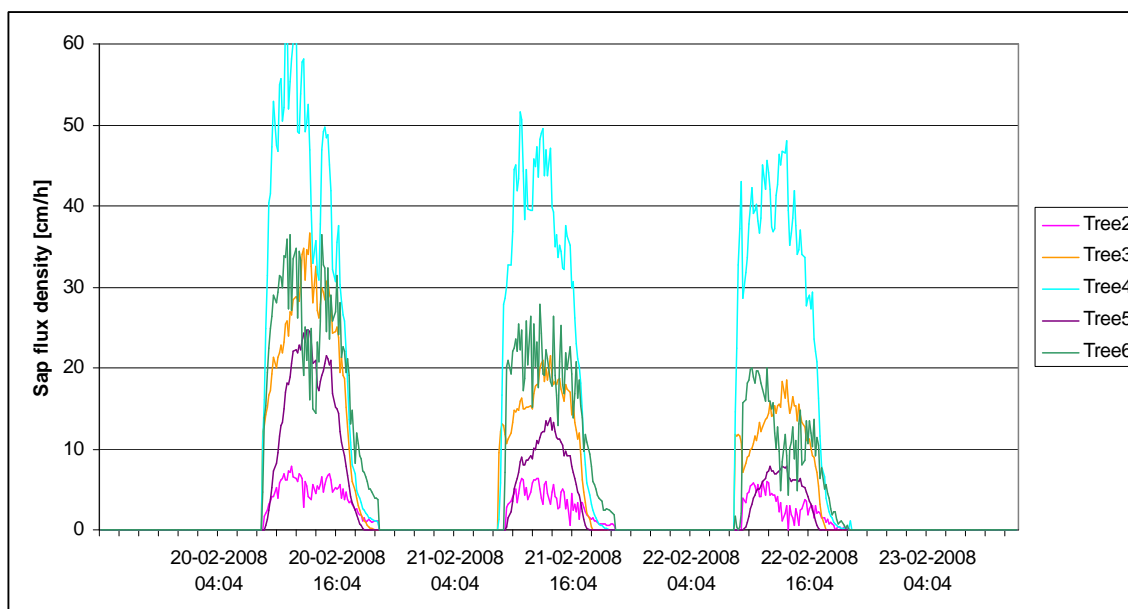


Figure 4-33: Calculated sap flux densities for five sample trees at site 5.

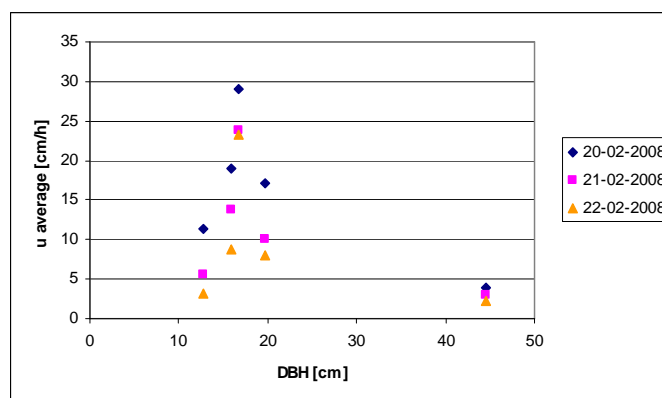


Figure 4-34: Calculated daytime average sap flux density plotted against DBH for trees 2-6 at site 5.

Tree and stand transpiration

Daily transpiration rates for trees 2-6 can be seen in Table 4-4. As for the sap flux velocity there seems to be no clear correlation between daily transpiration and DBH or basal area. There is, however, a rather consistent variation in transpiration between the three consecutive days: all five trees transpire most on February 20th, decreasing substantially on February 21st and decreasing a little more on February 22nd. Due to time limitations it was not possible to seek

4 Results

weather data from local stations to see if these fluctuations correlate with cloudiness, air temperature or other climatic variables.

Table 4-4: Calculated whole tree daily transpiration for five trees at site 5.

		Tree 2	Tree 3	Tree 4	Tree 5	Tree 6
DBH [cm]		44.6	19.7	16.7	12.7	15.9
F [L day ⁻¹]	20-02-2008	26.9	37.6	41.4	9.9	25.1
	21-02-2008	19.6	22.3	33.7	4.8	17.8
	22-02-2008	15.3	17.8	33.4	2.8	11.4

The sT calculated using two different biometric parameters is presented in Table 4-5. The scaling parameter resulting from DBH (6.45) was slightly lower than when using A_B (7.42).

Table 4-5: Estimated daily transpiration rates from stand at site 5 using two biometric parameters: DBH and A_B .

Date	T [mm day ⁻¹]	
	B=DBH	B= A_B
20-02-2008	6.1	6.9
21-02-2008	3.6	4.0
22-02-2008	3.0	3.4

4.6.4 Site 6

Trees

Within a plot size of approximately 800 m² there were counted in all 69 individual trees of a DBH larger than 3.2 cm. This corresponds to a tree density of 0.09, about half that observed at sites 3-5. Indeed the vegetation at this site looked very different from the previous ones, resembling more a mixture of woodland and small savanna areas than a tropical forest. Trees were found in clusters and some of them had shed their leaves. The surface at some places seemed to be covered with huge rocks and very little soil. Desert-like plants such as Agave (Genus *Agave*) and Nopal (genus *Opuntia*) were present between the trees. Photographs of the vegetation can be seen in Figure 4-35.



Figure 4-35: Two different views of the vegetation at site 6.

The biggest tree had a DBH of 64.8 cm and the mean DBH was 14.8 cm; size distribution is illustrated with the histogram in Figure 4-36(a). The trees belonged to 17 different species, of which three were very dominant: *Piscidia communis* (16), *Lisiloma bahamensis* (15) and *Dendropanax arboreus* (8). Measured depth of sapwood as a function of DBH is illustrated in Figure 4-36(b). Of the six trees sampled, it seemed that in three of them the whole radial profile of xylem was functional (thus the indicated sapwood depth is equal to their trunk radius subtracted the bark depth).

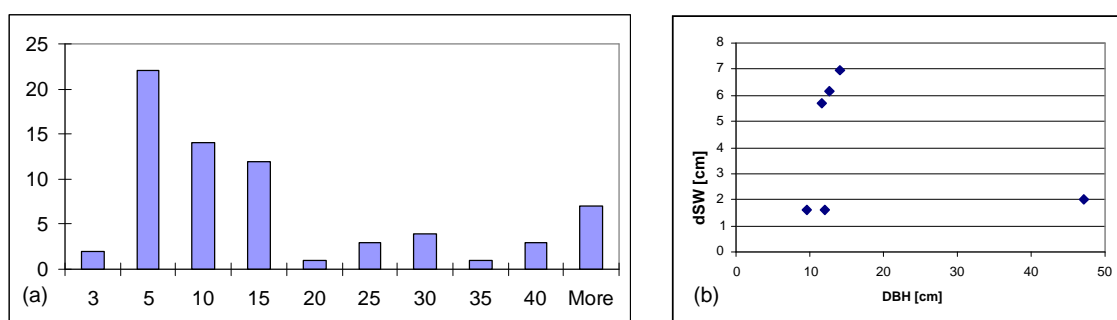


Figure 4-36: Characterization of trees at site 6: (a) Histogram of trees sizes within plot; (b) Measured depth of sapwood in sample trees.

Temperature data

The sap flow measuring equipment was set up at site 6 on February 24th, but in the effort of trying to get rid of the severe noise that was observed already at site 5, data gathering was intermittent and the only useful results are from February 27th to 29th. This data still suffers from noise problems, but since it is the only useful data obtained for a location with low NDVI it has been processed nonetheless.

Temperature differences between probes in the six sample trees averaged every 10 minutes can be seen in Figure 4-37. At this site there is no longer a single tree that exhibits considerably less structured data than the others. There cannot be seen as clear stable nighttime values for any of the trees as at previous sites, but considering the noise level it is still possible to detect relative stability for trees 1, 3 and 4. For trees 2, 5 and 6 it is unclear whether the apparent night trend is caused by data drift or whether these trees have sap flow during nighttime as well. This grouping of stable or unstable nighttime value does not correlate with species or with size. It has therefore been assumed in the further processing that sap flow took place only during daytime; the no-flow value (ΔT_M) was set to the ΔT value measured in the morning just a decrease in ΔT

4 Results

which could be assumed to correlate with morning sap flow onset. This introduces a high degree of subjectivity and uncertainty into the results.

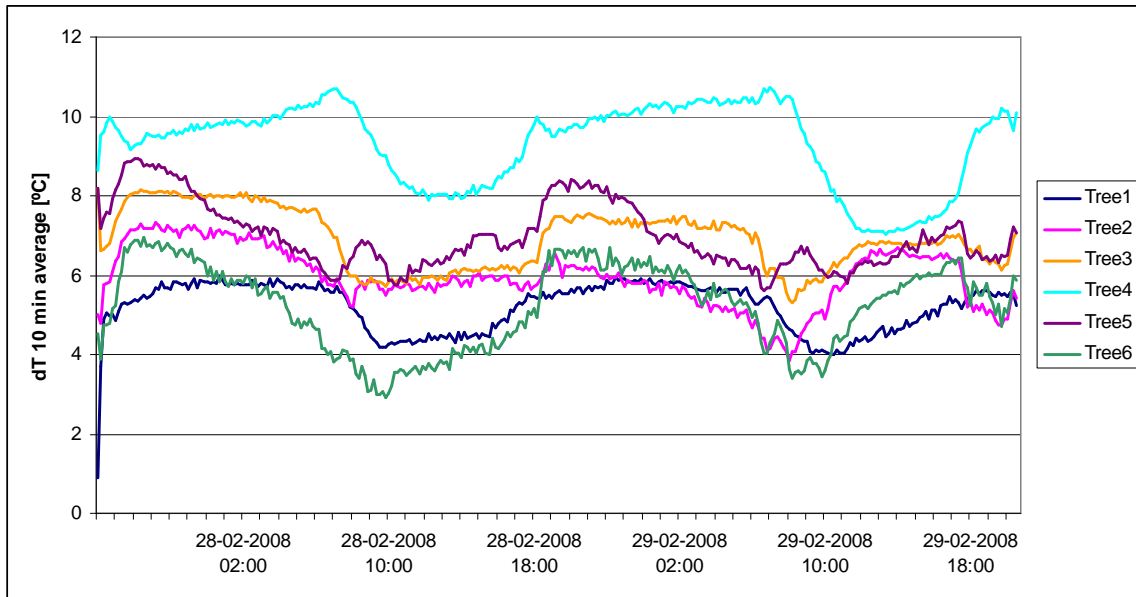


Figure 4-37: 10 minute averages of temperature differences between probes installed in six sample trees at site 6.

Sap flux density

As expected from the low quality of the raw data, the calculated sap flux densities vary a lot between trees and between days. Daytime averages range from 0.0 to 42.4 cm h^{-1} . These figures are considered very uncertain, and there is no correlation between days, DBH or A_B and sap flux density.

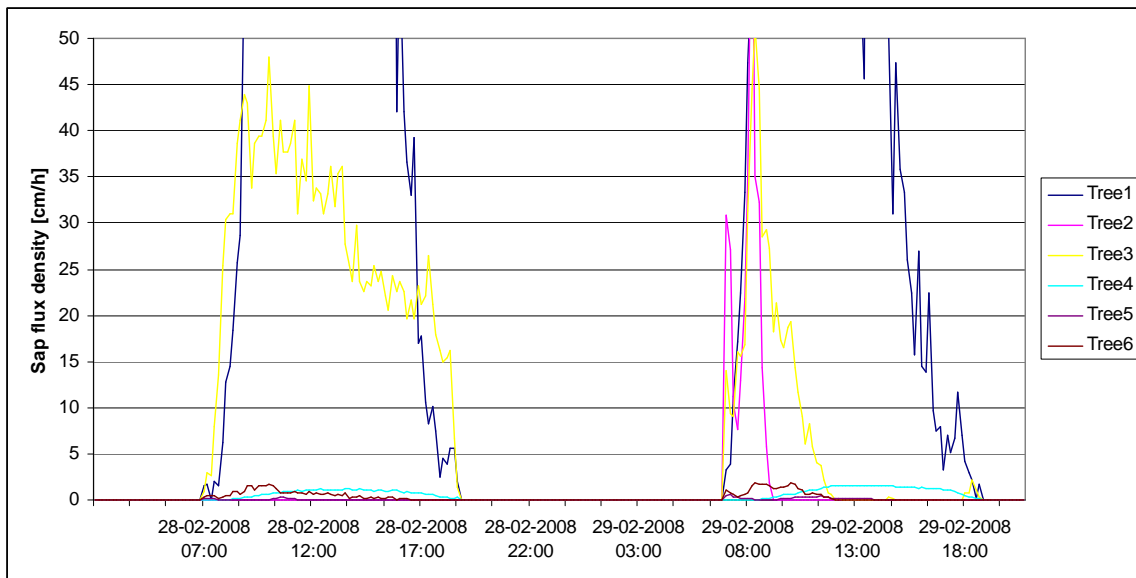


Figure 4-38: Calculated sap flux densities for six sample trees at site 6. Values for tree 1 reach up to 609 cm h^{-1} .

Tree and stand transpiration

Whole tree and sT rates can be seen in Table 4-6 and Table 4-7, respectively. As mentioned above, these figures are considered highly uncertain.

Table 4-6: Calculated whole tree daily transpiration for six sample trees at site 6.

		Tree1	Tree2	Tree3	Tree4	Tree5	Tree6
DBH [cm]		9.6	12.1	47.1	12.6	14.2	11.6
F [L day ⁻¹]	28-02-2008	26.4	0.0	54.3	0.8	0.0	0.2
	29-02-2008	23.6	0.0	1.0	1.2	0.1	0.1

Table 4-7: Estimated daily transpiration rates from stand at site 5 using two biometric parameters: DBH and A_B .

Date	T [mm day ⁻¹]	
	B=DBH	B= A_B
28-02-2008	1.0	1.1
29-02-2008	0.3	0.3

4.6.5 Site 7

Data recorded at site 7 was inspected after 48 hours, and it was found that the noise problems from previous sites were substantially reduced but three out of six sample trees were showing highly unexpected trends, as can be seen in Figure 4-39. Since there could be found no immediate explanation to this phenomenon and time for field work was running out, the setup was taken down already after these 48 hours. Consequently the probes and dataloggers were tested and found to be working properly (see Appendix H). Similar “reverse” patterns were observed at site 8, where they were found to correlate with the leaf shedding stage of the trees (see section below). The data was not further processed and the vegetation at the site was not characterized.

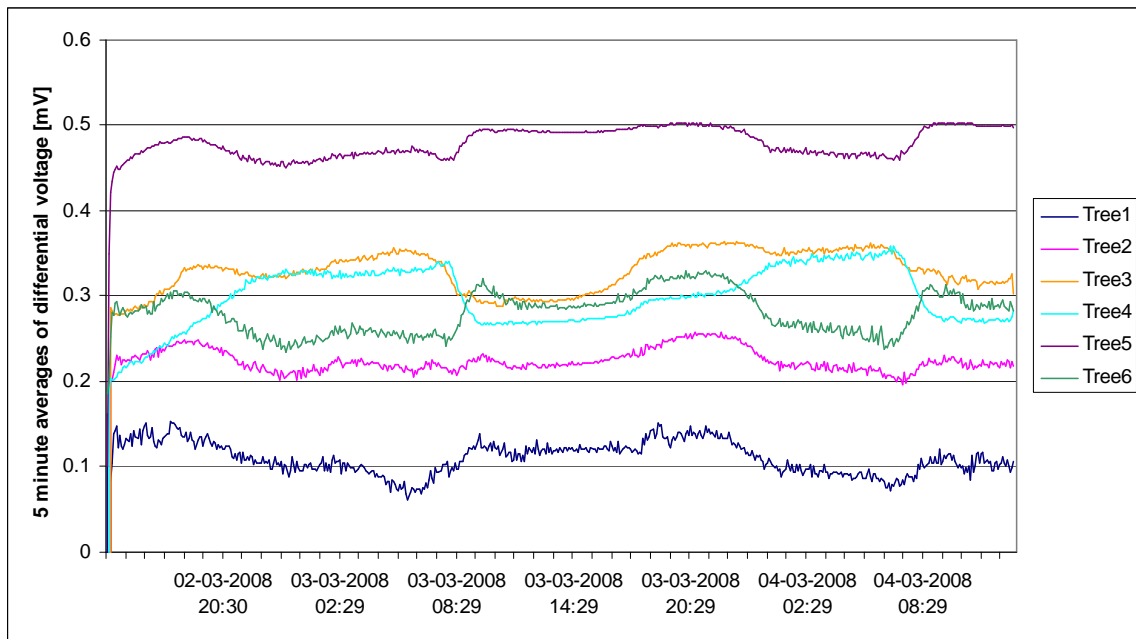


Figure 4-39: Raw measured differential voltages for six sample trees at site 7.

4.6.6 Site 8

Site 8 was installed on March 5th and left to be taken care of by local collaborators from ASK. Unfortunately, due to technical problems it has not yet been possible to extract data from the datalogger. The only data extracted is after the first 24 hours, which can be seen in Figure 4-40.

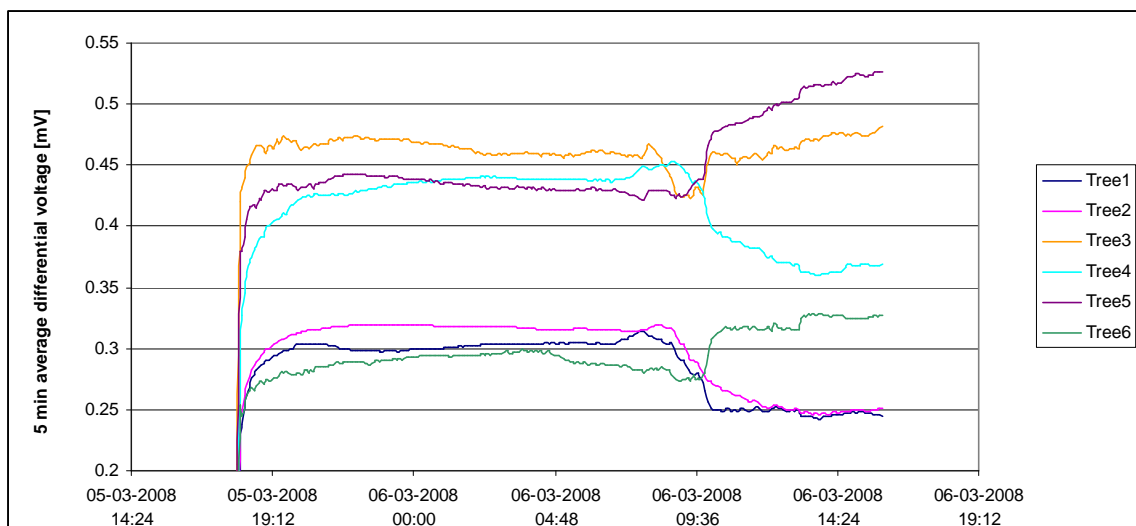


Figure 4-40: Raw measured differential voltages for six sample trees at site 8.

The tree composition and density at site 8 resembled those at sites 3-5, as expected. 205 individual trees of a DBH larger than 3.2 cm were counted within a plot of approximately 1200 m² (0.17 trees m⁻²). The biggest tree had a DBH of 78.0 cm and the mean DBH was 10.1 cm. The trees belonged to 39 different species, of which three were very dominant: *Gymnanthes lucida* (42), Lu'umché (name in Maya, Latin name unknown) (23) and Pukutzikil (name in Maya, Latin name unknown) (21). Depth of sapwood was only measured for two trees.

4.6.7 Summary

Trees

Tree densities at sites 3-5 and 8 were very similar, between 0.17 and 0.21 individuals of DBH larger than 3.2 cm per square meter. Size distribution was also quite similar, with most trees in the DBH category 5-10 cm and very few above 20 cm.

Sapwood depth was measured in 20 trees at four sites. As mentioned in Section 3.4.1, the method used for determining sapwood depth has some uncertainties. In Figure 4-41 the measured sapwood depths are plotted against the trees' DBH together with an empirical function derived by Meinzer et al (2001). Meinzer et al (2001) studied the relation between DBH and sapwood cross-sectional area, sapwood depth and sap flow density in 27 different tropical tree species in Panama. They found that DBH accounted for 98% of variation in A_{SW} and 67% of the variation in d_{SW} and fitted the presented curve to their data. It is obvious that the xylem depths estimated in this project are considerably lower than expected, the only exception being the three trees at site 6 for which it seemed that the whole radial xylem profile was active. Also Granier et al (1996b) in tropical trees in French Guiana measured deeper sapwood than found here, his results varying between 3.5 and 5.0 cm for trees with a DBH between 10 and 60 cm.

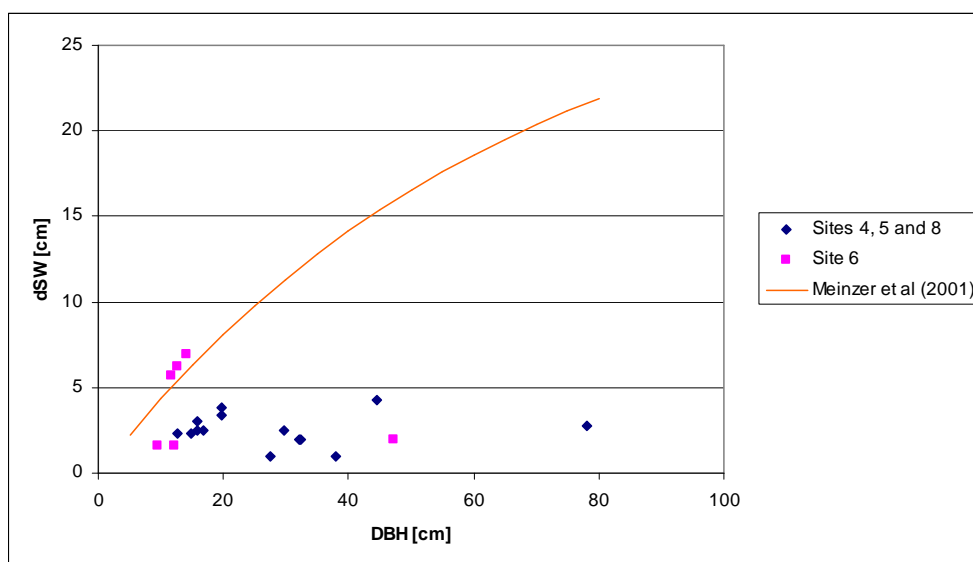


Figure 4-41: Measured sapwood in 20 different trees at four different sites together with a function relating sapwood depth to DBH derived by Meinzer et al (2001).

Sap flux densities

Average daytime sap flux densities at sites 4-6 varied approximately between 3 and 30 cm h^{-1} . Granier et al (1996b) reported sap flux densities between 10 and 40 cm h^{-1} , Meinzer et al (2001) between 5 and 25 cm h^{-1} , and Wu et al (2006) between 2 and 26 cm h^{-1} (all three studies done in tropical forests).

Tree and stand transpiration

Individual tree transpiration varied between 0.0 and 54.3 L day^{-1} for the low NDVI site to between 2.8 and 265.4 L day^{-1} for the high NDVI sites. Variations in daily tree sap flow of one order of magnitude between trees at same site are abundant in the literature (e.g. Granier, 1987,

4 Results

Köstner, 1992). Granier et al (1996b) found tree sap flow values on the order of 250-300 L day⁻¹ for large tropical trees in French Guiana. Meinzer et al (2005) summarized sap flow data for 18 tropical species of variable sizes from Panama and Brazil and found daily transpiration rates from near 0 to more than 800 L day⁻¹, with the trees of DBH below 20 cm mostly losing less than 100 L day⁻¹.

Calculated sT varied between 0.3 and 1.1 mm day⁻¹ for the low NDVI site to between 3.0 and 6.9 mm day⁻¹ for the high NDVI sites. Average daily pan evaporation calculated from the monthly mean pan evaporation climatic normal for February (calculated from the data presented in Section 1.3.3) at Chetumal and Merida is 4.6 and 5.0 mm day⁻¹, respectively. In this context a sT rate of 6.9 mm day⁻¹ seems unreasonably high but the remaining estimates are not unrealistic.

At site 4 DBH as scaling parameters yielded higher results than A_B, while at site 5 it was opposite, and at site 6 there was no significant difference. In the following the results for A_B as scaling factor are used.

Sites 4 and 5 were chosen as representative of high NDVI areas and are located close to each other (at a distance of ca. 42 km), therefore it was expected that sT rates would be similar, which is also the immediate impression from the results. A t-test shows that there is low probability that the mean of sT estimates at site 4 is significantly different from the mean site 5 (p-value of two-tailed t-test assuming equal variances is 0.35). However, the fact the means cannot be considered different is to a high degree a result of the large spread in the few data points at each site, which can be attributed both to measurement uncertainties as well as the influence of probable variability in driving forces of evaporation (climatic parameters) from day to day.

Site 6, chosen as representative of low NDVI areas, was expected to show lower sT rates than at sites 4 and 5, again confirmed by the immediate impression from the results. Indeed statistical comparison of sT means between site 6 and sites 4 and 5 does support the hypothesis that site 6 mean is significantly lower than at sites 4 and 5 (p-values of single-tailed t-tests are 0.004 and 0.03, respectively). However, the very low results for site 6 could be a result of the low data quality due to the technical problems with the datalogger at this site.

4.7 Comparison of actual evapotranspiration estimates from the triangle method and stand transpiration estimates from sap flow measurements

Estimates of aET in three specific pixels encompassing three sites of sap flow measurements (site 4 in X:240 Y:265, site 5 in X:281 Y:252 and site 6 in X:84 Y:119) for four triangle-method-successful days around February 2008 (January 29 and 31, February 25 and March 15) are shown in Figure 4-42, together with sT estimated from sap flow measurements at these sites on eight different days. Unfortunately, none of the sT estimate days coincide with aET estimate days. There was no valid pixel value for X:84 Y:119 on March 15, and only two days of useful data at site 6.

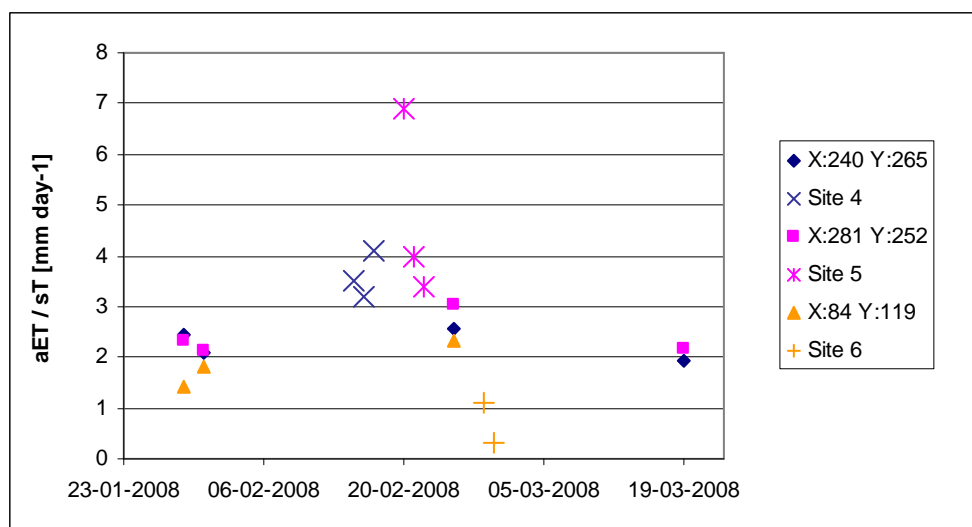


Figure 4-42: Estimated aET [mm day^{-1}] for three pixels (indicated by image sample number (X) and line number (Y)) which encompassing the locations of three sap flow measurement sites (number 4-6), whose location is indicated in Figure 4-22 (first figure in sap flow results section).

From immediate view of the figure it seems that sT estimates are much more “extreme” than aET estimates, yielding higher results for sites 4 and 5 and lower results for site 6. It was possible to show that statistically the mean sT at site 6 is lower than the mean sT at sites 4 and 5 (see Section 4.6.7). aET estimates for pixel X:84 Y:119 are lower than in pixels X:240 Y:265 and X:281 Y:252 on all three days, but the difference seems less pronounced. Statistics were used again to examine the differences, between pixels and between pixels and sites.

First a t-test was used to investigate whether the mean aET in X:240 Y:265 is significantly different from the mean in pixel X:281 Y:252, and it showed that they can be considered equal (p-value of two-tailed t-test assuming equal variances is 0.53).

Second, it was investigated whether the mean of pixel X:84 Y:119 is lower than the mean of pixels X:240 Y:265 and X:281 Y:252. Comparing each of the high NDVI pixels with the low NDVI pixel shows that at a significance level of 95% the means cannot said to be different, although a significance level of 90% would make it a reasonable statement (p-value of single-tailed t-tests for both pairs is 0.07). When pooling data for X:240 Y:265 and X:281 Y:252 together and comparing with X:84 Y:119 it would be reasonable to believe that the means are

significantly different (p-value 0.04), but the pooling somewhat violates the assumption of independence in the samples.

This can be considered to indicate that the triangle method and sap flow measurements agree that evapotranspiration at sites 4 and 5 is generally higher than at site 6, which is also in agreement with prior expectations.

Finally it was investigated whether the sT and aET estimates at the different sites/pixels could be considered directly comparable. Comparison of mean aET in pixel X:240 Y:265 and mean sT at site 4 suggests there is a significant difference, while mean aET in pixel X:281 Y:252 and mean sT at site 5 can be considered equal (p-values using a two-tailed t-test assuming different variances are 0.02 and 0.17, respectively). An ANOVA (analysis of variance) of sites 4 and 5 and their respective pixels suggests that they are statistically different (p-value equals 0.02), as is the case when pixels values are pooled together and compared with pooled sap flow values (t-test p-value is 0.02). Comparison of mean aET in pixel X:84 Y:119 and mean sT at site 6 suggests that there is no significant difference (p-value of two-tailed t-test assuming different variances is 0.14).

This can be considered to indicate that the triangle method and sap flow measurements results agree on the quantitative order of magnitude of evapotranspiration at site 5 and site 6. However, it must be kept in mind that the comparison is done between the mean of values for several days spread within a month and a half and not coinciding for the two methods. Thus the natural (weather driven) variability in ET is a strong factor contributing to the large spreading in the sample data. Another important contributor to data spreading is the uncertainties in the estimates of sap flow and scaling to sT. The large spreading in the data makes it more difficult to statistically prove differences between samples.

5 Discussion

Maps of estimated aET for the Yucatan Peninsula for 29 days in 2007 and 23 days in the first four months of 2008 were produced in this project, by using the triangle method slightly modified from Jiang and Islam (2001) with data from MODIS and ECMWF. It is, however, not clear how reliable these maps are.

The triangle method is basically an empirical method, although it does include theoretical considerations. In the cases described in the literature it has shown reasonable results when comparing with ground observations, but it cannot be said to have been proven to be a reliable method in all possible settings. Furthermore, the Yucatan Peninsula does not fulfill all the requirements for a study area as set by the method developers.

First, it does not include the desired complete variability in land cover: there is an overweight of dense vegetation pixels and very few pixels with low vegetation cover, probably none with bare soil and certainly not the whole range of soil moisture situations from dry to wet bare soil. This is the reason for the absence of a clear triangle/trapezoid shape in the scatter plots, where pixels at best “fill up” half of the imaginary triangle and the rest is left for interpolation/imagination. The situation changes over the year – it seems that in the dry season the variability is higher and in the rainy season it is lower, altering one of the main parameters which are fundamental for application of the method. It could be argued that the theoretical foundation of the triangle, i.e. the relation between surface temperature, vegetation density and partitioning of available energy at the surface, is sustainable also in a narrower range of land cover situations. But the concept of the triangle does not hold in the case of Yucatan. Hence, application of the theory requires development of a new concept for defining the extremes of EF, in the absence of extreme low soil cover, and for interpolating between them.

Second, it seems that there are no completely clear-sky days over Yucatan. Unlike some semi-arid areas the Yucatan Peninsula almost always has some clouds drifting by, also in the dry season. The presence of clouds not only decreases the availability of LST data but also affects the energy balance at the surface. This introduces a complication compared with situations where cloud free conditions allow the assumption that the whole study area received equal amounts of incoming radiation and that an instantaneous image of LST is representative of the whole day.

Third, the peninsula is rather flat but there are a few areas where the terrain has considerable slopes, but the effects of this have not been addressed in the current study.

Due to the empirical nature of the triangle method it is hard to estimate the effect of these disruptions, which associates a rather large uncertainty to the results. To increase reliability, the results need to be compared with observations. Strictly speaking there is no direct method for observing evapotranspiration, certainly not on a larger scale - the most direct method would be lysimeters, but they are very small. The method used for validation should ideally have the same spatial and temporal distribution as the RS images, but this is not feasible. Any ground observation is basically a point observation, which under certain conditions can be assumed to represent a larger area, at best at the scale of a pixel. It is necessary to have results from several, or at least two, such ground observation locations at several, or at least two, moments in time in order to account for the variability in time and space of aET as captured by the triangle method.

The attempt to use sap flow measurements for validation purpose proved to have several limitations. Set aside the intrinsic uncertainties of the method, which are discussed below, the

usefulness of the sap flow results obtained suffers from the discrepancy in time of observation. Considering the unstable weather with variable cloud cover and precipitation within the period considered (late January to early March 2008), stable aET rates from day to day cannot be assumed, and therefore the results cannot be compared directly. Even if a day of successful aET estimates coincided with a day of successful sT estimate, this would give only one point of comparison and could not be used to deduce directly about the reliability of estimates in other pixels.

Several uncertainties associated with the sap flow measurements were found, some related to the interpretation from measured temperature differences to sap flows, and some to the scaling from individual trees' sap flow to sT. A major source of uncertainty in the first group is the sapwood depth, which affects both the interpretation of sap flux density and the total sap flow. Another possibly important factor is the radial variability in sap flux density, which, depending on its magnitude, could cause significant errors in the calculation of sap flow. These uncertainties are probably more significant than usual due to the longer probes used (5 cm compared to 1-3 cm in most studies), especially since they were often longer than the measured sapwood depth. The lack of correlation between sap flux densities, sap flows and tree size is distressful.

The scaling to sT was done with a very simplified approach which is expected to result in some bias. Also, when comparing the sT results with aET, there is uncertainty related to the possible evaporation from canopy interception and from bare soil and understory vegetation. The latter are expected to be significant at site 6, while the former could be significant at sites 4 and 5.

A sensitivity analysis would be appropriate in order to quantify the uncertainty in results arising from uncertainty in measurement of sapwood depth, sap flux density etc. This was not done due to time limitations. It could also have been interesting to use some climatic variables to see if there is a correlation with variations in levels of sap flow measured on different days at the same site. A very careful estimate of the uncertainty in sT values would be 50-100%.

If sap flow measurements were to be used as a reliable source of sT estimates for comparison with aET estimates, several improvements to the method as applied in this project would be necessary. First, a more practical and accurate method for measuring sapwood depth is necessary. Second, the probes should be shorter, preferably 2-3 cm. It would be ideal with some probes of 1 cm length too, which could be inserted at variable depths to quantify radial variation and develop a model for accounting for such variation. Third, the number of probes installed simultaneously should be at least twice the current number, to better account for the variability in tree species and sizes, and a statistically based sampling strategy should be developed for each site in order to improve the scaling procedure. A more thorough investigation of the vegetation distribution might locate large patches of more mature forest (where the tree variability is lower). Finally, an installation should be set to run for longer time periods in order to increase the probability of having coinciding days of RS and ground measurements.

Despite the limitations of the sap flow method and the uncertainty of the results, estimates of sT were compared with aET estimates. Statistic analysis supports the hypothesis that the mean of sT observations at site 5 is not significantly different from the mean of aET estimates for the encompassing pixel (on different days within the same period), and the same is true for site 6 and its encompassing pixel, though not for site 4. Mean sT for site 5 is significantly higher than mean sT at site 6, and mean aET in the pixels encompassing sites 4 and 5 is significantly higher than mean aET in the pixel encompassing site 6. These statistics reflect the large spreading in the data points, but they show an agreement on the relative magnitude of evaporation between the results of the triangle method and the results of the sap flow measurements. It should be kept

in mind that this is based on mean values of a single period in time at two specific sites at the extremes of the evaporation range on the peninsula; this comparison does not allow making general conclusions on the quality of the aET maps.

The ideal means of getting ground observations for validating aET estimates would be the eddy covariance method. There is currently no flux observation tower installed on the peninsula (at least not any registered by the global network FLUXNET – the nearest points are in Florida, West Mexico and Costa Rica (ORNL, 2008)). The forest on the Yucatan Peninsula is considered a secondary forest while the preferred forest type for FLUXNET is primary (unaffected by human activities), but the relative homogeneity of the forest (on the scale of flux footprint sizes) seems quite appropriate. The options for setting up a flux tower in collaboration with other institutes should be investigated – flux tower measurements are relevant for many different study fields, and Risø is an obvious possible partner. It is probably not economically realistic to install more than one flux tower on the peninsula, but this would still be very useful. It will not be able to account for spatial variation, but the data continuity over time will be able to show whether the triangle method results reflect the right variation over time (the scale of variation in time at an appropriate site on the peninsula could be assumed similar to the scale of variation in space across the peninsula).

The aET results for 29 days in 2007 are not enough for use as input to a groundwater model. They probably do not represent the average evaporation, since that would imply a yearly aET for the peninsula which is almost as high as the yearly average precipitation. The estimates for these days are either too high or represent days of higher aET than the average, which is not unreasonable to assume since they probably represent days of lower cloud cover. This could be tested by comparing them with potential/reference evapotranspiration (PET) estimates. If it proves that there is a pattern of crop coefficients (K_c), and that days of aET estimates correspond to days of high PET, this would increase the reliability of the results. It would also provide a means of using the results to produce year-round estimates of aET using the concept of PET and K_c . It would probably be necessary to include more years in such analysis before a clear K_c pattern can be extracted, but the triangle method as applied in this project can be easily extended to longer periods.

An option for getting more “successful” days would be to use meteorological satellite data as done by Stisen et al (2008). This is expected to increase the number of days where LST data is available, although it will probably still not be enough to cover the whole year. The GOES East satellite operated by NOAA includes the Yucatan Peninsula and has three channels in the relevant thermal infrared range, which could be used for deriving surface temperatures (CLASS, 2008). Data for the “extended northern hemisphere” is acquired every 30 minutes, with a nominal square IGFOV (Instantaneous Geometric Field Of View) of 4 km at nadir, and available for public use through CLASS. However, the data is delivered in a complex format and almost-raw quality, thus requiring significant preprocessing before applicable in the triangle method.

There are several other options for improving the triangle method as applied in this project, which should be tested when a means of validation is found. If the source of surface temperature remains MODIS LST, it should be considered to normalize the temperature axis, and the view time of both night and day images should be analyzed. It is suspected that the viewing time is not equal for the whole peninsula and changing from day to day, which may contribute to explain the unexpected shape of the $\Delta LST/NDVI$ scatter on some days. It could also be tested if LST data can be used to estimate air temperatures for calculating $\Delta/(\Delta+\gamma)$, or maybe air temperature data from the ECMWF archive could be used.

Regarding the NDVI axis, it could be changed to e.g. EVI (enhanced vegetation index, a MODIS product). The motivation for changing to EVI would be that it was designed to improve sensitivity in high biomass regions, which is very relevant for the dense vegetation on Yucatan. Wang et al (2006) claim that the vegetation index does not have a significant impact on results from the triangle method, but the case of Yucatan is significantly different from other areas where the triangle method has been implemented before.

Estimation of the available energy at the surface was done in a very rough manner, and if the method results are to be used operationally it would probably be a good idea to improve this parameter. Furthermore, the question of time scale should be investigated thoroughly: the aim is to obtain daily (i.e. 24 hours integrated) actual evapotranspiration, but the triangle method is basically designed to estimate instantaneous EF. What can be done to turn this into a daily EF and what time scale of AE should be used? It would be an advantage if a source of ground measurements of net radiation and soil heat flux was found, thus AE estimates could be validated separately and allow for better evaluation of the isolated EF estimates.

Finally, it should be considered whether the triangle method is the most appropriate method for Yucatan. There are other methods in the literature for estimating actual evapotranspiration based primarily on RS data.

6 Conclusion

This project showed that it was possible to apply the triangle method to Yucatan to produce 29 maps of aET for the year 2007. However, given the lack of data to validate the results against, it is difficult to assess their reliability. The magnitude of the aET estimated is high; assuming the average of 2.99 mm day^{-1} represents the yearly average, the annual aET would be 1090 mm, which is close to the yearly precipitation. It is possible that the results do not reflect the annual average because the 29 days they are derived from days with lower cloud cover than the average. Another possibility is that the method is overestimating EFs because it does not capture the extremes of lowest and highest EF in each image correctly. This would be due to the fact that the scatter plots of ΔLST against NDVI did not resemble the triangle/trapezoid expected, which is attributed mainly to the fact that Yucatan does not feature the full variability in land cover that the triangle method requires. It is also possible that the high aET values are due to a bias in the estimation of available energy. The spatial distribution of aET/EF shows the pattern expected, with an overall trend of decreasing EF from southeast to northwest and maximum EF in wetlands. The distribution is more pronounced in the dry season than in the rainy season, which is also according to expectations. However, it could not be confirmed that the distribution is correlated with depth to the groundwater table.

Estimates of sT derived from sap flow measurements could not be used to directly validate aET estimates. First, because none of the days of successful sap flow measurements coincided with successful aET images. Second, because there were many uncertainties in calculating sap flows from the raw measurements and in scaling from trees to stand. The uncertainties in calculating sap flow are attributed mainly to uncertain measurements of sapwood depths, uncertain measurement of sap flux density (due to too long probes) and noise. Uncertainties in scaling are attributed mainly to non-representative sampling. Furthermore, discrepancies between aET and sT can be expected due to evaporation from canopy interception and bare soil, and evapotranspiration from understory (especially at low NDVI site).

Despite the uncertainties in sap flow results they were compared to aET results on the basis of periodic means. It was possible to statistically prove that both pixel aET and site sT in the corresponding pixels were higher at two high NDVI sites than at one low NDVI site, as expected. This is considered as a mild indication that the triangle method correctly captures the spatial variability in EF across the peninsula.

References

- Allen, G., Pereira L. S., Raes, D., Smith, M., 1998, Crop evapotranspiration - Guidelines for computing crop water requirements - FAO Irrigation and drainage paper 56, Rome, viewed on June 10, 2008, at <http://www.fao.org/docrep/X0490E/x0490e00.htm>
- AMS, 2008, Glossary of Meteorology by the American Meteorological Society, viewed on June 13, 2008 at <http://amsglossary.allenpress.com/glossary/browse?s=v&p=7>
- Bastiaanssen, W. G. M., Thiruvengadachari, S., Sakthivadivel, R., Molden, D. J., 1999, Satellite remote sensing for estimation productivities of land and water, Water Resources Developments 15:181-196, in Jiang and Islam (2001)
- Bauer-Gottwein, P., personal communication at DTU, 2008.
- Britannica Online, Wood, viewed on June 11, 2008 at <http://www.britannica.com/ebc/art-66141/Cross-section-of-a-tree-trunk>
- Carlson, T., 2007, an overview of the “Triangle Method” for estimating surface evapotranspiration and soil moisture from satellite imagery, Sensors 7:1612-1629
- CCRS, 2008, Tutorial: Fundamentals of remote sensing, The Canada Centre for Remote Sensing, viewed on June 13, 2008 at http://ccrs.nrcan.gc.ca/resource/tutor/fundam/index_e.php
- Cermak, J., Cienciala, E., Kucera, J., Lindroth, A., Bednarova, E., 1995, Individual variation of sap flow rate in large pine and spruce trees and stand transpiration: a pilot study at the central NOPEX site, Journal of Hydrology 168:17-27
- Cermak, J., Kucera, J., Nadezhdina, N., 2004, Sap flow measurements with some thermodynamic methods, flow integration within trees and scaling up from sample trees to entire forest stands, Trees 18:529-546.
- Cermak, J., Nadezhdina, N., 1998, Sapwood as the scaling parameter – defining according to xylem water content or radial pattern of sap flow?, Annales des Sciences Forestieres 55:509-521
- CLASS, 2008, Description of data available from GOES, a webpage under the Comprehensive Large Array –Data Stewardship System, viewed on July 9, 2008 at http://www.class.ncdc.noaa.gov/release/data_available/goes/index.htm
- Clearwater, M. J., Meinzer, F. C., Andrade, J. L., Goldstein, G., Holbrook, N. M., 1999, Potential errors in measurement of nonuniform sap flow using heat dissipation probes, Tree Physiology 19:681-687
- CNA, 2001, Capitulo II de: Actualizacion geohidrologica del acuífero de la zona norte del estado de Quintana Roo – Informe Final, Comisión Nacional del Agua - Infraestructura Hidraulica y Servicios

References

- CNA, 2008, Normales Climatológicas, online database of climatic products of the Servicio Meteorológico Nacional - Comisión Nacional del Agua, viewed on July 8, 2008 at <http://smn.cna.gob.mx/>
- Cocks, M., 2008, The Ecotree, educational webpage hosted by University of the Western Cape , viewed on June 11, 2008, at <http://www.botany.uwc.ac.za/ecotree/leaves/InsideLeaf2.htm>
- Cohen, Y., Cohen, S., Cantuarias-Aviles, T., Schiller, G., 2008, Variations in the radial gradient of sap velocity in trunks of forest and fruit trees, *Plant and Soil* 305:49-59
- Dagmar, B., 2008, Albedo, article in the online “encyclopedia of the earth” last updated March 19, 2008, viewed on June 10, 2008, at <http://www.eoearth.org/article/Albedo>
- Dingman, S. L., 2002, *Physical Hydrology*, 2nd Edition, Prentice-Hall, New Jersey.
- Drake, P. L., Franks, P. J., 2003, Water resource partitioning, stem xylem hydraulic properties, and plant water use strategies in a seasonally dry riparian tropical rainforest, *Oecologia* 137:321–329
- Dynamax, 2008, TDP brochure and manual, can be found on Dynamax Inc., homepage at <http://www.dynamax.com/tdp.htm>
- ENVI User’s Guide, 2007, Accompanying ENVI version 4.4, ITT visual information solutions
- EROS, 2007, FAQ on SRTM on webpage by Earth Resources Observation and Science – USGS, webpage last modified November 2007, viewed on July 9, 2008 at http://seamless.usgs.gov/faq/srtm_faq.php
- Gillies, R. R., Carlson, T. N., Cui, J., Kustas, W. P., Humes, K. S., 1997, A verification of the triangle method for obtaining surface soil water content and energy fluxes from remote measurements of the normalized difference vegetation index (NDVI) and surface radiant temperature, *International Journal of Remote Sensing* 18:3145-3166
- GO, 2008, Educational webpage on Remote Sensing from Geografforlaget, viewed on July 9, 2008 at <http://www.geografforlaget.dk/course/ENGLISH/basic/tele1.htm#udstrtemp>
- Gonzalez-Altozano, P., Pavel, E. W., Oncins, J. A., Doltra, J., Cohen, M., Paco, T., Massai, R., Castel, J. R., 2008, Comparative assessment of five methods of determining sap flow in peach trees, *Agricultural Water Management* 95:503-515
- Graham, L. E., Graham J. M., Wilcox, L. W., 2006, *Plant biology*, 2nd ed., Pearson Prentice Hall, Upper Saddle river NJ
- Granier, A., 1987, Evaluation of transpiration in a Douglas-fir stand by means of sap flow measurements, *Tree Physiology* 3:309-320
- Granier, A., Biron, P., Bréda, N., Pontailler, J. Y., Saugier, B., 1996a, Transpiration of trees and forest stands: short- and long-term monitoring using sapflow methods, *Global Change Biology* 2:265-274

- Granier, A., Huc, R., Barigah, S. T., 1996b, Transpiration of natural rain forest and its dependence on climatic factors, *Agricultural and Forest Meteorology* 78:19-29
- Granier, A., personal communication, e-mail sent in reply to a methodological question, June 19, 2008
- Harman, I. N., 2007, Canopy dynamics and the surface energy balance, Center for Australian Weather and Climate Research, viewed on June 10, 2008, at http://www.bom.gov.au/bmrc/basic/cawcr-wksp1/papers/Harman_CAWCR2007.pdf
- Howard, L., 2008, The Ripple electron microscope facility homepage at Dartmouth College, viewed on June 11, 2008, at <http://remf.dartmouth.edu/images/botanicalLeafSEM/source/16.html>
- Infoplease, 2008, a webpage viewed on July 8, 2008 at <http://www.infoplease.com/images/myucatan.gif>
- Jackson, R. B., Moore, L. A., Hoffmann, W. A., Pockman, W. T., Linder, C. R., 1999, Ecosystem Rooting Depth Determined with Caves and DNA, *Proceedings of the National Academy of Sciences of the United States of America* 96 :11387-11392
- Jacobsen, A., Hansen, B. U., 1999, Estimation of the soil heat flux/net radiation ratio based on spectral vegetation indexes in high-latitude Arctic areas, *International Journal of Remote Sensing* 20:445-461
- James, S. A., Clearwater, M. J., Meinzer, F. C., Goldstein, G., 2002, Heat dissipation sensors of variable length for the measurement of sap flow in trees with deep sapwood, *Tree Physiology* 22:277-283
- Jiang, L., Islam, S., 2001, Estimation of surface evaporation map over southern Great Plains using remote sensing data, *Water Resources Research* 37:329-340
- Köstner, B. M. M., Schulze, E. D., Kelliher, F. M., Holinger, D. Y., Byers, J. N., Hunt, J. E., McSeveny, T. M., Meserth, R., Weir, P. L., 1992, Transpiration and canopy conductance in a pristine broad-leaved forest of *Nothofagus*: an analysis of xylem sap flow and eddy correlation measurements, *Oecologia* 91:350-359
- Köstner, B., Granier, A., Cermák, J., 1998, Sapflow measurements in forest stands: methods and uncertainties, *Annales des Sciences Forestieres* 55:13-27
- Kustas, W. P., Daughtry, C. S. T., 1990, Estimation of the soil heat flux/net radiation ratio from spectral data, *Agricultural and Forest Meteorology* 49:205-223
- Kustas, W. P., Daughtry, C. S. T., Van Oevelen, P. J., 1993, Analytical treatment of the relationships between soil heat flux/net radiation ratio and vegetation indices, *Remote Sensing of environment* 46:319-330
- LPDAAC, 2008, Product description for V005 MOD13A2, viewed on June 27, 2008 at <http://LPDAAC.usgs.gov/modis/mod13a2v5.asp>

References

- McDaniel, A., 1997, Tree Roots – Where are they?, originally published in The Virginia Gardener Newsletter, viewed June 12, 2008, at <http://www.ext.vt.edu/departments/envirohort/factsheets2/tree/aug93pr1.html>
- McElrone, A. J., Pockman, W. T., Martínez-Vilalta, J., Jackson, R. B., 2004, Variation in xylem structure and function in stems and roots of trees to 20 m depth, *New Phytologist* 163: 507–517
- McMillin, L. M., 1975, Estimation of sea surface temperature from two infrared window measurements with different absorption, *Journal of Geophysical Research* 80:5113–5117
- Meinzer, F. C., Andrade, J. L., Goldstein, G., Olbrook, N. M., Cavelier, J., Wright, S. J., 1999, Partitioning of soil water among canopy trees in a seasonally dry tropical forest, *Oecologia* 121:29-301
- Meinzer, F. C., Bond, B. J., Warren, J. M., Woodruff, D. R., 2005, Does water transport scale universally with tree size?, *Functional Ecology* 19:558-565
- Meinzer, F. C., Goldstein, G., Andrade, J. L., 2001, Regulation of water flux through tropical forest canopy trees: Do universal rules apply?, *Tree Physiology* 21:19-26
- Mikkelsen, Teis, Senior researcher at the Biosystems Department, Risø DTU, personal comment made on May 23, 2008.
- Moran, M. S., Clarke, T. R., Inoue, Y., Vidal, A., 1994, Estimating crop water deficit using the relation between surface-air temperature and spectral vegetation index, *Remote Sensing of Environment* 49:246-263
- Motzer, T., 2004, Illustration of the heat dissipation method, viewed on July 8, 2008 at <http://www.geographie.uni-mannheim.de/inst/lpg/motzer/methodik.jpg>
- NASA, 2008, specifications sheet for MODIS, viewed on June 27, 2008 at <http://modis.gsfc.nasa.gov/about/specifications.php>
- Neuman, B. R., Rahbek, M. L., 2006, Modeling concepts for the sustainable management of the Sian Ka'an Biosphere Reserve, Quintana Roo, Mexico, MSc thesis at the Institute of environment and Resources, DTU.
- NIST, 1995, Type T Thermocouples - coefficients of approximate inverse functions, National Institute of Standards and Technology - an agency of the U.S. Commerce Department, viewed on June 22, 2008 at http://srdata.nist.gov/its90/type_t/tcoefficients_inverse.html
- Norman, J. M., Divakarla, M., Goel, N. S., 1995, Algorithms for Extracting Information from Remote Thermal-IR Observations of the Earth's Surface, *Remote Sensing of Environment* 51:157-168
- O'Grady, A. P., Cook, P. G., Howe, P., Werren, G., 2006, Groundwater use by dominant tree species in tropical remnant vegetation communities, *Australian Journal of Botany* 54:155-171

- ORNL, 2008, webpage of the global network of flux towers maintained by Oak Ridge National Laboratory – NASA, viewed on July 9, 2008 at <http://www.fluxnet.ornl.gov/fluxnet/index.cfm>
- Pal Arya, S., 2001, Introduction to Micrometeorology, 2nd Edition, Volume 79 in the International Geophysics Series, Academic Press, San Diego.
- Pidwirny, M., 2006, Net Radiation and the Planetary Energy Balance, in Fundamentals of Physical Geography, 2nd Edition, viewed on June 10, 2008 at <http://www.physicalgeography.net/fundamentals/7i.html>
- Pockman, W. T., McElrone, A. J., Bleby, T. M., Jackson, R. B., 2008, The structure and function of roots of woody species on the Edwards Plateau, Texas, USA, Eos Trans. AGU, 89(23), Jt. Assem. Suppl., Abstract H34A-02
- Price, J. C., 1990, Using spatial context in satellite data to infer regional scale evapotranspiration, IEEE Transactions on Geosciences and Remote Sensing 28:940-948
- Querejeta, J. I., Estrada-Medina, H., Allen, M. F., Jiménez-Osornio, J. J., 2007, Water source partitioning among trees growing on shallow karst soils in a seasonally dry tropical climate, Oecologia 152:26–36
- Rainforest Live, An educational website, viewed on June 12, 2008 at <http://www.rainforestlive.org.uk/media/Images/LAYER500copy.jpg>
- Ritchie, J. C., Rango, A., 1996, Remote Sensing applications to hydrology: Introduction., Hydrological sciences Journal 41:429-431
- Rzedowski, J., 1994, Vegetación de México, Editorial Limusa, México DF
- Sabins Jr., F. F., 1987, Remote sensing; principles and interpretation, W. H. Freeman, New York
- Sandholt, I., Rasmussen, K., Andersen, J., 2002, A simple interpretation of the surface temperature/vegetation index space for assessment of surface moisture status, Remote Sensing of environment 79:213-224
- Santanello, J. A., Friedl, M. A., 2003, Diurnal covariation in soil heat flux and net radiation, Journal of Applied Meteorology 42:851-862
- Saugier, B., Granier, A., Pontailler, J. Y., Dufrêne, E., Baldocchi, D. D., 1997, Transpiration of a boreal pine forest measured by branch bag, sap flow and micrometeorological methods, Tree Physiology 17:511-519
- Schultz, G. A., Engman E. T., (Eds.), 2000, Remote sensing in hydrology and water management, Springer-Verlag, Berlin Heidelberg
- SEMARNAP, 2000, digital map of land cover type from Secretaría de Medio Ambiente, Recursos Naturales y Pesca (today called Secretaría de Medio Ambiente y Recursos Naturales), obtained from Amigos de Sian Ka'an's GIS library.

References

- Short, N. M., 2008, The remote sensing tutorial, viewed on June 13, 2008 at <http://rst.gsfc.nasa.gov/Front/overview.html>
- Simon, R., 2007, Tropical deforestation, a feature on NASA's Earth Observatory internet publication, viewed on June 12, 2008 at <http://eobglossary.gsfc.nasa.gov/Library/Deforestation/index.html>
- Smith, D. M., Allen, S. J., 1996, Measurement of sap flow in plant stems, *Journal of Experimental Botany* 47:1833-1844
- Sobrino, J.,A., Romaguera, M., 2004, Land surface temperature retrieval from MSG1-SEVIRI data, *Remote Sensing of Environment* 92:247-254
- Stisen, S., Sandholt, I., Nørgaard, A., Fensholt, R., Jensen, K. H., 2008, Combining the triangle method with thermal inertia to estimate regional evapotranspiration - Applied to MSG-SEVIRI data in the Senegal River basin, *Remote Sensing of Environment* 122: 1242-1255
- Tucker, C. J., 1979, Red and photographic infrared linear combinations for monitoring vegetation, *Remote Sensing of Environment* 8:127-150
- UNEP-WCMC, 1996, Information sheet on the World Heritage Site Reserva de la Biosfera de Sian'Ka'an, online database maintained by United Nations environment Program – World Conservation Monitoring Centre, page last updated February 1996, viewed on July 7, 2008 at <http://www.unep-wcmc.org/sites/wh/sianka%27a.html>
- Wan, Z., 2006, MODIS LST products user's guide, viewed on June 30, 2008 at <http://www.icess.ucsb.edu/modis/LstUsrGuide/usrguide.html>
- Wang, K., Li, Z., Cribb, M., 2006, Estimation of evaporative fraction from a combination of day and night land surface temperatures and NDVI: A new method to determine the Priestley-Taylor parameter, *Remote Sensing of Environment* 102:293-305
- Wikipedia contributors, 2008a, Köppen climate classification, viewed on July 8, 2008 at http://en.wikipedia.org/wiki/K%C3%B6ppen_climate_classification
- Wikipedia contributors, 2008, Tropical and subtropical moist broadleaf forests, viewed on June 11, 2008, at http://en.wikipedia.org/w/index.php?title=Tropical_and_subtropical_moist_broadleaf_forests&oldid=217919874
- Williams, D. (responsible officer), 2008, Landsat 7 science data users handbook, NASA, viewed on June 12, 2008 at http://landsathandbook.gsfc.nasa.gov/handbook/handbook_toc.html
- Wu, W., Hall, C. A. S., Scatena, F. N., Quackenbush, L. J., 2006, Spatial modeling of evapotranspiration in the Luquillo experimental forest of Puerto Rico using remotely-sensed data, *Journal of Hydrology* 328:733-752

List of abbreviations

A _B	Basal area of tree trunk
AE	Available energy
aET	Actual evapotranspiration
ANOVA	Analysis of Variance
AVHRR	Advanced Very High Resolution Radiometer
CV	Coefficient of variance
DBH	Diameter at breast height
DE	Dry edge
DEL	Dry edge line
DEM	Digital elevation map
DMI	Danish Meteorological Institute
ECMWF	European Centre for Medium Range Weather Forecast
EF	Evaporative fraction
EO	Earth observation
ET	Evapotranspiration
G	Ground heat flux
GOES	Geostationary Operational Environmental Satellite
H	Sensible heat flux
IGFOV	Instantaneous Geometric Field Of View
LE	Latent heat transfer
LST	Land surface temperature
MODIS	MODerate-resolution Imaging Spectroradiometer
MRT	MODIS Reprojecting Tool
MSG-SEVIRI	Meteosat Second Generation Spinning Enhanced Visible and Infrared Imager
MSS	Multispectral scanners

List of abbreviations

NDVI	Normalized difference vegetation index
NIR	Near infrared
NOAA	National Oceanic and Atmospheric Administration
PBL	Planetary boundary layer
PET	Potential/reference evapotranspiration
ROI	Regions of interest
RS	Remote sensing
SAVI	Soil-adjusted vegetation index
SGP	Southern Great Plains
SRTM	Shuttle Radar Topography Mission
SSR	Surface solar radiation
sT	Stand transpiration
STR	Surface thermal radiation
SVAT	Soil vegetation atmosphere transfer
TDP	Thermal dissipation probe
UNAM	Universidad Nacional Autónoma de México
WDI	Water deficit index
WE	Wet edge
WEL	Wet edge line

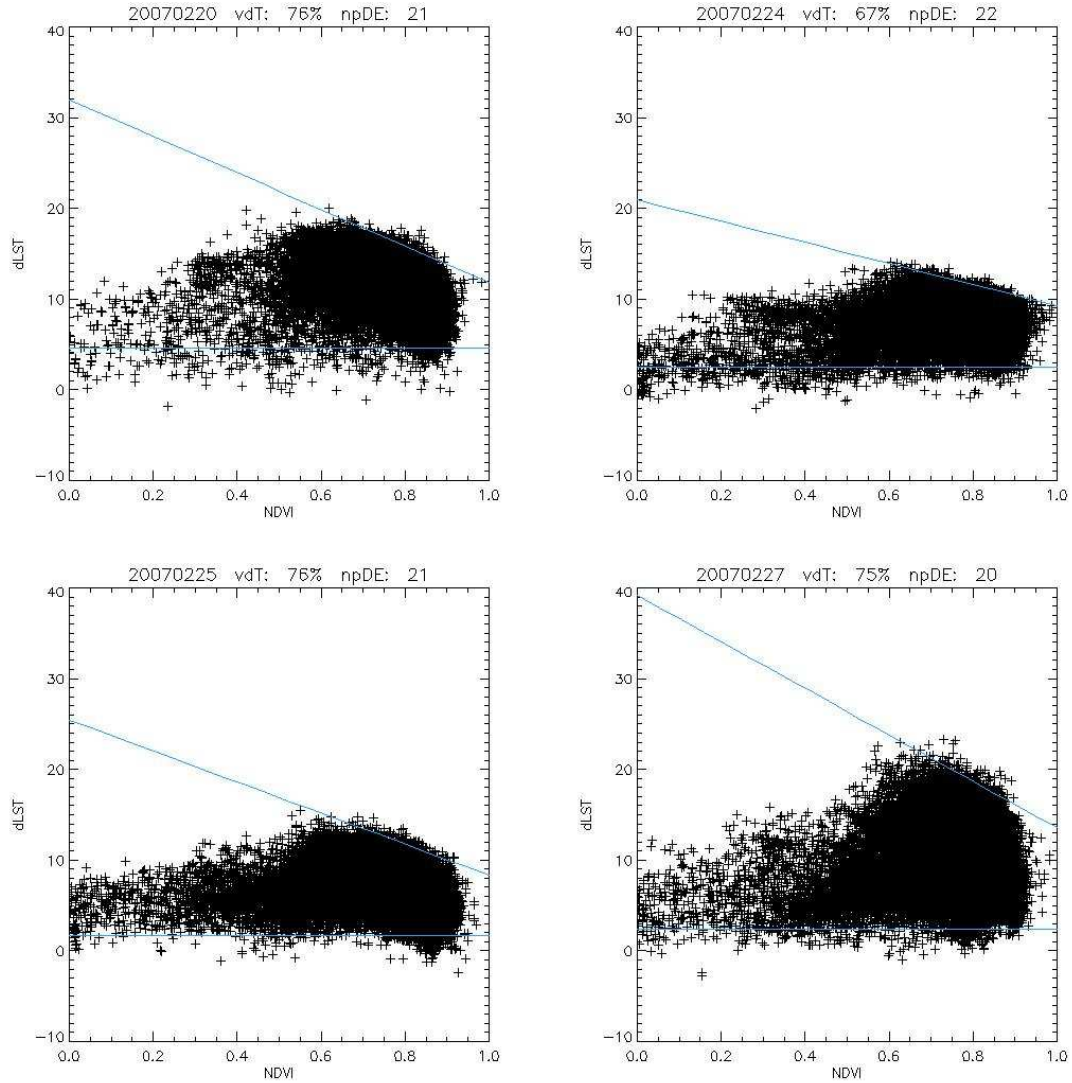
Appendix E

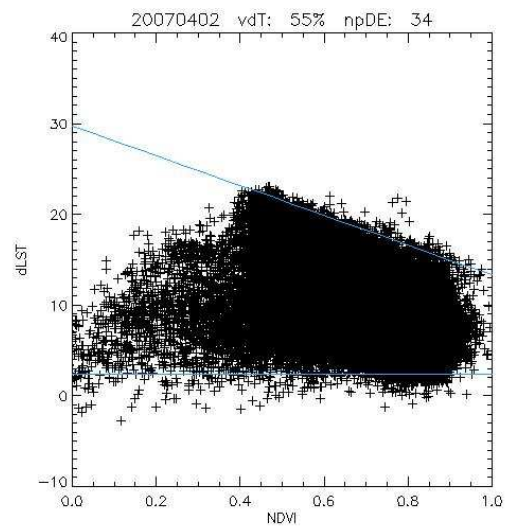
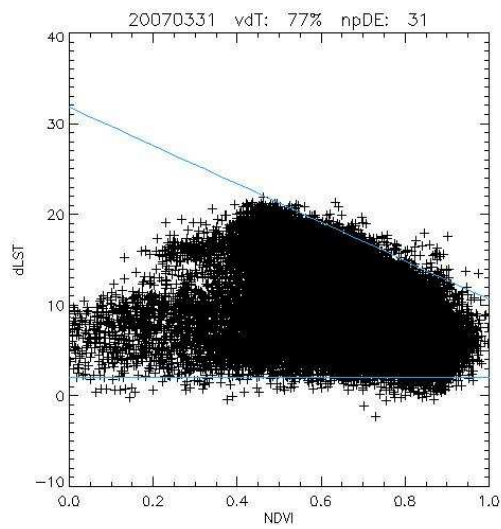
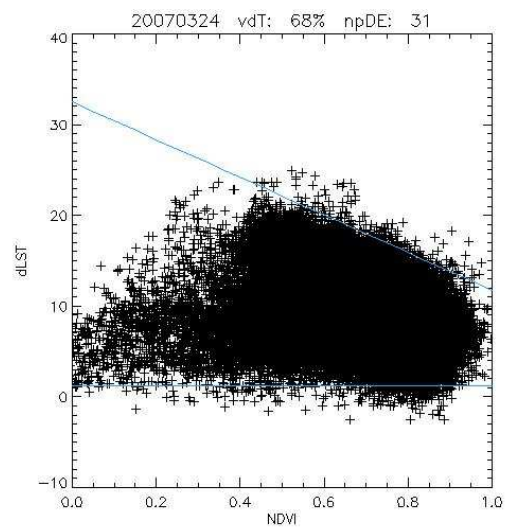
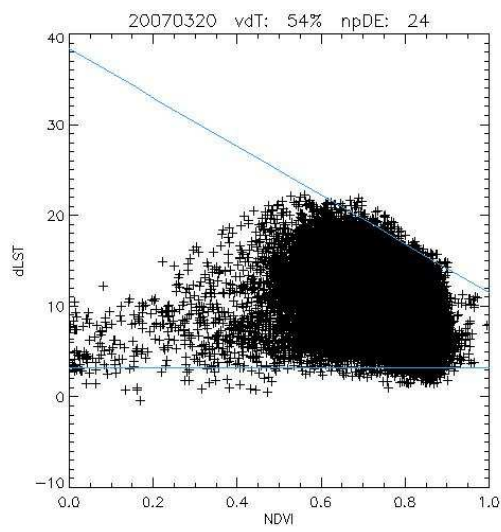
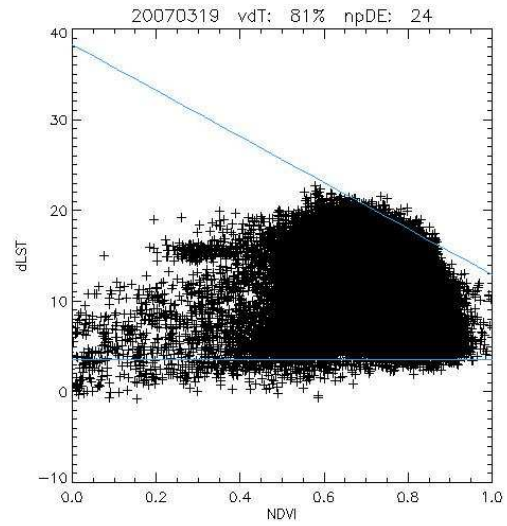
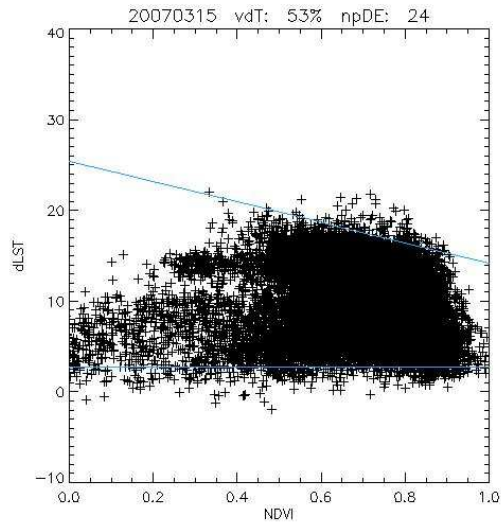
Coefficients for polynomial function translating thermocouple type T differential voltage into temperature for the temperature range 0 to 400 °C (used in Equation 3-12) (NIST, 1995):

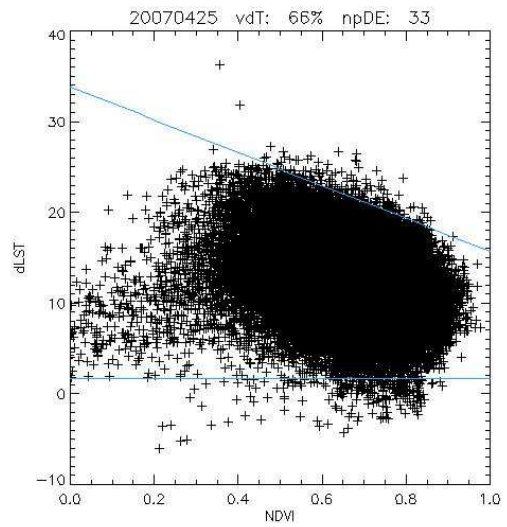
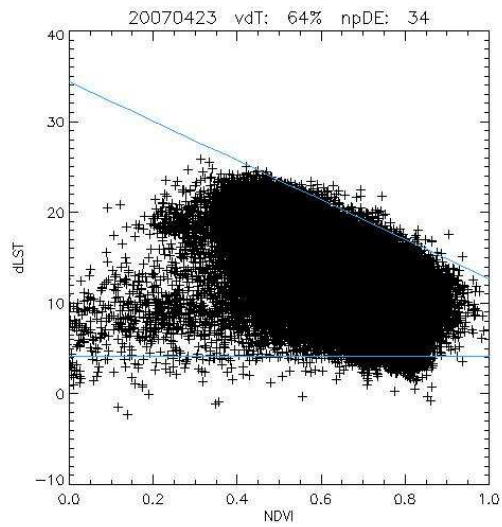
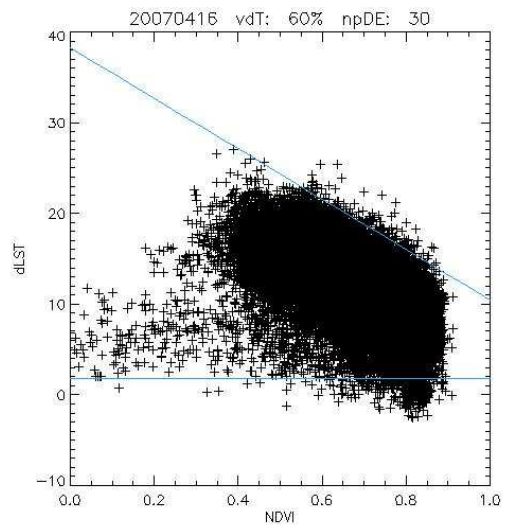
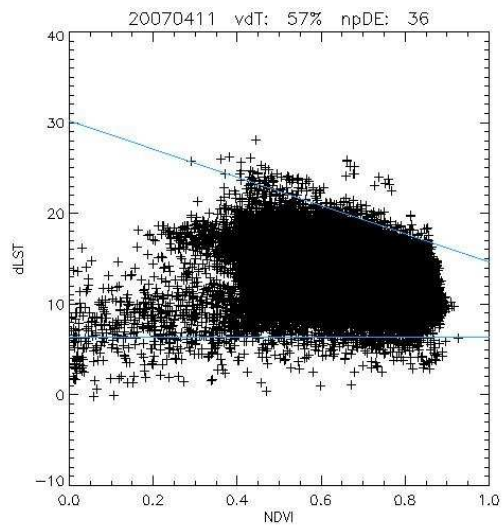
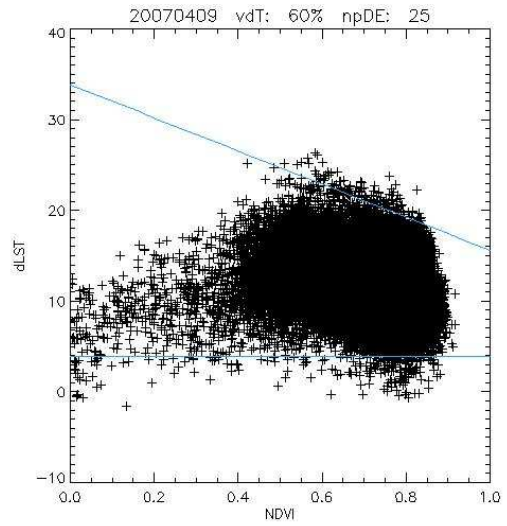
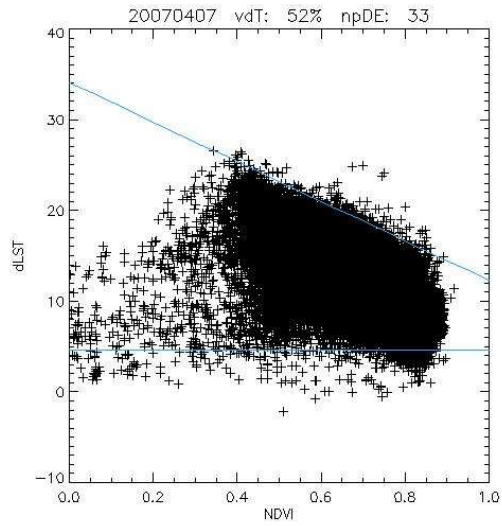
a_0	0
a_1	2.5928E-1
a_2	-7.602961E-1
a_3	4.637791E-2
a_4	-2.165394E-3
a_5	6.048144E-5
a_6	-7.293422E-7

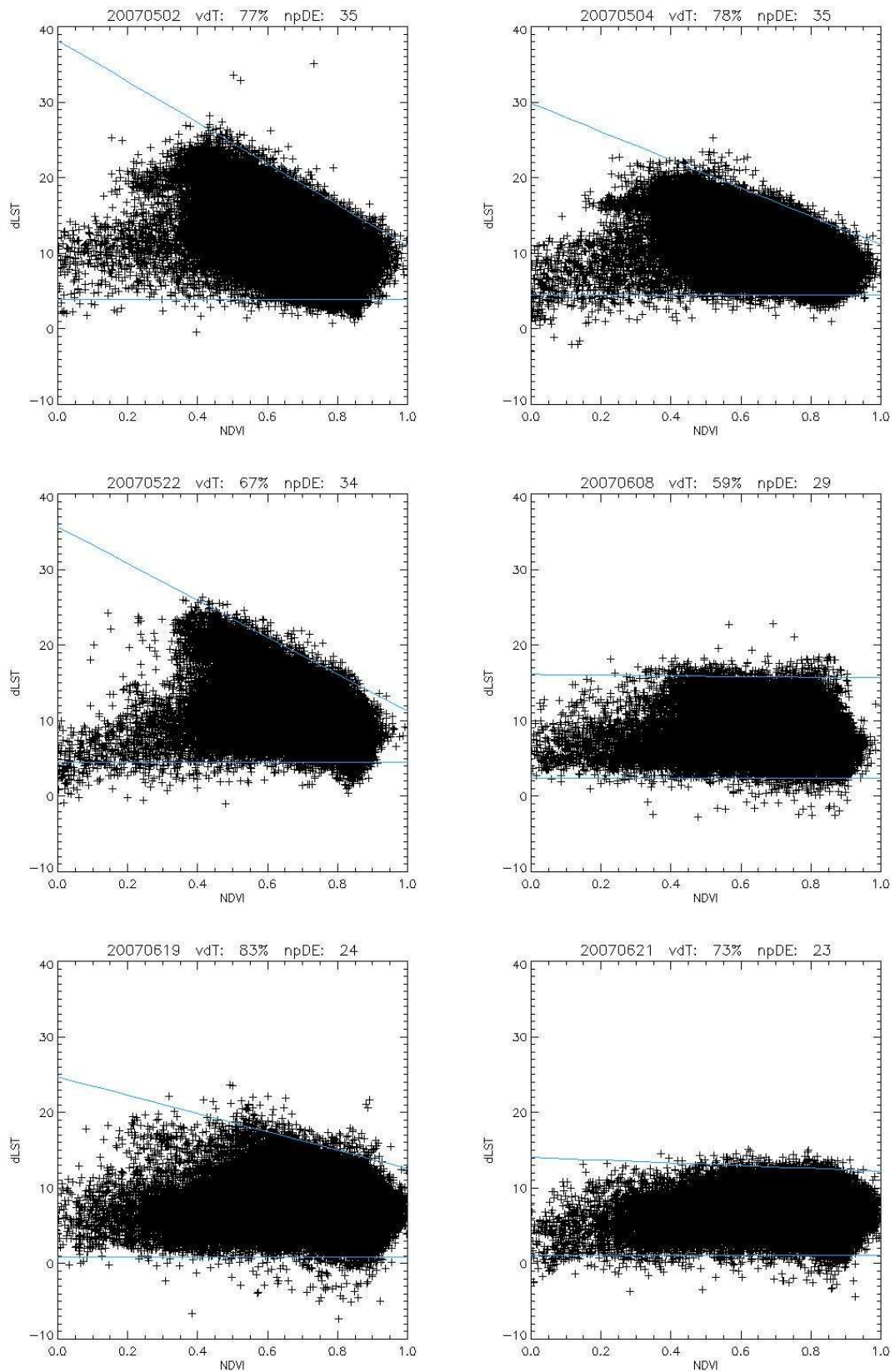
Appendix F

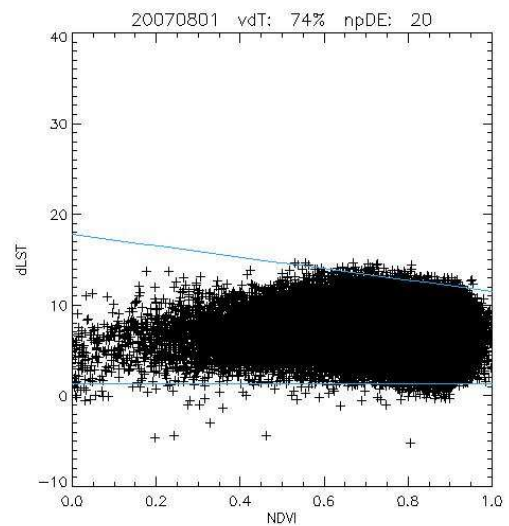
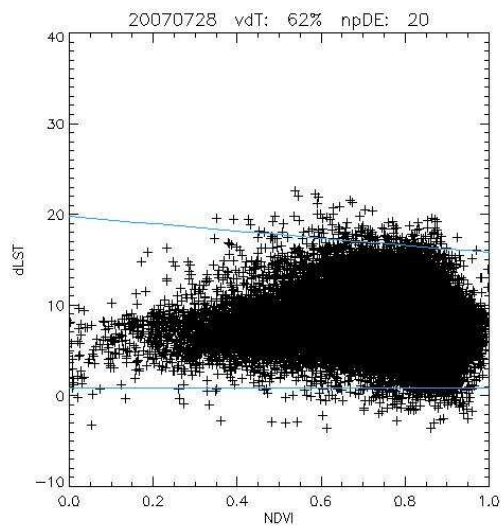
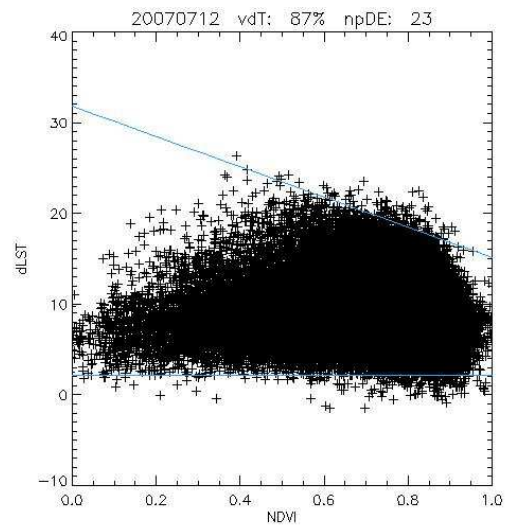
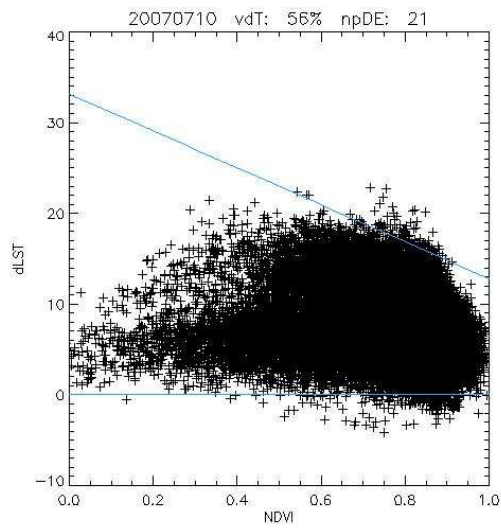
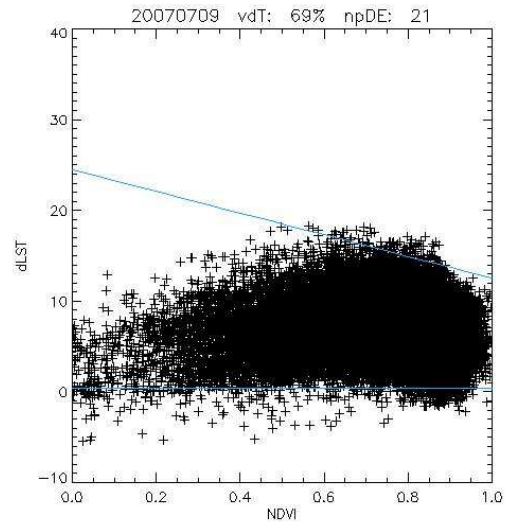
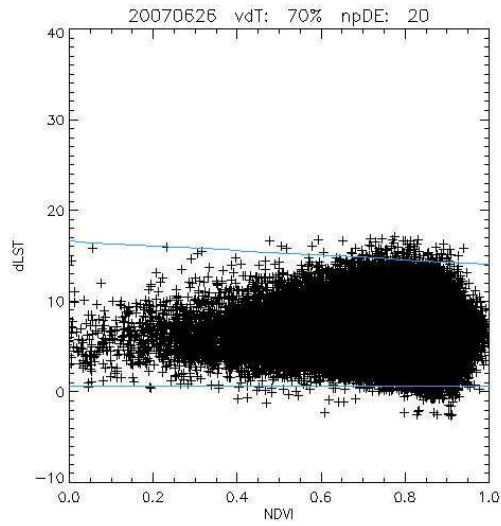
Scatter plots of Δ LST against NDVI for the days that passed the algorithm quality assurance in 2001 and the first four months of 2008.

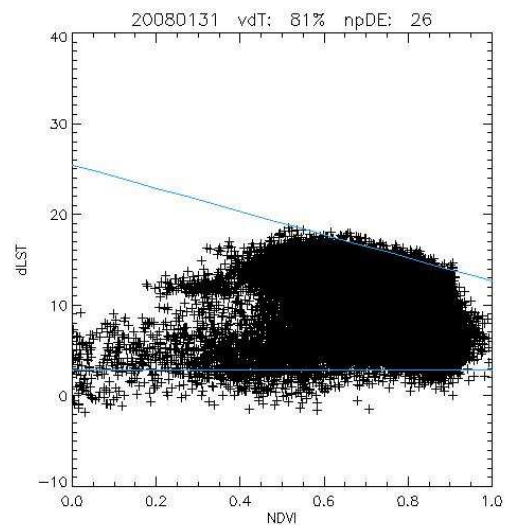
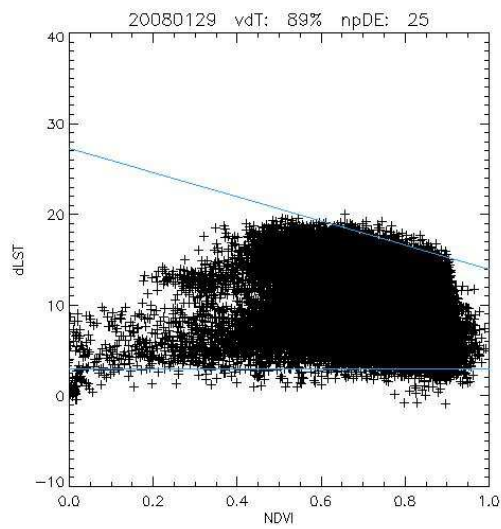
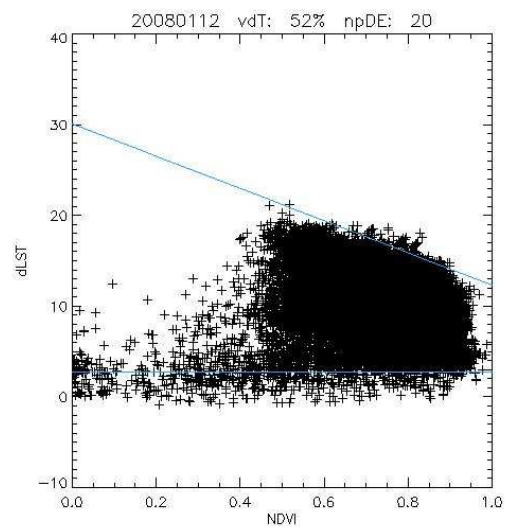
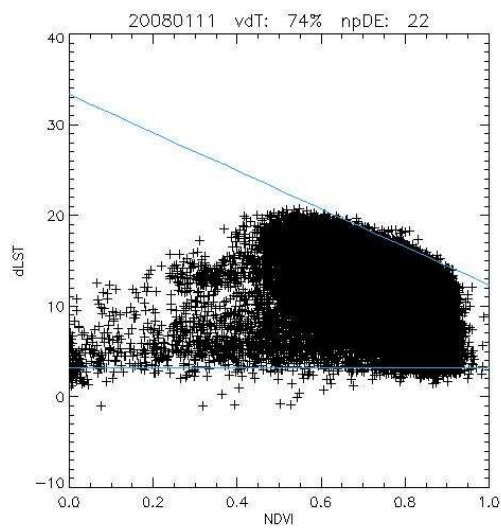
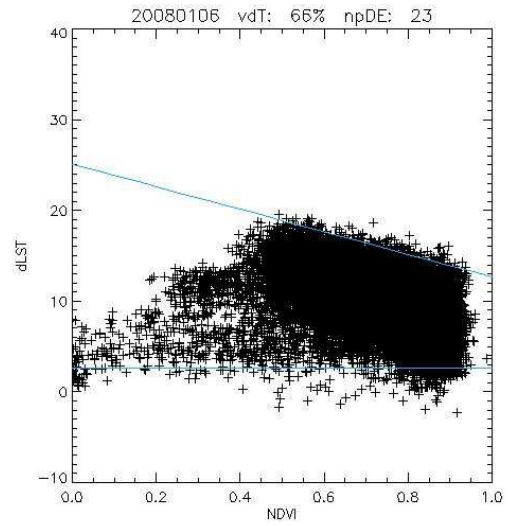
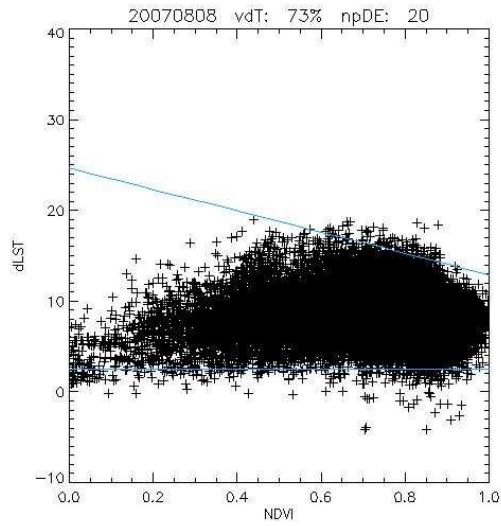


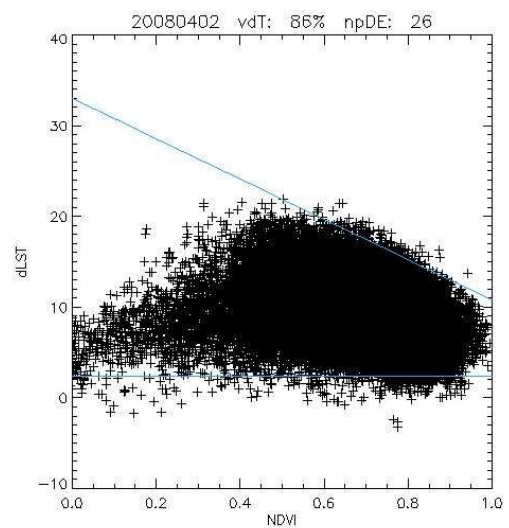
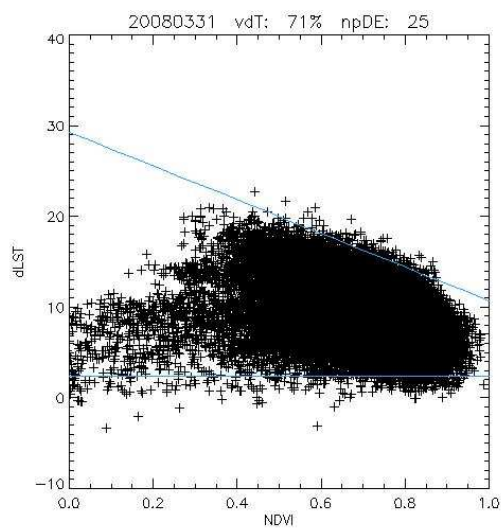
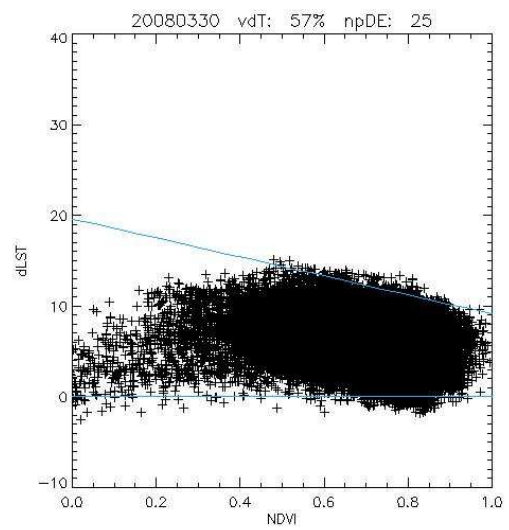
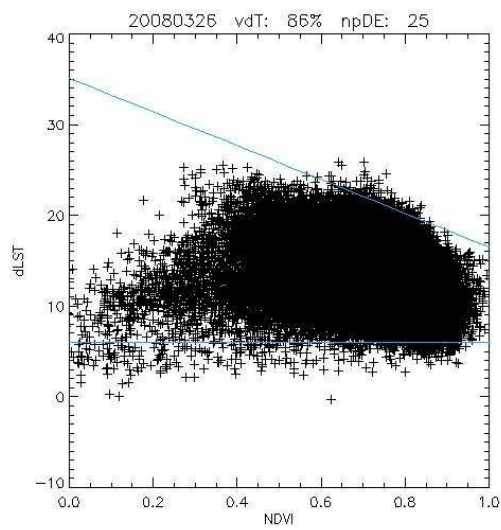
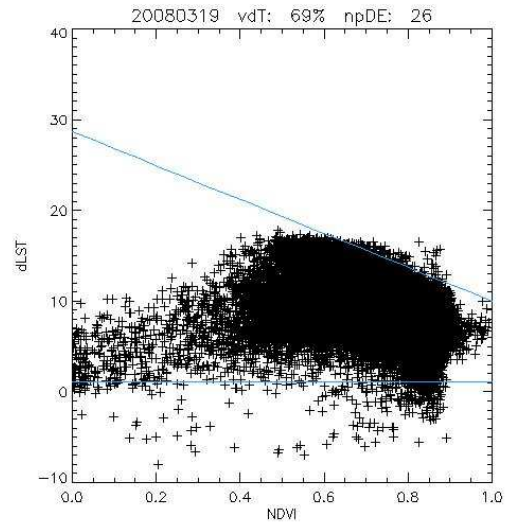
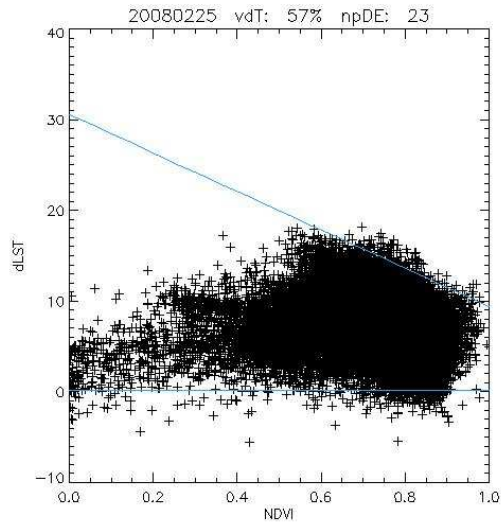


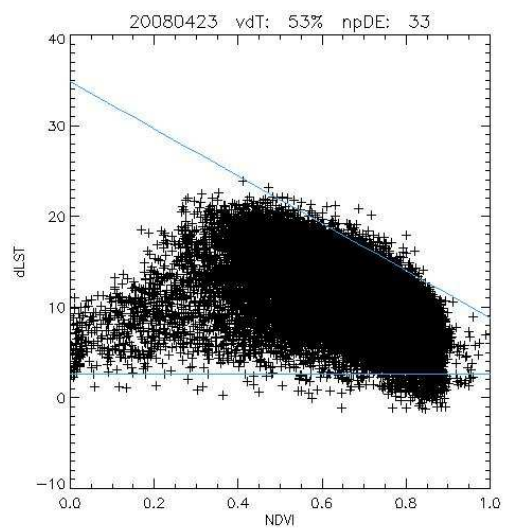
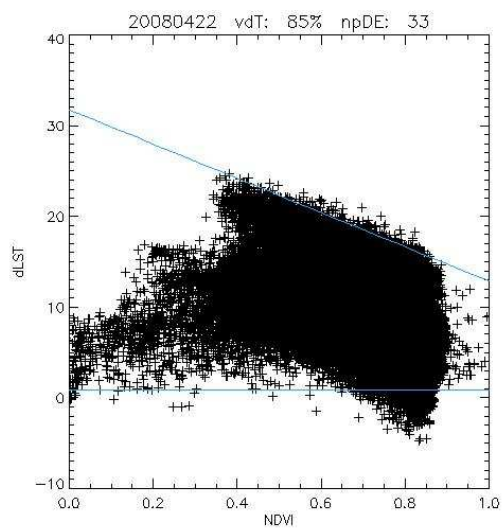
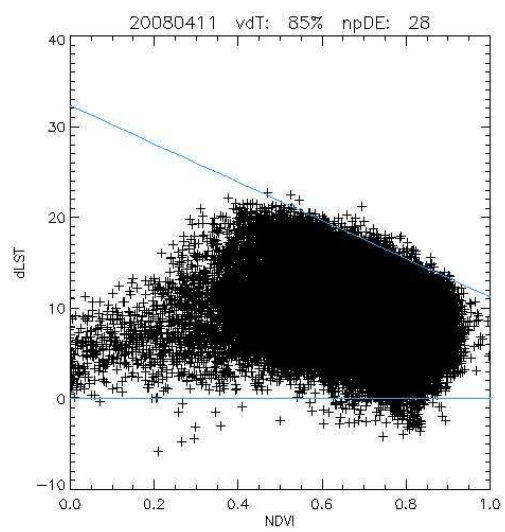
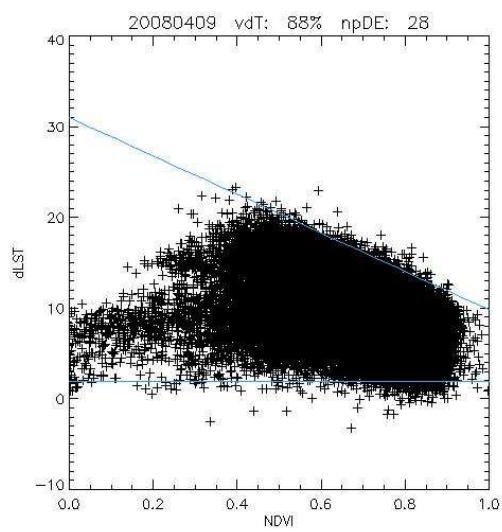
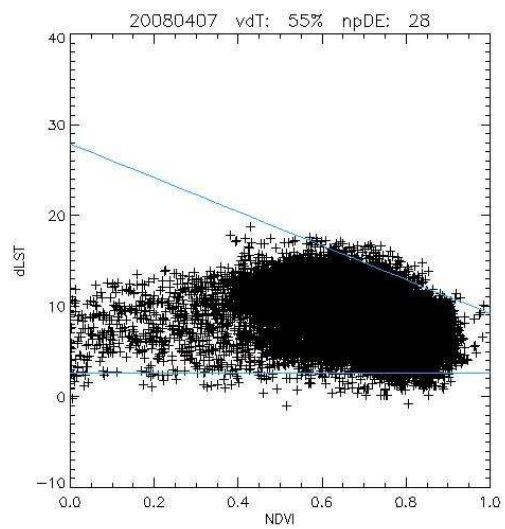
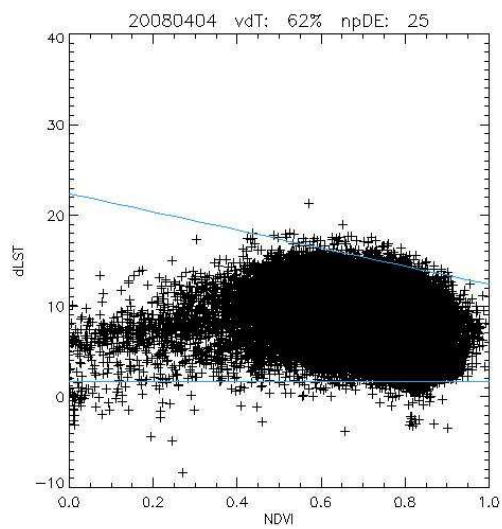


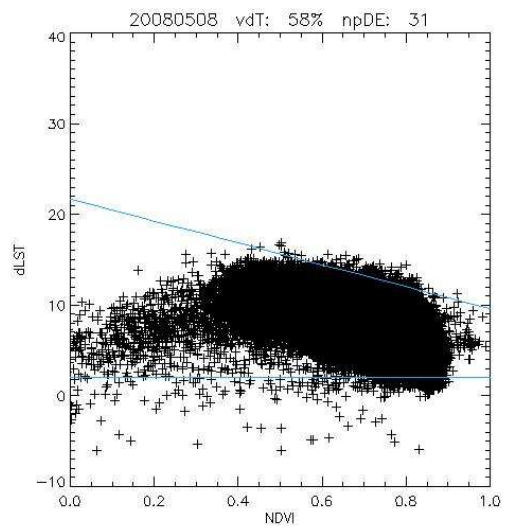
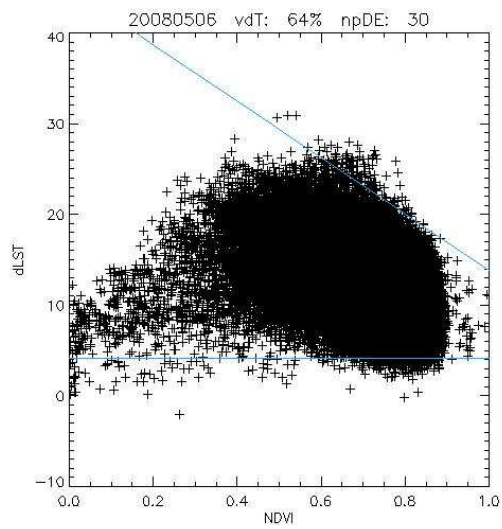
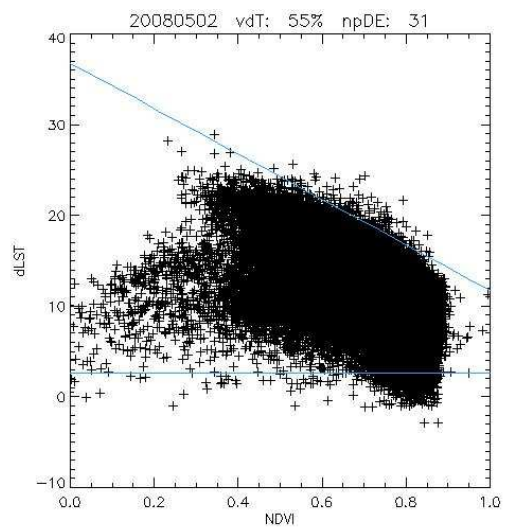
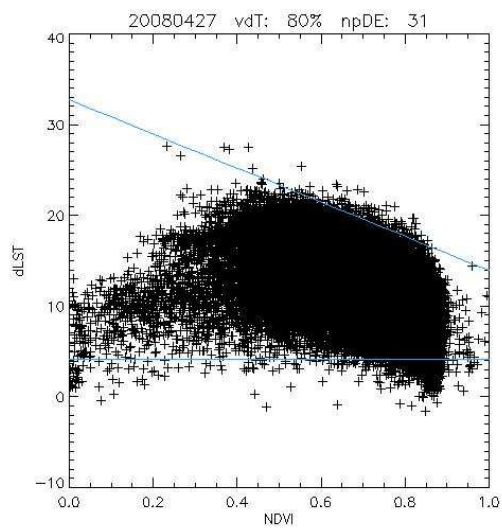
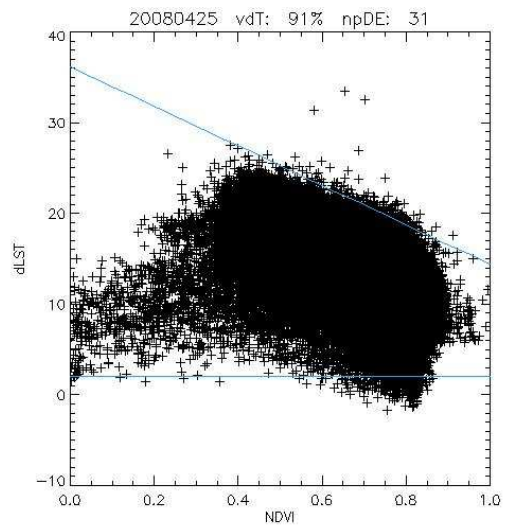
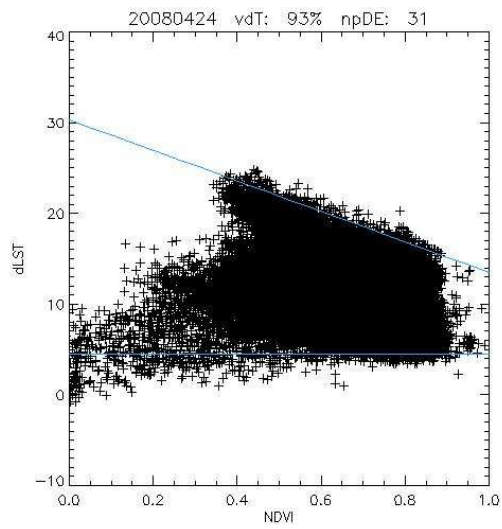












Appendix G

Description of sap flow measurement sites.

Test site nr. 1

Location: UTM zone 16N 389897E / 2154718N, WSG86.

Directions: turning left off the dirt road from the federal road 307 towards Laguna Ocom, in the state of Quintana Roo.

Forest type: medium sub-deciduous tropical forest.

Dates: installed on February the 7th and removed same day.

Setup: one sensor was partly installed (the drill battery had not been properly charged) and connected to the Grant datalogger for a few minutes.

Sapwood area: the tree was cut down and it was attempted to estimate the area by simple marking of the cross section with a marker, but there was no clear difference between the active and non active xylem.

Results: a signal was received, but since the setup was insufficient it was not analyzed.

Comments: This site demonstrated how difficult the drilling was going to be...

Test site nr. 2

Location: UTM zone 16N 390599E / 2165527N, WSG86.

Directions: in the front yard of the offices of ASK in the city of Felipe Carrillo Puerto, in the state of Quintana Roo.

Forest: none (not in a forest but in a city).

Dates: installed on February 8th and removed on February 10th (one full day, two nights).

Setup: three sensors were installed on the same quite large tree and connected using extension cables to the Grant logger which was placed indoors. The logger was set to store sample measurements every minute.

Sapwood area: no measurement was made.

Results: signals were received and stored in the file testsite2.L01, analysis is stored in the file testsite2.xls. The curve had the expected form and a reasonable level of noise.

Comments: It proved to be possible to do the drilling if just done slowly enough. Program setting of the datalogger was confusing but finally successful. Results extraction from the datalogger was difficult but finally successful. The datalogger proved to have a very coarse resolution and yet fine enough to detect the important trends. The three sensors showed overall reasonable agreement.

Test site nr. 3

Location: UTM zone 16N 381871E / 2156274N, WSG86.

Directions: off a lumbering path heading north from the village of Santa Isabel, near the Laguna Ocom, south-east of Felipe Carillo Puerto, in the state of Quintana Roo.

Forest: medium sub-deciduous tropical forest. Rather low and with few mature trees and many very young and small. Species in a 10x10 m area had their circumferences measured and were identified with the help of the commissioner of communal lands (in Spanish: comisariado ejidal) from Santa Isabel.

Dates: installed on February 10th and removed on February 13th (two full days, three nights).

Setup: three sensors were installed on three different trees and connected using extension cables to the CR10X datalogger. The logger was set to store sample measurements every minute.

Sapwood area: the dye method was attempted here for the first time, but it proved to be necessary with longer retention time than was available as well as the drilling was very hard, so no results were obtained.

Results: signals were received and stored in the file testsite3.dat, analysis is stored in the file testsite3.xls. The curves have distinct night-day trends, but the night values are not stable. Very low level of noise.

Comments: Again the drilling was a major problem, several drill bits were broken in the process and thus the drill battery lasted only enough to drill 3 trees out of 6 planned.

Full site nr. 4

Location: UTM zone 16N 320863E / 2135609N, WSG86.

Directions: off the dirt road between Plan de la Noria and Plan de la Nueva Noria, in the state of Quintana Roo.

Forest: medium sub-deciduous tropical forest. Forest somewhat higher than at site 3 and with a few more mature trees, yet also many very young and small; clear evidence of trees fallen due to hurricane as well as trees being lumbered. Species in a 20x20 m area had their circumferences measured and were identified with the help of an elder man referred by the commissioner of communal lands (in Spanish: comisariado ejidal) from Plan de la Nueva Noria.

Dates: installed on February 14th and removed on February 18th (three full days, four nights).

Setup: six sensors were installed on six different trees and connected using extension cables to the CR10X datalogger. The logger was set to store sample measurements every minute.

Sapwood area: the dye method was attempted here for the second time, this time with more success. Drilling was still very difficult and it was impossible to extract complete core samples; it was also hard to determine exactly how deep the dye had penetrated since it was very irregularly distributed in the samples.

Results: signals were received and stored in the file fullsite4.dat, analysis is stored in the file fullsite4.xls and fullsite4_new.xls. Four out of six curves have distinct night-day trends and stable night values, the fifth has an upward trend while the sixth lacks any clear trends. There seems to be some kind of irregular phase shift for all curves.

Comments: Very slow drilling and two drill batteries made it possible to do all six installations.

Full site nr. 5

Location: UTM zone 16N 361039E / 2148805N, WSG86.

Directions: off the lumbering road heading east from the road between Yoactún and Cha Santa Cruz, in the state of Quintana Roo.

Forest: medium sub-deciduous tropical forest. Forest slightly higher than at site 4 but seemingly less homogeneous – clearings due to hurricanes and/or lumbering. Species in a 25x15 m area had their circumferences measured and were identified with the help of the commissioner of communal lands (in Spanish: comisariado ejidal) from Yoactún.

Dates: installed on February 19th and removed on February 23rd (three full days, four nights).

Setup: six sensors were installed on six different trees and connected using extension cables to the CR10X datalogger. The logger was set to store sample measurements every minute.

Sapwood area: the dye method was used, with same problems as described at site 4. For the first time a species with active xylem through the whole trunk was encountered.

Results: signals were received and stored in the file fullsite5.dat, analysis is stored in the file fullsite5.xls. Five out of six curves have distinct night-day trends, but all had a severe noise during night-time, which got longer and longer from night to night. Three out of five had also some lower level noise during daytime. The sixth seems like complete rubbish, but it is unknown if it was connected to the same sensor as at the one showing rubbish at site 4. since the sensors had not been marked – this was done at this site

Comments: the sensors were marked at this site in order to be able to identify a possible consistency in the extremely bad channel data at next site.

Full site nr. 6

Location: UTM zone 16N 164550E / 2281595N, WSG86 (strictly speaking this point is slightly outside the eastern border of UTM zone 16 - in UTM zone 15 it has the coordinates 789974E / 2280756N).

Directions: off a small path to an orchard heading west from the road between San Mateo and Chunchucmil, in the state of Yucatán.

Forest: low deciduous and sub-deciduous tropical forest with secondary vegetation of shrubs and herbaceous plants. The tree population is mostly located in clusters, making the areas vegetation distribution quite heterogeneous compared to the previous sites. Species in a 20x40 m area had their circumferences measured and were identified with the help of the commissioner of communal lands (in Spanish: comisariado ejidal) from San Mateo.

Dates: installed on February 24th and removed on March 2nd (six full days, seven nights).

Setup: six sensors were installed on six different trees and connected using extension cables to the CR10X datalogger. The logger was set to store sample as well as averages plus internal temperature every minute.

Sapwood area: the dye method was used, with same problems as described at site 4.

Results: since efforts were continuously made to resolve the noise problems data was extracted several times and thus stored in a series of files – fullsite6a.dat to fullsite6h.dat. The main results are processed in fullsite6_CR10X.xls and fullsite6_combined_CR10X_&_Grant.xls. All data from this site has severe noise problems.

Comments: this site was one long fight to get the data free for noise, and several things were tested, i.a. eliminating outside electromagnetic disturbances, eliminating fluctuations due to long cables, reducing condensation in the datalogger, switching datalogger. Unfortunately the experiment had to move on to the next site before the problems were finally solved. There was found no consistency between the sensors yielding bad results at previous site with this site.

Full site nr. 7

Location: UTM zone 16N 173545E / 2260870N, WSG86 (strictly speaking this point is slightly outside the eastern border of UTM zone 16N - in UTM zone 15N it has the coordinates 799721E / 2260381N).

Directions: at a small ranch off the road between Nunkini and Chuc Holach, in the state of Campeche.

Forest: low deciduous and sub-deciduous tropical forest with secondary vegetation of shrubs and herbaceous plants. Like at site 6 the tree population is mostly located in clusters, but here the distinction is even more pronounced with the site being located in a tiny forest surrounded by areas of low vegetation. Due to the obvious challenges in determining tree concentration and the unexpected results there was not made any attempt of measuring and identifying species.

Dates: installed on March 2nd and removed on March 4th (one full day, two nights).

Setup: six sensors were installed on six different trees and connected using extension cables to the CR10X datalogger. The logger was set to store sample as well as averages plus internal temperature every 5 minutes.

Sapwood area: no measurements were made.

Results: data from this site is stored in the file fullsite7.dat, and processed in the file fullsite7.xls. Noise at this site is significantly reduced compared to last site (probably due changing of the moisture collecting bag inside the datalogger and the longer averaging time). However the curve trends are very different from expected.

Comments: data from this site unfortunately seems quite useless.

Full site nr. 8

Location: UTM zone 16N 400861E / 2170581N, WSG86.

Directions: about 30 m down a narrow dirt road branching to the east from the main dirt road leading from Felipe Carillo Puerto to Vigia Chico, about 10 km from Carillo Tecnológico, in the state of Quintana Roo.

Forest: medium sub-deciduous tropical forest. Forest slightly higher than at sites 4 and 5. Some trees were shedding or had shed their leaves. Species in a 20x30 m area had their circumferences measured and were identified with the help of a local expert sent by the commissioner of communal lands (in Spanish: comisariado ejidal) from Carillo.

Dates: installed on March 5th and removed on June 17th (by Waldemar from the ASK office in Carillo).

Setup: five sensors were installed on five different trees and connected, two directly and three using extension cables, to the CR10X datalogger. The logger was set to store 5 minute averages plus internal temperature every 5 minutes.

Sapwood area: measurements were made on two trees, and for the remaining three it was attempted to make regressions from other trees of same species but without luck.

Results: data from the first 24 hours is stored in the file fullsite8a.dat. Further data has not yet been extracted from the datalogger.

Comments: data seems promising, still waiting to get more.